UTILIZING THE SYSTEM INSTANTANEOUS FREQUENCY FOR THE STRUCTURAL HEALTH MONITORING OF BRIDGES

Neda Mostafa

UTILIZING THE SYSTEM INSTANTANEOUS FREQUENCY FOR THE STRUCTURAL HEALTH MONITORING OF BRIDGES

Neda Mostafa

UTILIZING THE SYSTEM INSTANTANEOUS FREQUENCY FOR THE STRUCTURAL HEALTH MONITORING OF BRIDGES

DISSERTATION

to obtain

the degree of doctor at the University of Twente,
on the authority of the rector magnificus,
prof. dr. ir. A. Veldkamp,
on account of the decision of the Doctorate Board
to be publicly defended
on Friday 26 April 2024 at 12.45 hours

by

Neda Mostafa

born on the 4th of July, 1982
in Tehran, Iran

This dissertation has been approved by:

Promotor
prof.dr.ir. T. Tinga

Co-promotors
dr.ir. R. Loendersloot
dr. D. Di Maio

Graduation Committee:

Chair / secretary: prof.dr.ir. H.F.J.M. Koopman

Promotor: prof.dr.ir. T. Tinga
                            Universiteit Twente, ET, Applied Mechanics & Data
                            Analysis

Co-promotors: dr.ir. R. Loendersloot
                            Universiteit Twente, ET, Applied Mechanics & Data
                            Analysis

                            dr. D. Di Maio
                            Universiteit Twente, ET, Applied Mechanics & Data
                            Analysis

Committee Members: prof. dr. M. Ghandchi Tehrani
                            University of Groningen, Science & Engineering

                            prof. dr. E.J.F. Figueiredo, Lusófona
                            University Portugal, Engineering

                            prof.dr.ir. A.G. Doree
                            Universiteit Twente, ET, Market Dynamics

                            prof.dr.ing. B. Rosic
                            Universiteit Twente, ET, Applied Mechanics & Data
                            Analysis

Dedicated to

my parents
my son, Nikan
my daughter, Nila
and
my husband, Mohammad

Summary

Bridges are continuously subjected to material aging, like corrosion of steel bars in reinforced concrete bridges or corrosion of steel structures and components. These processes combined with increasing traffic load result in overall deterioration and loss of structural integrity, which requires proper estimation of the maintenance needs to ensure safe operation of the asset. Vibration-based structural health monitoring is a non-destructive in-situ technology mainly based on performing three steps: 1) measure the dynamic response of the structure; 2) analyze the response; and 3) interpret the analyzed response for either system identification or damage detection. Structural Health Monitorin (SHM) then contributes to plan and perform maintenance or to provide early warnings of growing damage that can affect the safety and the bridge lifetime.

This thesis focuses on the time-frequency analysis of the vehicle-bridge dynamic interaction response to identify the time-dependent resonances of railway bridges which are incorporated into a damage detection approach, rather than only system identification. Most of the current system identification techniques applied to bridges are based on the free vibration response analysis. It is known that the bridge free vibration response is sensitive to environmental conditions such as temperature and it is not sufficiently sensitive to damage. Input-output modal analysis or output-only modal analysis are the other most used techniques for the bridge system identification. The train-bridge dynamic response, obtained during passage of the train is potentially more sensitive to damage, but also a more complex signal to analyze. First of all, it is a non-stationary signal that is not valid for modal analysis. In addition to the time-variant nature, the vehicle-bridge dynamic response can show closely-spaced spectral components response. These features disrupt the performance of the most advanced signal processing techniques. This thesis therefore applies a recently developed technique, Wavelet Synchrosqueezed Transform (WSST) to extract the Instantaneous Frequencies (IFs) of the Vehicle-Bridge Interaction (VBI) system response. A comparative study is performed on the various commonly used time-frequency analysis techniques. The obtained results were further validated using field measurements on a real bridge.

Subsequently, a concept for damage detection in (railway) bridges based on the instantaneous frequency analysis of the bridge's forced and free vibration responses

is proposed. Within this concept, based on the bridge natural frequency extracted from the bridge free vibration, a healthy baseline is obtained of the bridge forced vibration response. The shape correlation and the magnitude variation are proposed to distinguish between the global characteristics of the bridge baseline induced by variable operational conditions and the local deviations caused by damage. If the source of the baseline deviation is damage, then the magnitude variation can be used as a damage index. The proposed damage index is a preliminary step toward damage quantification. Furthermore, the local deviation of the baseline instantaneous frequency around the damage location shows the potential of the proposed method for damage localization. However, damage localization is out of the scope of the current study.

The proposed Vehicle-Induced Delta Frequency (VIDF) quantifies the influence of the vehicle dynamics on the response of the intact bridge. The Damage-Induced Delta Frequency (DIDF), as a damage sensitive feature, quantifies the influence of the vehicle dynamics on damage detection. The final objective of this study was to investigate the effectiveness of the proposed damage sensitive feature using different train types, specifically freight trains and passenger trains. Therefore, two vehicle models were employed to calculate VIDF and DIDF. The results of the numerical studies show that trains with single suspension systems cause more pronounced changes in the bridge's frequency response, specifically the Vehicle-Induced Delta Frequency (VIDF) and Damage-Induced Delta Frequency (DIDF), than dual suspension trains. This characteristic indicates that single suspension trains are better suited for efficient bridge health monitoring and damage detection.

The work in this thesis shows a methodology to use the non-stationary dynamic response of a bridge passing event of a train for structural health monitoring purposes. The method is applicable for relatively low-speed train passages (no high speed lines) and identifies a number of key points to take into account when implementing such a monitoring system. The signal processing technique is of great importance, but also the type of train passing the bridge is an elementary part of successful damage identification. These insights form the base for guidelines to design a monitoring system using the dynamic response to a train passing a bridge.

Contents

List of Figures

List of Tables

1

Introduction

This chapter provides an introduction to the PhD project, in the framework of the European project "DESTinationRAIL- decision support tool for rail infrastructure managers". It outlines the motivation behind the PhD project, presents an overview of the research process, and highlights the background and problem statement. Additionally, the chapter introduces the research questions and provides the thesis outline.

1.1 Background

Approximately 95% of European rail infrastructure was built prior to 1914 which underscores the importance of enhancing productivity in existing rail networks, prioritizing infrastructure renewal, and optimizing the construction of new sections[1]. Additionally, there is a need for infrastructure managers to enhance customer satisfaction and effectively address the impact of natural hazards and extreme weather events that have implications for the entire European rail network. These complex challenges necessitate the adoption of innovative approaches and the implementation of strategic decision-making by rail infrastructure managers throughout the continent. Currently, European rail infrastructure managers are facing challenges in making crucial investment decisions related to safety due to inadequate information, and data, and an excessive reliance on visual assessments of structures. The primary objective of the DESTinationRAIL project is to address these challenges by developing a decision support tool for rail infrastructure networks. The project's approach is illustrated in Figure 1.1 based on the FACT (Find, Analyze, Classify, Treat) principle.
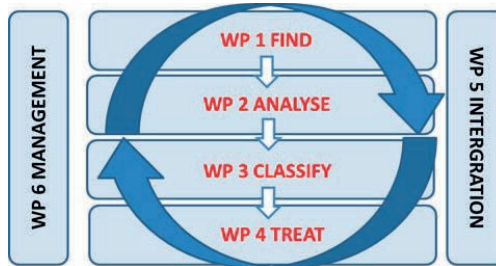
Figure 1.1: Destination RAIL aims to develop a decision support tool for infrastructure managers to make rational investment decisions.

- Find: Identify vulnerable critical assets in advance to prevent failures, understand asset performance, and assess the stability of the geological and engineering conditions surrounding these assets.

- Analyze: Utilize appropriate tools to process information and data in order to accurately evaluate asset conditions and the impact of different maintenance approaches.

- Classify: Understand the interrelationships between risks and individual components within the overall system, and comprehend how changes in the system affect the performance of individual components.

- Treat: Implement maintenance and repair strategies to ensure the safety and reliability of the entire rail network for both passengers and freight while considering limited maintenance budgets and the imperative to enhance sustainability.

The target critical components of the rail infrastructure are slopes, tunnels, tracks, retaining walls, switches, crossings, and bridges. The focus of this Ph.D. thesis, as part of the DESTinationRAIL project, is on developing a Structural Health Monitoring strategy for railway bridges to effectively identify damage.

According to statistical data provided by Rijkswaterstaat, part of the ministry of infrastructure and water management in the Netherlands, a significant number of bridges were constructed between 1960 and 1980 with an intended service life of 50 years [2]. This trend is likely similar in other European countries as well. The service life of a bridge refers to the period during which it is expected to function safely. Therefore,

alongside the design of new and modern bridges, some of which are equipped with Structural Health Monitoring (SHM) systems right from the start, there are existing bridges that have surpassed their expected service life [2]. The collapse of the Morandi bridge in Genoa, Italy, on August 14, 2018, after 51 years of service, resulted in a tragic event that claimed the lives of 43 individuals. A post-collapse analysis [3] indicated that inadequate maintenance practices and construction flaws contributed to this devastating accident. The collapse of the Morandi bridge serves as a stark reminder of the critical importance of addressing the condition of aging bridges and implementing additional maintenance and structural health monitoring strategies.

1.2 Problem statement

The development of an SHM system contains a sequence of actions initiated by the instrumentation of the target structure, data acquisition, data analysis, and the assessment of the structure's condition. The core part of a SHM system is the applied methodology or approach on the sensor data to extract information about the condition of the structure and damage. Various sensors are available for bridge condition assessment, including corrosion sensors, displacement sensors, vibration sensors and vision systems, such as high-speed cameras. Given the widespread adoption of vibration sensors, this study centers its attention on vibration-based damage detection techniques.

In general, vibration-based damage detection techniques can be classified into four groups. The first group consists of model-based techniques that update the parameters of an analytical or numerical model to match real measurements [4–6]. However, these techniques may not be efficient for all bridges, particularly those with complex geometries where model accuracy plays a crucial role. The second group comprises data-driven methods, such as neural networks, machine learning, feature extraction, and pattern recognition techniques [7–13]. These two groups are beyond the scope of the current study. The third group includes traditional modal-based damage detection techniques that monitor changes in modal properties caused by damage [14, 15]. However, these techniques rely on analyzing the bridge's free vibration response, which may not be as sensitive as the forced vibration response. The fourth group involves time-frequency analysis of the Vehicle-Bridge interaction (VBI) response using advanced signal pro-

cessing techniques. The proposed Structural Health Monitoring (SHM) scheme in this study falls under the fourth group.

The efficiency of extracting bridge dynamic properties from its free vibration response for the purpose of damage detection is questioned due to the belief that the bridge's transient response carries more information, including damage-induced singularities. However, several challenges arise in this context. Firstly, the coupled system of the bridge and heavy vehicles becomes time-variant due to vehicle-induced effects, resulting in a non-stationary system response. Consequently, approaches like operational modal techniques or output-only analysis, which assume broad-band white noise excitation, fail to provide accurate results.

The vehicle-bridge interaction response is the response of the bridge when a passing vehicle acts as excitation. Signal processing techniques commonly used for other systems face difficulties when applied to Vehicle-Bridge Interaction (VBI) responses. The difficulties arise from the characteristics of these systems. The closely-spaced modes in VBI systems lead to mode-mixing problems, making it challenging to decompose and analyze the responses accurately.

Therefore, analyzing VBI responses poses challenges in 1) comprehending the dynamic interactions within the coupled system, 2) accurately extracting and isolating the time-dependent dynamic properties of each sub-system (the vehicle and the bridge) under various conditions, including both healthy and damaged states, 3) developing a technique to identify damage based on the analysis of VBI responses, 4) understanding the impact of vehicle dynamics on the coupled system response enables efficient SHM strategies.

1.3   Rationale of the proposed approach

The proposed approach is a physic-based technique based on the time-frequency analysis of the VBI acceleration response by applying wavelet-synchrosqueezed transform to extract the instantaneous frequencies of the system. The approach is based on the following considerations;

- The bridge free vibration (the global response of the structure) and the bridge forced vibration (the VBI response) both contain information on the damage event. However, the bridge free vibration response may not be as sensitive to

damage as the forced vibration response where the damage is triggered by the passing vehicle.

- Damage is a local event which imposes a local stiffness reduction at the damage location, and hence causes a local effect on the dynamic response of the system.

- Damage-induced changes in the structure's stiffness can manifest as singularities in the Vehicle-Bridge Interaction (VBI) response when a passing vehicle encounters the damage.

- The local stiffness change due to damage affects the instantaneous frequency (IF) of the bridge at the damage location. Therefore, the target frequency range is around the bridge natural frequency which for a typical bridge, such as studied in the current study, is about 1-10 Hz.

- Besides the bridge, the dominant vibrating sub-system in the target frequency range is the vehicle which can induce a bridge IF variation.

- For small and medium span bridges, 20-80m, the mass of a train is not negligible in comparison with the mass of a bridge.

- To accurately extract the bridge IF variation due to damage, the bridge IF variation due to operational conditions should be identified and excluded.

- The dynamic response of a vehicle-bridge interaction response is a noisy, multi-component signal with closely spaced spectral components. Therefore, the applied technique should overcome the mode-mixing issue and enable the proper mode decomposition.

- The objective is to outperform approaches relying on the free vibration principles. Therefore, to capture damage at an early stage a higher frequency resolution is required that enables to capture the damage-induced IF variation.

1.4   Research objective and research questions

The objective of this research is developing a vibration-based health monitoring strategy for railway bridges and the main research question is formulated as:

How to efficiently utilize the vehicle-bridge dynamic interaction response to detect damage by means of monitoring the instantaneous frequencies of the system?

In order to answer the main research question, the following sub-questions need to be answered:

1. What are the failure mechanisms for bridges and how do these influence the bridge dynamics?

2. How to accurately extract the instantaneous frequency of the vehicle-bridge coupled system which carries time-dependent and local event information, i.e. damage information?

3. How to identify damage based on the extracted instantaneous frequencies and distinguish between operational conditions and damage?

4. How do the dynamics of a passing vehicle affect the instantaneous frequency of the intact and damaged structure?

5. What type of vehicle is most suitable for damage detection?

1.5   Research approach & thesis outline

In order to achieve the aim of this research, a robust research approach is adopted that can also be used for road bridges and probably other time-variant coupled systems other than the VBI. The research approach contains the following steps:

1. Find the failure mechanisms and the leading causes of deterioration of the bridge structure and their physical effects on the bridge dynamic properties.

2. Find a method to accurately extract the time-dependent resonances or the instantaneous frequencies (IFs) of the intact vehicle-bridge interaction response.

3. Develop a damage detection approach by utilizing the extracted instantaneous frequency of the vehicle-bridge interaction response and use numerical models to validate the approach.

4. Investigate the influence of operational conditions by varying the vehicle dynamics and assess the effect on the ability to identify damage.

By following the above mentioned research steps, the research was divided into several parts which will be discussed in the remaining chapters of this thesis.

Chapter 2 The chapter provides an overview of the various failure mechanisms observed in bridges, with a focus on identifying key causes addressable through proper maintenance. Additionally, it reviews the current state-of-the-art in recent bridge monitoring campaigns, specifically examining instrumentation and analysis approaches for vibration-based bridge monitoring.

Chapter 3 While most available structural health monitoring (SHM) systems analyze the bridge's free vibration response, it is essential to consider the vehicle-bridge interaction (VBI) response, as it captures the damage-induced singularities when the vehicle encounters the affected area. This chapter will focus on understanding and extracting the time-dependent resonances of the VBI system using various time-frequency analysis techniques. The main challenges are overcoming the mode-mixing issue, providing accurate results in terms of instantaneous frequencies (IFs) of the system and handling noisy responses. Furthermore, the method(s) are tested on field data obtained from the Boyne bridge, to check their reliability and applicability.

Chapter 4 From the previous chapter, it can be concluded that by utilizing a high-resolution time-frequency method, the bridge's instantaneous frequency can be accurately extracted from the coupled system response. This chapter introduces a damage detection approach based on the bridge's instantaneous frequency. Since the vehicle dynamic properties have an influence on the bridge's instantaneous frequency, the proposed approach excludes the influence of the operational conditional and utilizes the shape of the bridge's instantaneous frequency as a damage-sensitive feature. Moreover, a Damage Index is proposed as an attempt to quantify the damage.

Chapter 5 The dynamic interaction between vehicles and bridges (VBIs) is characterized by the frequency ratio between the vehicle (super-system) and the bridge (sub-system), meaning that the vehicle dynamics have an influence on the instantaneous frequency of a bridge in both intact and damaged conditions. Therefore, the Vehicle-Induced Delta Frequency and Damage-Induced Delta Frequency are introduced

to quantify the influence of the vehicle dynamics on the bridge instantaneous frequency. The vehicle-bridge dynamic coupling has been investigated through two vehicle models; 1) single suspension and, 2) dual suspension vehicles. The results show that not all vehicle types are equally efficient for the health monitoring of bridges. The trains with single suspension outperform the passenger trains.

Chapter 6 A reflection on the research questions, in light of the results obtained from the individual chapters, is presented in this chapter. It also discusses a number of limitations of the present approach and presents potential solutions for these.

Chapter 7 and 8 Chapter 7 provides conclusive insights derived from the research conducted, summarizing key findings and implications. Also a list of recommendations, both for future research and practical application, is presented. Chapter 8 compiles a list of publications stemming from the research, showcasing the scholarly contributions resulting from the study.

Bibliography

[1] I. Stipanović Oslaković, K. Gavin, and M. S. Kovacevic, "Developing decision support tools for rail infrastructure manager," in *4th International Conference on Road and Rail Infrastructure, CETRA 2016*, pp. (pp. 627–633).

[2] N. Mostafa, R. Loendersloot, T. Tinga, A. Reitsema, and D. Hordijk, "Monitoring dynamic stiffness that predicts concrete structure degradation,"

[3] M. Morgese, F. Ansari, M. Domaneschi, and G. P. Cimellaro, "Post-collapse analysis of morandi's polcevera viaduct in genoa italy," *Journal of Civil Structural Health Monitoring*, vol. 10, no. 1, pp. 69–85, 2020.

[4] M. I. Friswell, "Damage identification using inverse methods," *Philos Trans A Math Phys Eng Sci*, vol. 365, no. 1851, pp. 393–410, 2007.

[5] R. V. Farahani and D. Penumadu, "Damage identification of a full-scale five-girder bridge using time-series analysis of vibration data," *Engineering Structures*, vol. 115, pp. 129–139, 2016.

[6] J. Li, S. S. Law, and H. Hao, "Improved damage identification in bridge structures subject to moving loads: Numerical and experimental studies," *International Journal of Mechanical Sciences*, vol. 74, pp. 99–111, 2013.

[7] D. Li, Y. Wang, W.-J. Yan, and W.-X. Ren, "Acoustic emission wave classification for rail crack monitoring based on synchrosqueezed wavelet transform and multi-branch convolutional neural network," *Structural Health Monitoring*, vol. 20, no. 4, pp. 1563–1582, 2020.

[8] L. Sun, Z. Shang, Y. Xia, S. Bhowmick, and S. Nagarajaiah, "Review of bridge structural health monitoring aided by big data and artificial intelligence: From condition assessment to damage detection," *Journal of Structural Engineering*, vol. 146, no. 5, 2020.

[9] A. Malekjafarian, F. Golpayegani, C. Moloney, and S. Clarke, "A machine learning approach to bridge-damage detection using responses measured on a passing vehicle," *Sensors (Basel)*, vol. 19, no. 18, 2019.

[10] M. Silva, A. Santos, E. Figueiredo, R. Santos, C. Sales, and J. C. W. A. Costa, "A novel unsupervised approach based on a genetic algorithm for structural damage detection in bridges," *Engineering Applications of Artificial Intelligence*, vol. 52, pp. 168–180, 2016.

[11] G. Comanducci, F. Magalhaes, F. Ubertini, and A. Cunha, "On vibration-based damage detection by multivariate statistical techniques: Application to a long-span arch bridge," *Structural Health Monitoring-an International Journal*, vol. 15, no. 5, pp. 505–524, 2016.

[12] A. Santos, E. Figueiredo, M. Silva, R. Santos, C. Sales, and J. C. W. A. Costa, "Genetic-based em algorithm to improve the robustness of gaussian mixture models for damage detection in bridges," *Structural Control & Health Monitoring*, vol. 24, no. 3, 2017.

[13] H. Babajanian Bisheh, G. Ghodrati Amiri, M. Nekooei, and E. Darvishan, "Damage detection of a cable-stayed bridge based on combining effective intrinsic mode functions of empirical mode decomposition using the feature selection technique," *Inverse Problems in Science and Engineering*, vol. 29, no. 6, pp. 861–881, 2020.

[14] M. B. P. Scott W. Doebling, Charles R. Farrar, "A summary review of vibration-based damage identification methods," *The Shock and Vibration Digest*, 1998.

[15] J. J. Moughty and J. R. Casas, "A state of the art review of modal-based damage detection in bridges: Development, challenges, and solutions," *Applied Sciences-Basel*, vol. 7, no. 5, 2017.

2

Failure mechanisms of bridges and bridge monitoring state-of-the-art[1]

2.1 Introduction

Bridge health monitoring systems are essential for safeguarding public safety, optimizing resource allocation, and extending the operational life of bridges. To build effective monitoring strategies and choose suitable sensors and methods, it is crucial to comprehend the causes and consequences of deterioration. Therefore, delving into the various failure modes and mechanisms that affect both steel and concrete bridges is required to lay the foundation for the development of advanced bridge-monitoring systems. This chapter will provide an overview of the failure modes and mechanisms typically encountered in steel and concrete bridges. After that, the state-of-the-art in bridge structural health monitoring will be described. Many of the currently developed SHM systems go beyond merely identifying dynamic characteristics and instead focus on assessing the bridge's condition and on damage detection.

---

[1]This chapter is reproduced from: N. Mostafa & R. Loendersloot (2018). Implementation of a Complete Vibration Monitoring System on Irish Rail Bridge. Deliverable 1.5, DESTination RAIL – Decision Support Tool for Rail Infrastructure Managers
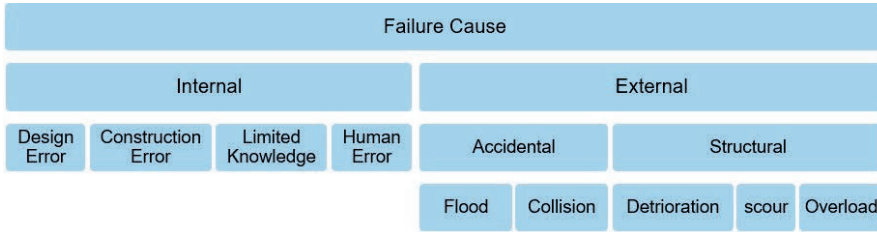
Figure 2.1: Failure cause of bridges [3]

2.2 Failure modes and failure mechanisms

The approach for the development of a bridge-monitoring system followed in this research relies on the conviction that it is necessary to first understand the failure modes and mechanisms of bridges. Using that information, it is possible to define the best monitoring approach, given other constraints that are to be met in a field application.

2.2.1 Failure classifications

On the one hand, it is known that any imperfection in a bridge design, construction, or maintenance can cause a failure. On the other hand, it is known that Structural Health Monitoring (SHM) is aimed for improving maintenance decision-making, with the ultimate goal of reducing maintenance costs and increasing system availability [1]. Therefore, an efficient SHM system should be designed based on the corresponding maintenance strategy, bearing in mind that maintenance activities attempt to prevent failure. Failure causes of bridges have been classified by Imhof [2] in limited knowledge, natural hazard, design error, overloading, accidental impact, human error (not design related), vandalism, and deterioration. Another classification, proposed by Caglayan et al. [3] has assigned all these causes to three categories: the principal cause, the enabling cause, and the triggering cause. The principal and enabling causes are related to human error in design and construction, limited knowledge, etc., while the third cause, the triggering cause, refers to external effects such as deterioration, scour, collision, and overload. These are referred to in this document as External-Structural failure cause (see Figure 2.1). Having identified the different categories of failure causes does not allow for a condition assessment, let alone an estimation of the remaining useful life (RUL). The deterioration of bridges during their operational life needs to be studied

to this end. Firstly, the distinction is made between different building materials for bridges: concrete and steel. Although the Boyne Viaduct, the cases study used in this project, is a steel bridge, the deterioration of concrete bridges is also touched upon. Despite the significant differences in material and construction, corrosion is a shared failure mechanism of bridges. The associated failure modes however show differences and will — possibly — lead to differences in the monitoring systems for each type of bridge.

2.2.2 Deterioration of Steel Bridges

Damage to steel members typically results from corrosion, fatigue, and impact. If the damage from any of these causes is extensive, either a portion or the entire member may have to be replaced [4]. Corrosion is considered a leading cause of bridge deterioration, according to the technical report of the National Bridge Inventory in the U.S. [5]. A steel girder bridge can be affected by five main forms of corrosion [6]:

1. General corrosion

2. Pitting corrosion

3. Galvanic corrosion

4. Crevice corrosion

5. Stress corrosion

The most prevalent form is a general loss of surface material; this condition will lead to the gradual thinning of members. General corrosion accounts for the largest percentage of corrosion damage. Pitting corrosion also involves the loss of material at the surface. However, it is restricted to a very small area. Pits can be dangerous because they extend into the metal, showing little evidence of their existence. Pit occurrence is serious in high-stress regions because it can cause local stress concentrations. Galvanic corrosion occurs when two dissimilar metals are electrochemically coupled. Such situations may occur at bolted or welded connections. Galvanic corrosion can be local, leading to pit formation. Crevice corrosion occurs in small confined areas, such as beneath peeling paint or between facing surfaces. It is usually caused by a low concentration of dissolved oxygen in the moisture held within a crevice. Deep pits can also provide locations

for crevice corrosion to occur. Stress corrosion occurs when metal is subjected to tensile stress in a corrosive environment. For mild carbon steel in ordinary bridge environments, stress corrosion is usually not a problem [6].

There are three basic changes that can occur in a steel bridge due to corrosion: loss of material, reduction of section parameters, and build-up of corrosion products. The effect of corrosion on the bending behavior will depend on whether the section is in the positive or negative momentum region. For a continuous span, a reduced lower flange thickness may cause local buckling above an interior support (see Figure 2.2a) and for the positive momentum regions, corrosion loss will cause a reduction in the tensile capacity of the lower flange [7] (see Figure 2.2b).

A capacity-loss analysis was carried out for both composite and non-composite wide flange girders, in positive bending [6] and the results are shown in Figure 2.3. The reduction in bending capacity and stiffness is shown to be linearly proportional to the section loss [6].

2.2.3   Deterioration of Concrete Bridges

Concrete members are subject to spalling due to corrosion of the underlying reinforcement; scaling caused by freezing and thawing; and cracking caused by shrinkage, flexure, or differential settlement [4]. In a concrete bridge structure, corrosion of reinforcing steel and other embedded metals is the leading cause of deterioration. There are two main types of corrosion of the steel rebar embedded in reinforced concrete bridges:

1. Chloride corrosion

2. Concrete carbonation

Chloride penetrating through existing cracks in the concrete induces corrosion of the steel reinforcement (see Figure 2.4a). Concrete carbonation occurs naturally over the service life of a concrete structure, where carbon dioxide reacts with calcium hydroxide within the concrete to form calcium carbonate. Carbon dioxide can come from either the atmosphere or from external water sources. While carbonation can increase the strength capacity of concrete, it also reduces its alkalinity. The reduced alkalinity decreases the corrosion protection capabilities of the reinforcement steel, often leading to spalling as a result (see Figure 2.4b). When steel corrodes, the resulting rust occupies
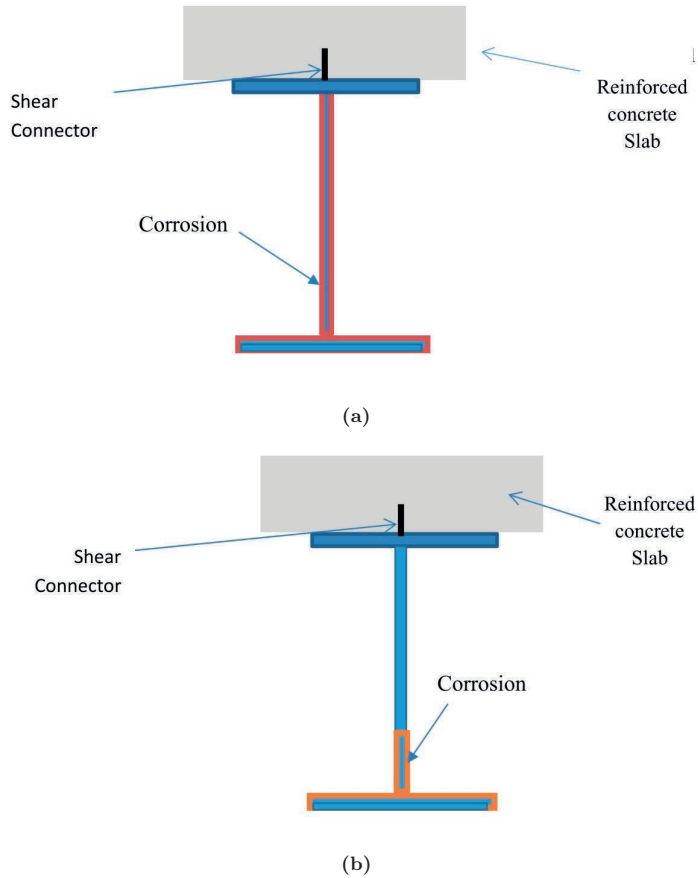
Figure 2.2: Corrosion models for (a) supports (shear section model) and, (b) the mid-span (moment section model) of a steel bridge girder [7].

a greater volume than the steel. This expansion creates tensile stresses in the concrete, which can eventually cause cracking, delamination, and spalling. The mechanical behavior of reinforced concrete beams due to corrosion of the rebars is investigated by Zhu [8], following a similar approach as the research on the corrosion of steel bridges. The mid-span deflection was measured via a Linear Variable Displacement Transducer (LVDT). Figure 2.5 displays the Load-Displacement curves for uncorroded (BT1-C) and corroded beams with different levels of corrosion. Corrosion of the rebars reduces
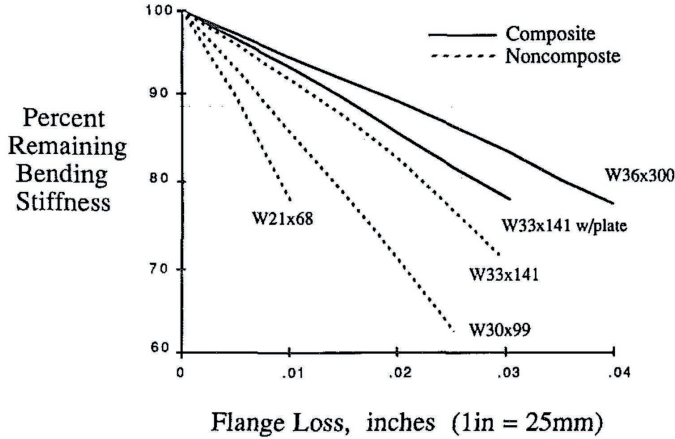
Figure 2.3: Reduction in bending stiffness due to corrosion [6]

the bending stiffness of the beam, hence the bending stiffness of the bridge appears to be an eligible structural dynamic property to monitor.

2.2.4   Concluding Remarks on Bridge Deterioration

Despite differences in materials, constructions, and mechanisms, corrosion appears to be a common denominator in the deterioration process of bridges. Eventually, a stiffness loss will occur, resulting in a decrease in load bearing capacity of the bridge. The monitoring strategy and the sensors selected for monitoring depend on the type of deterioration expected and the level at which this is to be detected. The earlier a problem is to be identified, the more dedicated the sensor needs to be. Often, this also implies measuring close to the expected location of failure (hot-spot monitoring). A compromise is to measure changes in global behaviour and further inspect and/or take maintenance actions on regions of the bridge. One way of identifying global changes in bridge behaviour is Vibration-Based Monitoring. This topic is further elaborated in the next section.
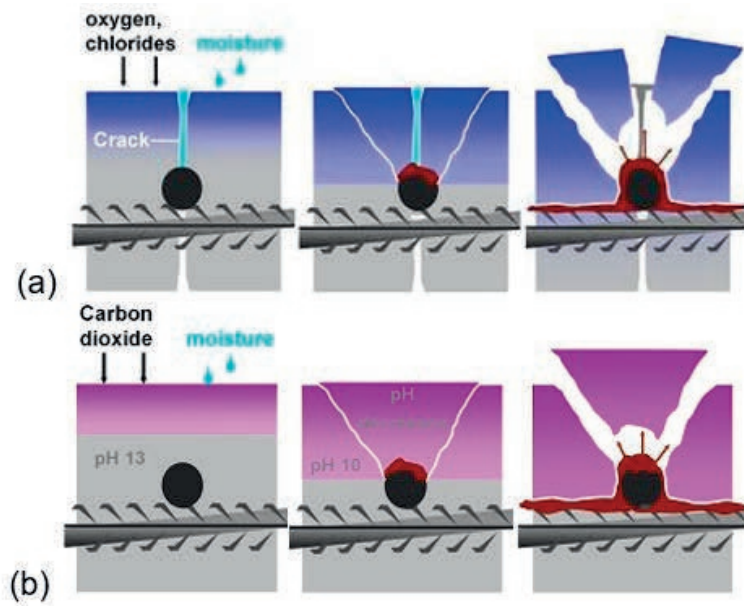
Figure 2.4: (a) Chloride Penetration (b) Carbonation Process [8].

2.3 Vibration Based bridge Structural Health Monitoring

A vibration based Structural Health Monitoring (SHM) system for bridges refers to the extraction of the basic dynamic properties such as: the modal parameters, natural frequencies, damping ratio and mode shapes. These are inherent properties of the structure, only related to mass distribution, stiffness and boundary conditions. Variations in these properties can be an indication of changes in the inherent properties of structure, by which structural damage can be detected [9–11]. Therefore, modal parameters often serve as indicators in damage identification techniques. Structural health monitoring (SHM) schemes are commonly classified based on their capability [12]. Typically, a level I SHM scheme has the capability to determine if damage is present in a structure. A level II scheme can identify damage and determine its location. A level III scheme is capable of identifying damage determining its location, and estimating the severity of the damage. Lastly, a level IV scheme has the capability of identifying damage, determining its location, estimating the severity of the damage
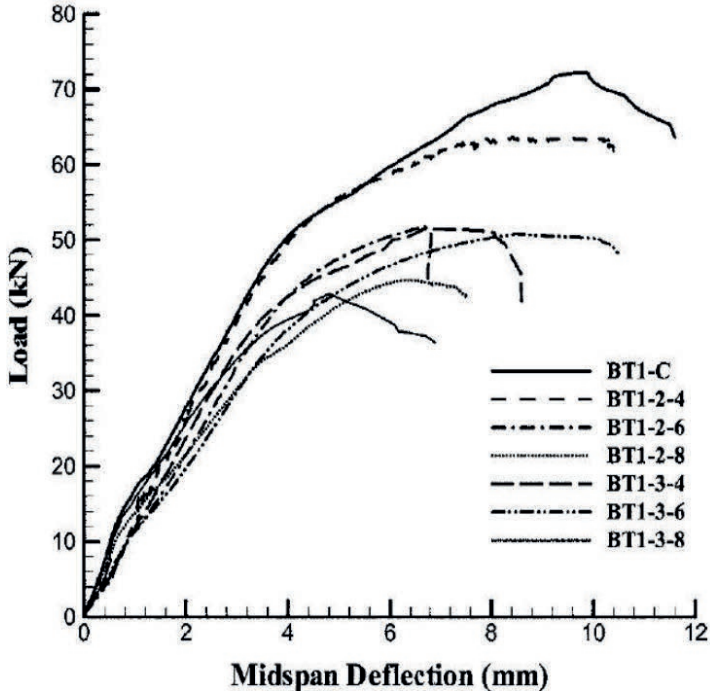
Figure 2.5: Mid-span deflection versus bridge load for uncorroded (BT1-C) and corroded rebars [8].

and predicting the durability of the structure. A level I SHM system is considered as global health monitoring system. However, to achieve the higher level SHM system, a local health monitoring system is required.

2.3.1   Instrumentation and Measurements

In bridge health monitoring concepts, instrumentation is considered as both measurements and data acquisition. Measurements can be classified in four categories; deformation and displacement measurements, load measurements, dynamic measurements, electrochemical and environmental measurements [13, 14]. The next step after finding the related failure mechanisms is the selection of appropriate transducers. The selection of the sensors for long term monitoring should be based on their durability,

cost, installation limitation and power requirement [14]. A variety of sensors such as camera, optical fibres, electrochemical, laser Doppler, accelerometer, strain and relative displacement, temperature sensors and acoustic emissions sensors have been used for structural health monitoring [15]. However, accelerometers, strain gauges and displacement sensors are the most widely used among them [3, 16–22]. Accelerometers have been utilized in all above references. They are useful for measuring a wide range of frequencies. Strain gauges have been applied in various cases [18, 19] to monitor the traffic loads and implementing bridge weigh in motion. In some research articles [3, 21–23] strain gauges have been used to study the structural behaviour, to subsequently assess the condition of the structure. Displacement sensors are available in both contacting and non-contacting. The contacting type usually measures a relative displacement. Non-contacting sensors include camera, laser displacement sensors, global positioning systems and GPS [14, 15].

Accelerometers can measure over a wide range of frequencies and they are relatively easy to install and use. Accelerometers capture the more global response of the structure while a strain sensor captures the more localized behaviour [24]. Strictly taken, strain gauges measure the strains at the locations of the sensors and these data should reflect damage in the vicinity of the gauge.

2.3.2 Structural Assessment by Modal Analysis

A common method of assessing the structural integrity is by determining the dynamic response. Input-output methods or experimental modal analysis (EMA) involve applying a known input, such as a Dirac impulse load to the structure and measuring its output vibration response and to create a desired forcing function, devices such as impact hammers, shakers, or drop weights have been used [22, 25]. This method is impractical for large structures. In those cases, the well-defined input function is replaced either by an operational or by an environmental source: the output only or operational modal analysis (OMA) [26, 27].

In most cases, the nature of the ambient excitation can only be considered by statistical descriptions (for example wind loading, rain loading and traffic density based on the urbanization of region) or by assuming the excitation spectrum to be concentrated within a frequency range (for example. $2 - 4$ Hz for vehicular excitation of

bridges [12, 28]. If the loading spectrum is limited to a narrow band of frequencies, only a limited picture of the dynamics of the structure can be monitored.

The operational modal analysis (OMA) approaches are classified into frequency domain methods and time domain methods [26, 27]. Examples of frequency methods are Pick Peaking (PP) from the power spectral density [29], frequency domain decomposition (FDD) [30] and operational PolyMax method [31]. Examples of time domain methods, are auto regressive moving average (ARMA) [32], natural excitation method (NexT) [29, 33], the least square complex exponential (LSCE) [33] and the stochastic subspace identification (SSI) [27]. The Operational Modal Analysis is based on the following assumptions [34]:

- Linearity: the response of the system to a given combination of inputs is equal to the same combination of the corresponding outputs.

- Stationarity: the dynamic characteristics of the structure do not change over time, so that the coefficients of the differential equations governing the dynamic response of the structure are independent of time.

- Observability: the sensor layout has been properly designed to observe the modes of interest, avoiding, for instance, nodal points.

In general, the acceleration time histories resulting from the passage of trains are considered not to be a reliable means for obtaining the dynamic characteristics of the bridge itself, since the bridge-train system and the bridge itself have different modal parameters that both influence the measured dynamic response. This is due to the relatively high mass of the trains compared to the total mass of the system [35]. For this reason, system modal identification of bridges has been done in [35–37] based on the following types of recorded signals:

- Acceleration records during the passage of road traffic only

- Acceleration records immediately after the passage of trains

- Acceleration records of the ambient vibration.

Traffic-induced bridge vibration is considered as non-stationary vibration, due to the time-dependent mass distribution on the bridge of the traversing moving mass [38, 39].

Wavelet analysis and Empirical Mode Decompositions (EMD), as part of Hilbert-Huang Transform (HHT), are two widely researched time-series analysis methods applicable for non-stationary signal [40, 41]. Yet, the application of these types of methods on rail bridges is limited.

2.3.3 Recently Applied SHM Systems on Existing Bridges

The number of bridges being monitored is growing steadily. However, there is a significant difference between monitoring the dynamic behaviour of a bridge and effectively applying structural health monitoring. An overview of the monitoring systems used on a series of bridges is presented. A comparison is made between the type of sensors used, the algorithms implemented and the capabilities in terms of identifying the modal parameters of the bridge and of assessing the state or condition of the bridge. A distinction between identification and the ability to remove noise and operational effects is made for the model identification capabilities. The condition assessment is split in three levels: detection, localisation and state estimation. The results are summarised in table 2.1, details on the monitoring and monitored assets are discussed in the following paragraphs.

Japanese Bridge [42]: A simply supported through-type steel Warren truss bridge with 59.2 m length and 3.6 m width, designed for a single lane road bridge. The bridge vibration induced by a passing of a two-axle vehicle were measured by 8 accelerometers, but only the free vibration responses are taken into account for modal-parameter identification. Observations collected in the undamaged condition are treated as a reference dataset (or training dataset in the machine learning field). Candidate observation are compared with these reference data sets and can be either from a damaged or undamaged condition. If the candidate is identified as an outlier; it implies a damaged condition of the bridge. Field experiments with four artificial damage scenarios were applied sequentially: a half cut in a vertical tension member at the mid-span, a full cut in that member, a recovery of the cut member, and a full cut in a vertical tension member at the 5/8th-span. Both univariate (modal frequency, damping ratio, or modal assurance criteria value of a specific mode) and multivariate features (modal frequencies, damping ratios, or MAC values of a couple of modes) were examined. Various combinations of modal parameters identified by multivariate autoregressive (AR) time series models are considered as damage-sensitive features. Their main conclusions are

that the model frequencies and mode shapes of the bridge can be identified accurately and the damage can be identified, provided a proper damage sensitive feature selection procedure is followed.

I-40 USA Bridge [43]: A composite bridge with concrete deck supported by five steel girders. The bridge was 52.10 m long consisting of three spans (11.34 m, 27.28 m, 13.48 m). The bridge was instrumented with inexpensive geophones (passive-velocity sensors) to measure vertical vibrations of the bridge. The bridge was excited by dropping a 22.7 kg drop source (sandbag) from a height of one meter onto the bridge deck at a total of nine different locations. The bridge vibrations were recorded at a total of 120 measurement locations that were dived into five groups along bridge beams (girders). Three damage scenarios were induced in the girders such that the bridge girders was incrementally cut upward from the bottom flange, and the drop tests were repeated to obtain vibration data in damaged bridge conditions. A time series-based damage identification technique, autoregressive with exogenous input (ARX) models and sensor clustering, is evaluated using the measured and simulated bridge data. ARX models and sensor clustering damage identification techniques, both output-only methods, are employed. The authors propose a new damage sensitive feature, which corresponds to the ratio of the standard deviation of the prediction error in the damaged bridge condition to the standard deviation of the prediction error in the healthy bridge condition, to enhance identification of the induced damage to this highly indeterminate bridge. To identify damage, an outlier analysis method is employed. The implemented damage identification technique was reported to detect outliers for all three damage scenarios, induced in this bridge, which indicates that damage is successfully detected for all considered damage scenarios. However, localisation of the damage and an estimate of the severity of the damage proved to be impossible with this damage feature.

S101 Austria Bridge [44]: This bridge is a post-tensioned concrete highway bridge with a main span of 32 m, side spans of 12 m, and a width of 6.6 m. In an on-site test, ambient vibration data of the bridge was recorded through 15 triaxial accelerometers while different damage scenarios were introduced on the bridge. 14 sensors were place on one side, while one was placed on the opposite side, allowing for the identification of bending and torsion modes. The latter are assumed to be antisymmetric bending modes. Two artificial damage scenarios were induced to the bridge. Output-only methods combined with statistic techniques (covariance-driven and statistical subspace

iteration methods) were applied for the identification of the damage. The advantage of the method is, according to the authors, that no modal parameter extraction is necessary: the system response is compared implicitly and not only the first modes. This alleviates the requirement to extract modal parameters, as required in other methods. The results showed however, that the method was only successful for one of the damage cases – the more global damage. On the other hand, the method proves to be successful in the elimination of environmental effects.

The Infante D. Henrique Bridge [45]: is a highway bridge composed of two mutually interacting fundamental elements: a very rigid pre-stressed reinforced concrete box beam, supported by a very flexible reinforced concrete arch that spans 280 m. A total of 12 force balance accelerometers were installed inside the deck box girder. The measurement system was complemented with strain gauges, inclinometers and temperature sensors. Output-only techniques were employed for the modal parameter identification (FDD, SSI-COV and p-LSCF). The measurement lasted three years (2007-2010). Environmental and operational effects are removed from the identified natural frequencies using a regression model. An additional correction of the natural frequencies was applied to account, for, as the authors specify, unmeasured factors. The first twelve corrected natural frequencies of the bridge were used for the construction of a multivariable control chart. To test the ability of control chart to detect damage, several damage scenarios were simulated with a numerical model of the bridge previously tuned. Damage was simulated in a simplified form as a bending stiffness reduction of 10% over length of 5 m at selected regions along the bridge. This led to frequency variation in some modes of the order of 0.15%. These variations, quantified with the tuned numerical model, were applied to the experimental data collected after March 2009. The authors claim to that the points of the control chart are outside the control area after the introduction of the frequency shifts due to the simulated damage. Hence, they concluded that it is possible to automatically detect a small frequency variation in the bridge with the installed monitoring system. It should be note though that the frequency shift is due to a relative large damage.

US 30 Bridge [46]: A composite highway bridge made of reinforced concrete and steel beams. It used for field experiment to validate the transmissibility technique for local damage detection. The proposed algorithm for vibration-based measurements was

based on localizing sensors around failure–critical joints and on establishing transmissibility ratios. The methodology was tested on laboratory experiments, resulting in a successful damage detection, localisation and quantification. The preference of using the transmissibility rather than the frequency response function (FRF) is motivated by the fact that the FRF contains global information and may be less sensitive to local changes. Moreover, the FRF is more (negatively) affected by operational input forces. The transmissibility between sensor pairs provides local data and is deemed more useful for damage identification. Statistical methods are applied to determine whether a specific transmissibility is different from a baseline. The percentage of transmissibility ratios of all sensors around a failure critical joint that is significantly different from the baseline is used as a measure for the likelihood of damage of that joint. Field tests, under normal traffic loading, showed that damage warnings were issued correctly, but environmental effects caused a significant number of false alarms. Moreover, quantification of damage proved to be unsuccessful, which was also attributed to environmental effects.

Songtoujiang Bridge – China [47]: A four span pre-stressed concrete bridge located at the mountain in China. It is a continuous box girder bridge with a span arrangement of (60+2×100+60) m. The width of the bridge deck is approximately 12.5 m, with two railway lines. In total 3 accelerometers were used for a multi-setups test with 2 reference nodes and 47 roving measurement points. All measurement points were placed at the centre of the bridge deck. Three output-only methods were used: Peak-Picking, SSI-COV and improved EMD based modal identification. The latter either used random decrement based techniques or SSI-COV to extract the modal parameters from the Intrinsic Mode Functions. The main argument for using EMD is that it can handle nonstationary situations better than the other techniques. No significant changes in performance of the three techniques in terms of modal parameter extraction are reported.

Nanjing Yangtze Bridge – China [24]: The bridge consists of three units of three-span continuous steel truss and a simply-supported steel truss. Each unit of three-span continuous steel truss has a span of 160 m and the simply supported steel truss has a span length of 128 m. The width of the bridge is 14 m which carries both highway and railway traffic. The monitoring system comprises a total of approximately 150 sensors, including accelerometers, strain gauges, displacement transducers, temperature sensors,

weight-in-motion sensors, anemometers and seismographs. A total of 30 accelerometers are installed in the middle section of all ten spans. The acceleration response by railway traffic is prominent due to its heavy loading. A distinction between train induced, road traffic induced and ambient induced responses is made, based on the vibration amplitude. EMD is used to identify the modal frequencies and damping ratios for the first three modes in all three situations. The authors state that no differences in modal parameters were found for the three cases. Hence, neither traffic nor trains affect the modal properties of the bridge.

Brazil – Bridge [36]: The bridge has total length of 2310 m and a width of 19.40 m. The structure system consists of pre-stressed concrete deck slabs, carrying the rail and road traffic, on top of steel girders. The study was carried out in the central part of the bridge which consists of two 44 m long spans and one 77 m long central span, which is partially supported by a steel arch. In total, 32 low frequency piezoelectric accelerometers were installed. The positions were determined based on the results of a numerical model and taking accessibility into account. The dynamic tests were performed for cases of ambient excitation due to wind, river current and operational excitation due to passage of loaded and unloaded trains, as well as road traffic. The nonstationary effects during passage of a train turned out to be too significant to reliably extract the modal parameters from the bridge. Note that the nonstationary effects stem from the fact the train mass is not negligible compared to that of the bridge. Hence a bridge-train system is formed, which dynamic characteristics differ from that of the bridge alone. For this reason the modal identification was performed by using the acceleration records during the passage of road traffic and the acceleration records immediately after the passage of loaded trains. The output-only methods "Stochastic Subspace identification – unweighted main component" (SSI-UPC, a time domain method) and "Enhanced Free Domain Decomposition" (EFDD, a frequency domain method) were used. Limited differences between the methods were found, be it that the SSI method performed slightly better. The main contribution of this study is that it revealed the importance of the vibration amplitude and length of the time record on the accuracy of the identification of the dynamic characteristics of structures.

Jalon Bridge – Spain [37]: A six-span girder railway bridge for high-speed trains at Spain. In order to determine the dynamic characteristics of the bridge, a vibration measurement campaign was performed on 18 and 19 September 2011. Acceleration

Figure 2.6: Aerial view of the Boyne Viaduct superstructure

were measured under both ambient (wind) and trains passages (free vibration only). 12 GeoSIG wireless sensors were used for the measurements. In total 303 nodes were measured in 3 orthogonal directions. The measurements were performed in 38 different setups. There were four reference nodes common to all setups, which were measured by sensors at fixed locations where the modes of interest are well present. The system identification is performed by using the reference-based covariance-driven stochastic subspace identification algorithms (SSI-COV). Limited differences were found between the ambient vibration-based analyses and those based on the free vibration, be it that the modes are more real valued in the first case, indicating a higher phase collinearity. A higher phase collinearity is beneficial for the extraction of mode shapes.

2.4   The Boyne viaduct

The Boyne viaduct, the central case study in this research, was constructed in the early 1930s and consists of fifteen semi-circular masonry arch spans and three simply supported steel-girder spans. This assessment only considered the central steel-girder span. Figure 2.6 shows a view of the steel superstructure of the Boyne viaduct.

The central span is approximately 81m and consists of a truss with 10 bays. The top chord has a curved profile and the maximum distance from the bottom chord to the top chord is approximately 10.6m. The bridge is supported on 4 bearings at each end.

Table 2.1: Case Studies on Structural Health Monitoring of Bridges

Case study	Type of bridge	Excitation	Sensors	Method(s)	System Identification	Remove operational effect	Damage detection
D. Henrique bridge	road bridge	road traffic	accelerometer, strain gauge, inclinometer, temperature	OMA, p-LSCF, SSI-COV, FDD	successful	successful	successful- numerical study
Milau Viaduct	road bridge	ambient vibration	seismograph, accelerometer, GPS	OMA, p-LSCF, SSI-COV	successful	NA	NA
US 30 bridge	road bridge	road traffic	accelerometer (uniaxial)	Transmissibility ratio	NA	NA	successful
Japanese Bridge	road bridge	vehicle induced, free vibration	accelerometer	modal parameters	successful	NA	NA
I-40 bridge	Road bridge	drop weight	accelerometer	Autoregressive with exogenous, ARX & NA	successful - numerical study		NA
S-101 Bridge	Road bridge	Ambient vibration	Accelerometer (triaxial)	output-only response analysis	successful	NA	NA
Songtoujiang bridge	rail bridge	ambient vibration	SSI-COV and EMD-based output-only modal analysis	successful	NA	NA	NA
Nanjing Yangtze	rail and road bridge	ambient, road and rail traffice	Accelerometer, strain gauges, displacement and temperature	EMD-based out-put only modal analysis	successful	NA	NA
Z-24 bridge	road bridge	road traffic	accelerometer	ARMA modelled, RD + SSI / WT / HHT	successful	NA	successful
Brazil bridge	composite bridge	ambient, road traffic	accelerometer	Stochastic Subspace identification	successful	NA	NA
Jalon bridge	steel	ambient and free vibration	Accelerometer	Sstochastic subspace identification	successful	NA	NA

Figure 2.7: Scaffolding on the Boyne Viaduct

Figure 2.8: Localised corrosion (a) and heavy pitting (b) on the Boyne Viaduct

The ballasted track is supported on timber sleepers which transfer the load through a steel deck plate to the two main longitudinal 'rail bearer' beams. The rail bearers span between cross beams which are located every 8.1m at the nodes of the bottom chord of the truss. Bracing is provided at the top of the structure as shown in Figure 2.6.

At the beginning of the DESTinationRAIL project, scaffolding was in place throughout the structure (Figure 2.7), including beneath the deck, allowing safe access to the structure. This was put in place in order to perform patch repairs and painting. The majority of the patch repairs were done to the end-spans. It is for this reason that only the central span was analysed.

Although the structure was deemed to be in good condition, there was some evidence of corrosion to the structure, as shown in Figure 2.8.

2.5   Concluding remarks

The main points that can be concluded from the review in this chapter are:

- Corrosion is a dominant failure mechanism in steel bridges, manifesting in different forms such as general corrosion, pitting corrosion, galvanic corrosion, crevice corrosion, and stress corrosion. This gradual corrosion process results in material loss and diminished section parameters, weakening the structural elements, and ultimately compromising the bridge's stiffness.

- The primary cause of deterioration in concrete bridge structures is the corrosion of reinforcing steel and other embedded metals.

- Existing Structural Health Monitoring (SHM) systems employed on real bridges have predominantly focused on identifying the global dynamic characteristics of the structures, with a primary emphasis on resonance frequencies.

- Current Structural Health Monitoring (SHM) systems excel at capturing the dynamic characteristics of structures. The future of SHM lies in its potential to move beyond characterizing dynamic behavior and toward the effective detection and assessment of structural damage.

Bibliography

[1] T. Tinga and R. loendersloot, "Aligning phm, shm and cbm by understanding the physical system failure behaviour," in *European Conference of the Prognostic and Health Management Society.*

[2] D. Imhof, *Risk Assessment of Existing Bridge Structures.* PhD thesis, University of Cambridge, 2004.

[3] O. Caglayan, K. Ozakgul, and O. Tezer, "Assessment of existing steel railway bridges," *Journal of Constructional Steel Research*, vol. 69, no. 1, pp. 54–63, 2012.

[4] G. Hearn, R. L. Purvis, P. Thompson, W. H. Bushman, K. K. McGhee, and J. Wallace T. McKeel, "Bridge maintenance and management, a look to the future," *TRB 81st Annual Meeting: A3C06: Structures Maintenance and Management*, pp. 1–7.

[5] S.-K. Lee, "Current state of bridge deterioration in the u.s.-part 2," *Materials Selection & Design*, vol. 51, no. 2, 2012.

[6] J. R. Kayser and A. S. Nowak, "Capacity loss due to corrosion in steel-girder bridges," *Structural Engineering International*, vol. 115, no. 6, 1988.

[7] M. S. A. Badran, *Structural Reliability analysis of Corroded Steel Girder Bridge.* Master Thesis, University of Nebraska-Lincoln, 2013.

[8] W. Zhu, *Effect of corrosion on the mechanical properties of the corroded reinforcement and the residula structural performance of the corrosded beams.* Thesis, 2014.

[9] W. Fan and P. Z. Qiao, "Vibration-based damage identification methods: A review and comparative study," *Structural Health Monitoring-an International Journal*, vol. 10, no. 1, pp. 83–111, 2011.

[10] P. C. Chang, A. Flatau, and S. C. Liu, "Review paper: Health monitoring of civil infrastructure," *Structural Health Monitoring*, vol. 2, no. 3, pp. 257–267, 2016.

[11] E. P. Carden and P. Fanning, "Vibration based condition monitoring: A review," *Structural Health Monitoring*, vol. 3, no. 4, pp. 355–377, 2016.

[12] A. P. Ojeda, *MATLAB Implementation of an Operational Modal Analysis Technique for Vibration-Based Structural Health Monitoring.* Master of science, 2012.

[13] K. Bergmeister and U. Santa, "Global monitoring concept for bridges," in *Nondestructive Evaluation of Highways, Utilities, and Pipelines IV*, vol. 3995, pp. 14–25.

[14] R. S. Yongtao Dong, *Bridges Structural Health Monitoring and Deterioration Detection - Synthesis of Knowledge and Technology.* Thesis, 2010.

[15] I. González, *Study and Application of Modern Bridge Monitoring Techniques.* Licentiate thesis, comprehensive summary, 2011.

[16] M. Enckell, *Lessons Learned in Structural Health Monitoring of Bridges Using Advanced Sensor Technology.* Thesis, 2011.

[17] K. Przemysław, S. Jacek, S. Krzysztof, w. Andrzej, M. Krzysztof, and G. Piotr, "Structural health monitoring of a railway truss bridge using vibration-based and ultrasonic methods," *Smart Materials and Structures*, vol. 20, no. 3, p. 035016, 2011.

[18] R. Karoumi, J. Wiberg, and A. Liljencrantz, "Monitoring traffic loads and dynamic effects using an instrumented railway bridge," *Engineering Structures*, vol. 27, no. 12, pp. 1813–1819, 2005.

[19] A. Liljencrantz, R. Karoumi, and P. Olofsson, "Implementing bridge weigh-in-motion for railway traffic," *Computers & Structures*, vol. 85, no. 1–2, pp. 80–88, 2007.

[20] D. Inaudi, "Overview of 40 Bridge Structural Health Monitoring Projects ," *Proceedings of International Bridge Conference*, 2009.

[21] J. Wiberg, *Railway bridge response to passing trains : Measurements and FE model updating.* Doctoral thesis, KTH Royal Institute of Technology, 2009.

[22] J. Rodrigues, "Dynamic performance of a steel truss bridge under railway traffic," *Proceedings of Imac-Xx: Structural Dynamics Vols I and Ii*, vol. 4753, pp. 14–20, 2002.

[23] B. J. A. Costa and J. A. Figueiras, "Evaluation of a strain monitoring system for existing steel railway bridges," *Journal of Constructional Steel Research*, vol. 72, pp. 179–191, 2012.

[24] X. H. He, X. G. Hua, Z. Q. Chen, and F. L. Huang, "Emd-based random decrement technique for modal parameter identification of an existing railway bridge," *Engineering Structures*, vol. 33, no. 4, pp. 1348–1356, 2011.

[25] J. Zwolski and J. Bien, "Modal analysis of bridge structures by means of forced vibration tests / tilto konstrukciju modaline analize taikant priverstines vibracijos testus," *Journal of Civil Engineering and Management*, vol. 17, no. 4, pp. 590–599, 2011.

[26] S. A. Schanke, *Operational Modal Analysis of Large Bridges*. Master thesis, Norwegian University of Science and Technology, NTNU, 2015.

[27] L. Zhang and R. Brincker, "An overview of operational modal analysis: Major development and issues," in *International Operational Modal Analysis Conference*, pp. 179–190.

[28] V. G. R. Patel S G, "Ambient vibration testing of bridges - state of the art," *International Journal of Advances in Engineering & Technology*, 2015.

[29] G. James, T. Carne, J. Lauffer, and A. Nord, "Modal testing using natural excitation," in *Proceedings of the 10th International Modal Analysis Conference*, vol. 2.

[30] R. Brincker, L. M. Zhang, and P. Andersen, "Modal identification of output-only systems using frequency domain decomposition," *Smart Materials & Structures*, vol. 10, no. 3, pp. 441–445, 2001.

[31] B. Peeters and G. De Roeck, "One-year monitoring of the z24-bridge: environmental effects versus damage events," *Earthquake Engineering & Structural Dynamics*, vol. 30, no. 2, pp. 149–171, 2001.

[32] P. Andersen, R. Brincker, and P. H. Kirkegaard, "Identification of civil engineering structures using vector arma models,"

[33] D. Brown, R. Allemang, Zimmerman, R., and M. Mergeay, "Parameter estimation techniques for modal analysis," in *7th International Seminar on Modal Analysis*.

[34] C. Rainieri and G. Fabbrocino, *Operational Modal Analysis of Civil Engineering Structures*. 2014.

[35] M. Cardoso, R. A. C. Sampaio, R. M. d. Souza, and E. Silva, "Operational modal analysis of road-rail bridge," in *MATEC*, EDP Sciences, 2015.

[36] L. He, S. Qin, T.-T. Bui, E. Reynders, M. Cuadrado, P. Museros, and G. De Roeck, "Operational modal analysis of a high-speed railway bridge: the jalon viaduct," in *ISMA*.

[37] V. Zabel and J. Gössinger, *Dynamics of Civil Structures*, vol. 4. 2014.

[38] M. D. Spiridonakos and S. D. Fassois, "Fs–tarma models for non–stationary vibration analysis: An overview and comparison," in *15th IFAC Symposium on System Identification*.

[39] A. G. Poulimenos and S. D. Fassois, "Parametric time-domain methods for non-stationary random vibration modelling and analysis — a critical survey and comparison," *Mechanical Systems and Signal Processing*, vol. 20, no. 4, pp. 763–816, 2006.

[40] J. Meredith, A. Gonzalez, and D. Hester, "Empirical mode decomposition of the acceleration response of a prismatic beam subject to a moving load to identify multiple damage locations," *Shock and Vibration*, vol. 19, no. 5, pp. 845–856, 2012.

[41] M. B. P. Scott W. Doebling, Charles R. Farrar, "A summary review of vibration-based damage identification methods," *The Shock and Vibration Digest*, 1998.

[42] K.-C. Chang and C.-W. Kim, "Modal-parameter identification and vibration-based damage detection of a damaged steel truss bridge," *Elsevier*, 2016.

[43] R. V. Farahani and D. Penumadu, "Damage identification of a full-scale five-girder bridge using time-series analysis of vibration data," *Engineering Structures*, vol. 115, pp. 129–139, 2016.

[44] M. Döhler, F. Hille, L. Mevel, and W. Rücker, "Structural health monitoring with statistical methods during progressive damage test of s101 bridge," *Elsevier*, 2014.

[45] A. Cunha, E. Caetano, F. Magalhães, and C. Moutinho, "Recent perspectives in dynamic testing and monitoring of bridges," *Structural Control and Health Monitoring*, vol. 20, no. 6, pp. 853–877, 2013.

[46] S. Rahmatallah, C. Schallhorn, and G. Swadi, "Integration of bridge damage detection concepts and components, volume ii: Acceleration-based damage detection," report, 2013.

[47] S. Q. Qin, Q. P. Wang, and J. T. Kang, "Output-only modal analysis based on improved empirical mode decomposition method," *Advances in Materials Science and Engineering*, vol. 2015, pp. 1–12, 2015.

[48] L. Connolly, L. Prendergast, N. Mostafa, and R. Loendersloot, "Report on assessment of bridges," report, 2017.

3

Extracting the time-dependent resonances of a vehicle-bridge interacting system by wavelet synchrosqueezed transform[1]

Abstract

The dynamic response of a Vehicle-Bridge Interaction (VBI) system is a noisy, non-stationary and, multi-component response with closely spaced spectral components. Considering the ultimate goal as utilizing the VBI system instantaneous frequencies (IFs) for bridge condition monitoring, this paper carries out a systematic study to investigate the performance of four advanced time-frequency analysis techniques on a series of VBI responses: Hilbert-Huang transformation (HHT), Continuous Wavelet Transformation (CWT), Robust Local Mean Decomposition (Robust-LMD) and Wavelet Synchrosqueezed Transform (WSST). The novel contribution of this study is the application of the two latter techniques. The synthesized tests demonstrate that the WSST is the best method to precisely separate and localize in time the closely spaced resonances. Therefore, the WSST is applied to field measurements obtained from the Boyne viaduct in Ireland, as well. The results verify the capacity of this method to

---

deal with time-varying vibrations adequately.

3.1   Introduction

Structural Health Monitoring (SHM) is a growing technology that can be used for condition assessment and developing an efficient maintenance strategy [1]. Dynamic properties of a system such as modal frequencies, modal damping and mode shapes are key elements towards the application of SHM and damage detection techniques on structures, amongst which bridges [2]. Among the various dynamic properties, eigen-frequencies can provide a simple high-level condition assessment using only a limited number of sensors, while mode shapes and their derivatives are more noise sensitive and require a higher sensor density [3].

In order to study the frequency content of the dynamic response of a bridge, as excited by a moving train, the characteristic of the signal should be investigated. The full vibration response of a typical bridge, induced by a moving train contains: 1) The Entrance Phase response, which corresponds to the time period before the train actually enters the bridge; 2) The Traverse Phase response, which corresponds to the time period when a train is either partly or completely on the bridge, and 3) The Leaving Phase response, which is the bridge vibration when the train has left the bridge. Measuring the Entrance Phase response enables to measure the true start of the Traverse Phase signal, i.e. when the train enters the bridge. However, the detailed dynamic analysis of the Entrance Phase is not included in the current study, as it does not provide additional insights. The Leaving Phase is a free decay response and represents a stationary process, whereas the Traverse Phase is a non-stationary process due to the time-dependent mass distribution of the train on the bridge. The Traverse Phase represents the response of a coupled system of both bridge and train which is also known as a Vehicle-Bridge Interaction (VBI) response. Since the Traverse Phase response is characterized by non-stationarity, time-frequency techniques are required to extract the time-dependent system resonances or Instantaneous Frequencies (IFs).

The common input-output modal analysis is developed for linear time-invariant sys-tem and is not a proper tool for a time-variant system [4]. There is a vast literature on the output-only identification of a time-varying systems [5]. Dziedziech et al [6] developed an algorithm for modal identification of time varying systems excited by a

series of random impacts by applying a wavelet-based Frequency Response Function (FRF) where the excitation signal must be measured. He et al [7] proposed a mass-normalized mode shape identification method to enrich the mode shape resolution for bridge structures by using a parked vehicle on the bridge under environmental excitation. Lin et al [8] identified the modal frequencies of a short-span concrete bridge before and after bridge deck widening by applying Frequency domain decomposition techniques to the bridge under a blocked traffic condition. Spiridonakos et al [9] proposed a method to consider the problem of parametric output-only identification of a time-varying structures based on autoregressive moving average technique to capture the varying frequencies of a laboratory scaled bridge-like structure. The proposed method was applied to the random vibration response to capture the varying frequency. Staszewski et al. [4] proposed a time-variant FRF based on applying the continuous wavelet transform to the random vibration response of a sprung mass system as well as the same laboratory setup as presented in [9] to capture the varying frequency. The majority of the developed techniques are applicable when the excitation is random vibration that can be considered as white noise. Moreover, the developed techniques are aimed at identification of general time-varying systems, while it is known that a VBI response contains closely-spaced spectral components due to the vehicle-bridge dynamic coupling. This feature distinguishes the VBI system from the common time-variant systems. Therefore, the literature review in further limited to the application of the techniques on the VBI system response and field measurement.

In recent years, signal processing techniques have been widely used to analyze VBI responses in different research fields. The basic idea of the time-frequency analysis of a bridge vibration is to devise a joint time-frequency distribution function that describes the energy density of a signal in both the time and the frequency domain [10]. The Hilbert-Huang Transform (HHT), as the combination of the Empirical Mode Decomposition (EMD) and Hilbert Transform (HT), and Continuous Wavelet Transform (CWT) have been widely used for the condition assessment of bridges in many research studies. Many different versions of these methods, have been proposed, each optimized for specific applications. In this work, the intention is not to optimize the parameters, but use the default settings of the Matlab built-in functions as the benchmark for each technique in this study.

The conventional technique to identify the modal parameters of a bridge is using the bridge free vibration or the Leaving Phase response. Modal frequencies of Tsing Ma railway bridge in China identified by the spectral analysis of the bridge acceleration [11]. HHT and CWT have been applied on the free vibration response of bridges despite the fact that this response is a stationary process. The modal frequencies of Donghai bridge in China were identified by applying a wavelet-based technique on the bridge free vibration. Yan et al. [12] performed a comparative study of modal parameters obtained from applying FFT, HHT and CWT to the ambient vibration response of the Z24-bridge. CWT and HHT were applied to the bridge free decay to perform output-only modal analysis. The well-separated bridge modal frequencies were successfully identified by applying both techniques. Similarly, He et al. [13] applied an EMD-based Random Decrement (RD) technique on the ambient vibration of the NYR steel truss bridge in China while Sayed et al. [14] applied CWT on the acceleration response of the Kaya bridge in the Seoul-Busan railway induced by a high speed train. Both were able to extract the modal parameters from the free vibration response of the bridge. Unlike these cases, the free vibration response of the Xining Beichuan bridge in China contained closely-spaced modes [15]. The proposed EMD-based stochastic subspace identification technique was used to identify the bridge modal parameters using the ambient excitations measured before the opening of the bridge to traffic. Specified intermittency frequencies were used for each mode while EMD was used to avoid mode-mixing. It can be concluded that for a bridge structure with closely-spaced frequency components, EMD is confronted with the mode-mixing issue and for the free vibration of a bridge with well-separated spectral components both techniques, CWT and HHT, can perform successfully. Apart from the mode-mixing, there are further limitations to perform SHM based on the bridge free vibration response only. Firstly, the identified natural frequencies from the free vibration responses are dependent on the variable environmental conditions such as temperature [16]. Secondly, the extracted modal parameters using the free vibrations are actually global features which may not be sensitive to damage as a local event [17]. Therefore, investigation of the Traverse Phase response is proposed since the changes in the dynamic properties of the bridge structure due to damage are believed to be amplified by the presence of a moving vehicle on the bridge. The focus of the current study is therefore finding an accurate method to

extract the time-variant frequencies of the structure by exploiting the Traverse Phase response as it has the potential to improve the existing condition monitoring techniques.

The Traverse Phase signal is a broad spectrum, noisy, non-stationary and multi-component response of a vehicle-track-bridge interacting system. Generally, the vehicle frequencies are distributed in the low frequency range, 1-10 Hz [18] and it is also known that the first two bending frequencies of a bridge structure are usually in the same frequency range. Therefore, the low frequency part of a Traverse Phase response is of great interest for the current study. It is worth to mention that CWT and HHT have been widely used on the Traverse Phase response for damage detection and finding singularities, which do not exist in a healthy bridge and only appear in the response of the damaged structure [19–25]. However, those singularities, abrupt changes or signal discontinuities typically appear in a higher frequency range (i.e. well above 100 Hz) whereas, a low frequency (i.e. below 10 Hz) is the target frequency range in this paper, since for the majority of the railways VBI systems the fundamental frequency of the bridge as well as the vehicle frequencies are distributed in the target low frequency range.

There are few studies on extracting the modal frequencies of a VBI system from a simulated Traverse Phase response. Nguyen [26] identified the bridge IF from the mid-span displacement response of a simulated VBI system with well separated modes. Li et al. [27] modelled a moving vehicle on a simply supported beam and obtained the fundamental frequency of the bridge numerically by a step-wise solution of the eigenvalue problem at each step of numerical integration rather than from a time-frequency analysis of the bridge dynamic response. The same approach was used on a modelled bridge [28] to calculate the bridge relative frequency change (RFC) while a vehicle is moving. Roveri et al. [29] simulated the mid-span displacement of a simply supported Euler-Bernoulli beam subjected to a moving constant point load, so effectively neglecting the vehicle dynamics, and the first IF of the beam was extracted by applying HHT. Yan et al. [12], next to extracting the modal parameters of the Z24-bridge using the Leaving Phase, also performed a comparative study on extracting the modal parameters of a modelled bridge using the Traverse Phase by applying HHT and CWT. EMD was not successful to separate the close spectral components of the simulated signal and Chebyshev filters were applied to overcome the mode-mixing issue. The modified Morlet wavelet function was used for the same simulated signal and the

close modes were presented in a blurred time-frequency representation due to the low frequency resolution.

As an experimental study, Marchesiello et al [30] applied CWT and short-time stochastic subspace identification (ST-SSI) on the acceleration response of a scaled bridge-like structure under a moving train without any suspension systems. The bridge time-dependent resonance was successfully extracted with both techniques.

Considering the field measurements, the acceleration response of the Kaya bridge showed that the bridge resonance frequencies were mixed with other frequency components [14]. Cantero et al. [31] applied the Wavelet transform in combination with the modified Littlewood-Paley method on the response of the Skidtrask bridge in Sweden. The proposed method was not successful in identifying the bridge resonance from the Traverse Phase response and they concluded that the dynamic interaction between the vehicle and the bridge is complex and highly dependent on the mechanical properties of the suspension systems and the distribution of the masses within the vehicle.

In the following, the contributions of the current study are presented to fulfill the research gaps. Firstly, a number of studies were conducted on a modelled bridge mid-span displacement response. However, an accurate assessment of a bridge displacement induced by external action may be currently challenging and costly [1]. Moreover, the bridge acceleration signal is more sensitive to damage than the deflection signal [21]. Thus, the current study aims for the time-frequency analysis of the bridge acceleration response. Secondly, in the majority of the studies, only the IF corresponding to the bridge first resonance has been investigated. Either the vehicle dynamics were not included at all or the time-dependent resonance originating from the vehicle dynamics was not investigated, which Cantero et al [31] showed to be of significant importance. Therefore, the second aim of this study is to include the vehicle dynamics in the analysis of the VBI system. To fulfill the research gap, the two methods commonly used in literature, CWT and HHT are complemented with two recently developed methods, Robust Local Mean Decomposition (Robust-LMD) [32, 33] and Wavelet Synchrosqueezed Transform (WSST) [34] are considered. The performance of these methods to extract the time-variant resonances of the coupled system are assessed by applying them to a series of simulated Traverse Phase responses. Robust-LMD is investigated as it is reported by Wang et al. [35] to outperform EMD, while WSST is considered because it is reported to overcome some limitations such as mode-mixing and blurred

time-frequency representations [36, 37]. The major contribution of this study is the application of Robust-LMD and WSST on the non-stationary response of the coupled vehicle-bridge system with closely spaced spectral frequencies. A verification with the field acceleration measurements of the Boyne viaduct in Ireland is performed by using WSST method.

The outline of this study is as follows. Section 2 presents a brief introduction of the aforementioned time-frequency analysis techniques. The vehicle-bridge numerical model is presented in Section 3. Various numerical test cases will be presented in Section 4. Results of and discussions associated with each technique are elaborated in Section 5. Section 6 presents the application of WSST to the field measurement of Boyne viaduct, Ireland. Finally, Section 7 forwards the conclusions.

3.2 Time-frequency analysis techniques

3.2.1 Hilbert-Huang Transform

The definition and application of the instantaneous frequency have been studied elaborately by Huang et al [38–40]. There is consensus that the instantaneous frequency of a non-stationary response of a system only has a physical meaning when the signal is a mono-component frequency signal. Therefore, EMD aims for decomposing a multi-component signal into a series of mono-component frequency signals (IMFs). Subsequently, the HT aims for extracting the IF of each of the IMFs and capturing the variation of these frequency components in time. Therefore, the prerequisite of being mono-component must hold to link the physics of the system to the extracted IF.

3.2.2 Robust Local Mean Decomposition

Smith [32] developed local mean decomposition (LMD) in 2005 after which it was further optimized by Liu et al [33] referring to it as Robust-LMD. It has been reported in literature that Robust-LMD outperforms EMD [35] regarding decomposing non-stationary signals into a set of mono-component signals. The LMD algorithm progressively separates a frequency modulated (FM) signal $s(t)$ from an amplitude modulated (AM) envelope signal $a(t)$. This separation is obtained in three steps; 1) calculate the local mean, $m_{ij}(t)$ and the local magnitude, $a_{ij}(t)$, where the i denotes the number of the Product Function (PF) and j denotes the number of the iteration. 2) compute

the smooth $m_{ij}(t)$ and $a_{ij}(t)$. 3) calculate the frequency modulated signal $s_{ij}(t)$, the estimated zero-mean signal, $h_{ij}(t)$ and the estimated envelope signal, $a_{ij}(t)$. For PF_i, this process continues for p iterations until a purely frequency modulated signal, s_i is obtained. The corresponding envelope signal, $a_i(t)$ is given by:

$$a_i(t) \prod_{j=1}^{p} a_{1j}(t) \tag{3.1}$$

The obtained purely FM signal can be written as:

$$s_i(t) = \cos \theta_i(t) \tag{3.2}$$

where $\theta(t)$ is the instantaneous phase and the instantaneous frequency is defined by Equation (4.2). Multiplying $s_i(t)$ by the corresponding envelope function, $a_i(t)$, provides PF_i. Similar to the EMD procedure, PF_i from the time signal results in a new time signal and the whole process is repeated until the residual time signal $r(t)$ contains no oscillation anymore. Then after m iterations, the original signal can be represented by:

$$x(t) = \sum_{i=1}^{m} PF_i(t) + r(t) \tag{3.3}$$

It has been mentioned that each PF is a mono-component AM-FM signal and that the instantaneous frequency can reveal the time varying frequency components [32]. In the present study Robust-LMD is applied to VBI to investigate to what extent it outperforms EMD.

3.2.3 Continuous Wavelet Transform

Sadowsky [41] introduced continuous wavelet transform (CWT) as a tool for signal processing. A comprehensive and detailed mathematical description is provided in [42]. The basics are briefly explained here.

The definition of CWT is [42]:

$$W_x(a,b) = \int x(t) a^{-1/2} \psi \left(\frac{t-a}{b} \right) \tag{3.4}$$

where a and b are the translation and the scale variables respectively and $x(t)$ is the time signal. The natural sampling of the scale variable is dyadic, i.e. logarithmic to the

base 2. The function ψ is called the 'mother' wavelet. The basic idea of the CWT is similar to the short time Fourier transform (STFT). The signal is windowed in time and subsequently a Fourier frequency decomposition is performed on the windowed signal as the window slides along the time axis [42]. In STFT the width of the time window is constant, while the width of the time window of a wavelet function is variable and is adapted to its frequency. At low frequencies, the wavelets have better frequency resolution and at high frequencies they have better time resolution. The wavelets perform better than STFT in case of a non-stationary signal since wavelet functions are irregular, of limited duration and often non-symmetrical [43]. The performance of the wavelet approach depends on the selection of a mother wavelet, which is potentially inconvenient as the optimal choice is unknown a priori, and some wavelets may work better than others in capturing specific types of damage [24]. To extract the instantaneous frequency, it has been recommended in [36] to use 'bump' as the mother function because it is band-limited and performs well for frequency localization. Therefore, in the current study,'bump' is used as the mother function.

3.2.4 The Wavelet Synchrosqueezing Transform

The continuous Wavelet transforms the one-dimensional time signal $x(t)$ into a two-dimensional quantity, $W(a,b)$, see equation Equation (4.1). $W(a,b)$ is spread out over a region around a on the time-scale which provides a somewhat blurred time-frequency picture [44]. The synchrosqueezing procedure aims to sharpen the resulting time-scale picture of CWT. During the time-frequency analysis of audio signals for speaker identification, Daubechies et al. [44] have observed that, despite $W(a,b)$ is smeared out in a (scale), the oscillatory behaviour of the signal at time b shows the original frequency ω, regardless of the magnitude of a.

In summary, WSST [34] has three steps. The first step is calculating the continuous wavelet transform of a time signal, $x(t)$ by Equation (4.1). The second step is calculating the instantaneous frequency by:

$$\omega_x(a,b) = \frac{\frac{\partial W_x(a,b)}{\partial b}}{2\pi i W_x(a,b)} \tag{3.5}$$

where the frequency variable ω_x and the scale variable a are binned and computed only at discrete values a_k, with $a_k - a_{k-1} = (\Delta a)_k$. The last step is to re-assign the scale

variable a to the frequency variable ω by calculating the Synchrosqueezed transform, T_x as:

$$T_x(\omega_l, b) = (\Delta\omega)^{-1}\sum_{a_k} W(a_k, b)a_k^{-3/2}(\Delta a)_k \tag{3.6}$$

The transform function $T_x(\omega_l, b)$ is determined over time, only at the centers ω_l of the successive bins $[\omega_l - \frac{1}{2}\Delta\omega, \omega_l + \frac{1}{2}\Delta\omega]$, with $\Delta\omega = \omega_l - \omega_{l-1}$.

Daubechies et al. [34] developed WSST as an empirical mode decomposition-like tool because it provides an adaptive time-frequency decomposition, which is also the goal of EMD. It has been claimed that WSST overcomes some limitations such as mode-mixing [36, 37], which is the reason to apply this method on the test cases of the current study.

3.3   Numerical model

An extended version of a simply supported beam in 2D space is used in the current study to numerically simulate the Traverse Phase (the response of a coupled system) and the Leaving Phase (the response of the bridge only, without the vehicle). In the current model, entrance and leaving sections have been added to the bridge(beam) to allow for generating the bridge vibration response corresponding to the Entrance and the Leaving Phase. The entrance and the leaving sections are modelled by beam elements that are fully constrained at all their nodes, as schematically shown in Figure 3.1. The added parts are connected to the bridge at the bridge supports by linking displacement degrees of freedom, while the rotational degree of freedom is left unlinked.

The dynamic response of an elastic system carrying a moving elastic subsystem has no steady state solution [45]. The mass slides through a node-to-surface inter-action with a hard contact model where no friction is considered. The simulation is performed in ABAQUS and the applied analysis scheme is the Newmark implicit time
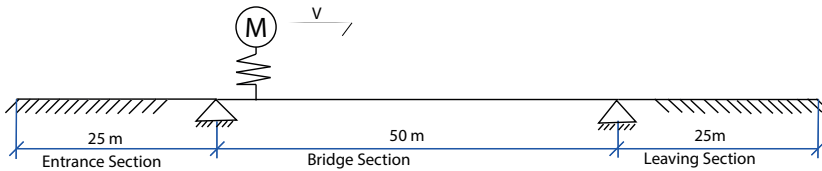
Figure 3.1: Schematic representation of the numerical model

integration method with a fixed time increment of $0.001\,\mathrm{s}$ which provided sufficient numerical stability and accuracy, and frequency resolution. Three dynamic analysis steps are implemented, corresponding to the mass approaching, crossing and leaving the bridge. The entrance part is not strictly necessary. The dimensions and material properties of the bridge model (Table 3.1) are selected such that they are representative for the case study of the current study, Boyne viaduct (see Figure 3.20). The first two fundamental frequencies of the bridge model obtained by Abaqus are 2.33 and 9.2 Hz. These frequencies match well with the analytical solution and the first two frequencies of the Boyne bridge, i.e. 2.9 Hz and 9.2 Hz (see Section 3.5). The bridge is modelled with 200 Euler-Bernoulli beam elements. A sprung-mass system slides with a speed of $5\,\mathrm{m/s}$ over the bridge. The mass of the vehicle is constant for the all test cases and is 20% of the bridge mass. The mass ratio is inspired by the mass ratio between a loco-motive and the Boyne bridge. The stiffness of the vehicle spring is selected such that the frequency of the vehicle oscillation (3 Hz), is close to the fundamental frequency of the bridge (2.3 Hz).

Table 3.1: Properties of the bridge model

Length	Cross section area	Young's modulus	Density	mass
$50\,\mathrm{m}$	$1.25\,\mathrm{m}^2$	$210\,\mathrm{GPa}$	$7860\,\mathrm{kg/m}^3$	$314.4\,\mathrm{ton}$

Modal analysis simulations are carried out on the coupled system (vehicle-bridge), by moving the vehicle every 5 m. This step-wise analyses are performed to create a trivial relationship between the resonances of the VBI system and the actual vehicle positions as is displayed in Figure 3.2. Figure 3.2 displays the two resonances of the system along a virtual time axis. The step-wise relocating of the vehicle can be con-sidered as a quasi-static moving. Therefore, the time is equal to the displacement of the vehicle divided by the its velocity, since the velocity of the vehicle is assumed to be constant along the bridge. It takes 10s for the vehicle to pass the bridge with a speed of $5\,\mathrm{m/s}$. In this way the first two resonances of the vehicle-bridge interacting system are reconstructed by doing modal analysis. Figure 3.2 shows that when the vehicle is on the bridge supports, the resonances are the same as those of the bridge (2.3 Hz) and vehicle (3 Hz). When the vehicle is located somewhere between the supports, the res-onances of the system vary with the vehicle location. For all cases, the first resonance is close to the bridge fundamental frequency and the second one is close to the vehicle

Table 3.2: The first two resonance frequencies $F_{R,i}$ of the vehicle-bridge coupled system corresponding to different vehicle parking locations

	Relative vehicle position.										
	0	0.1	0.2	0.3	0.4	0.5	0.6	0.7	0.8	0.9	1
$F_{R,1}$ [Hz]	2.33	2.23	2.06	1.93	1.85	1.82	1.85	1.93	2.06	2.23	2.33
$F_{R,2}$ [Hz]	3.00	3.09	3.30	3.54	3.74	3.82	3.74	3.54	3.30	3.09	3.00
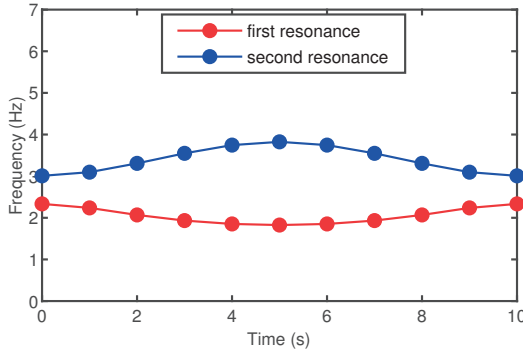
Figure 3.2: The first two resonance frequencies of the coupled system while the vehicle is located at 11 diffrent locations on the bridge

frequency. The result of the step-wise modal analysis creates an underlying behaviour which would be expected to observe once the signal processing will extract the IFs of the coupled system.

3.4   Results and discussion

This section presents the results in two main parts. First, the simulated signals corresponding to the test cases are presented and then the application of the time-frequency techniques on the simulated signals are presented. Each of the four methods is applied to the first test case and if the results are satisfactory, it proceeds to the next test case which is more complex. The performance of each method is discussed for each test case it is applied to.

To investigate the performance of the time-frequency analysis techniques three test cases have been designed. The bridge structure is subjected to:

1. a moving unsprung mass

2. a moving sprung mass

3. a moving sprung mass in a noisy environment

The goal is to investigate the proficiency of each method, 1) in detecting and separating the frequency components of the coupled system, and 2) in localizing each frequency component in time.

The vehicle for the first test case is a mass moving along the bridge while in the second test case the vehicle is represented by a mass-spring system. The last test case aims to study the performance of the methods in a noisy environment by adding white noise to the result of the second case. As stated in Section 3.1 mode-mixing occurs due to closely spaced frequency components [37, 46]. Thus, to elaborate on that, in the second test case, the spring constant is tuned with a stiffness of 22.35 MN/m to have a frequency close to the fundamental frequency of the bridge (3 Hz vs 2.3 Hz, see Table 3.2).

3.4.1 Simulated acceleration response of the test cases

Test case 1

Figure 3.3a displays the simulated bridge full vibration response due to the moving single point mass. The Entrance Phase is not included in the results. The signal in the first 10 seconds corresponds to the Traverse Phase response when the mass is moving on the bridge and the last 10 seconds corresponds to the Leaving Phase response, when the mass has left the bridge. A comparison between the Traverse Phase and the Leaving Phase reveals that firstly: the Traverse Phase is a non-stationary signal, since the wave length changes with time, while the Leaving Phase signal represents a stationary process; secondly: the Traverse Phase contains numerical noise which appears as small spikes in the response, whereas the Leaving Phase is perfectly smooth.

Figures 3.3b and 3.3c show the power spectral density of the bridge forced and free vibration responses respectively. The Traverse Phase contains a first resonance around 2 Hz, the second resonance of the bridge of 9 Hz and another frequency component around 20 Hz. It worth reminding that the acceleration signal has been calculated at the bridge mid-span due to which the second resonance of the bridge (9 Hz) is captured with a very low vibration amplitude. The last frequency component (20 Hz) is an
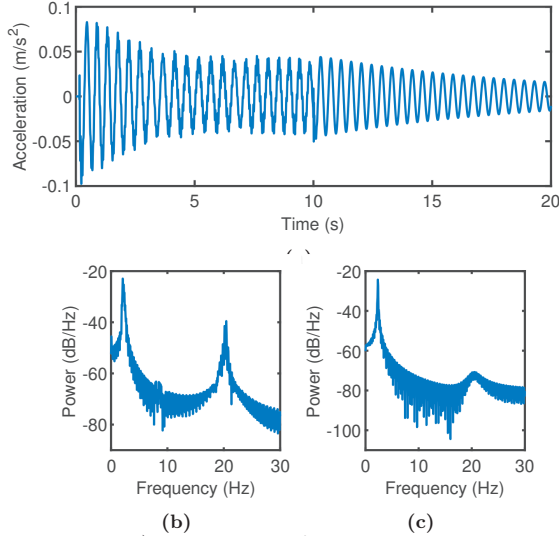
Figure 3.3: Test case 1: a) Full response of the bridge including the Traverse Phase (0-10s) and the Leaving Phase (10-20s) response, b) the power spectral density of the Traverse Phase response and c) the power spectral density of the Leaving Phase response.

artificial effect of the numerical simulation referred to as the *driving frequency*. This corresponds to the inverse of the time taken by the mass for passing a numerical grid [47], in this case equal to the speed ($5\,\text{m/s}$) divided by the numerical grid size ($0.25\,\text{m}$).

Test case 2

In this test case, the sprung mass has its own dynamics. Therefore, the bridge forced vibration signal contains the vehicle-bridge dynamic interactions. The Traverse Phase response and its power spectral density are presented in Figure 3.4a and Figure 3.4b. Figure 3.4a shows less distortion in the response due to the presence of a spring and the more moderate contact force in comparison with the case represented by Figure 3.3a which is reflected by the lower amplitude of the driving frequency. Figure 3.4b shows three peak frequencies: 1) the first resonance of the coupled system around $2\,\text{Hz}$, 2) the second resonance of the system around the sprung mass frequency $3\,\text{Hz}$ (see Table 3.2); and 3) the driving frequency around $20\,\text{Hz}$.

<div align="center">(a)</div> <div align="center">(b)</div>
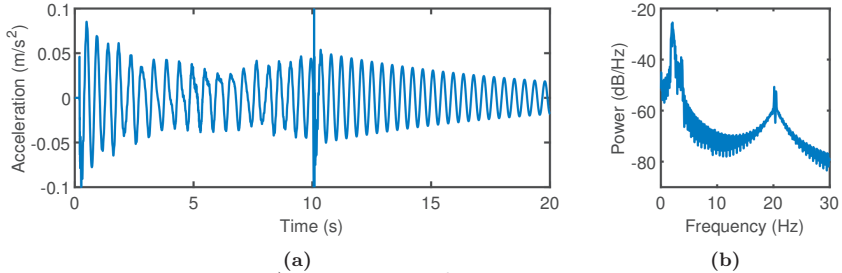
Figure 3.4: Test case 2: a) Full response of the bridge including the Traverse Phase (0-10s) and the Leaving Phase (10-20s) response. b) The power spectral density of the Traverse Phase response.

Test case 3

In this test case, white noise is added to the bridge response of the second test case. Gaussian white noise with a zero mean and a signal-to-noise ratio (SNR) of 10 dB is generated by the build-in Matlab function *awgn* and is added to the Traverse Phase signal. The noise is Gaussian in nature as its amplitude can be modeled with a normal probability distribution. The chosen SNR of 10 dB corresponds to the noise level of the field measurements of the Boyne bridge (see Section 3.6). Figure 3.5a shows the Traverse Phase signal including the white noise, while the power spectral density of the Travres Phase response is again shown in Figure 3.5b. In the following subsection, the four analysis methods will be applied to these three test cases and the results will be discussed.

<div align="center">(a)</div> <div align="center">(b)</div>
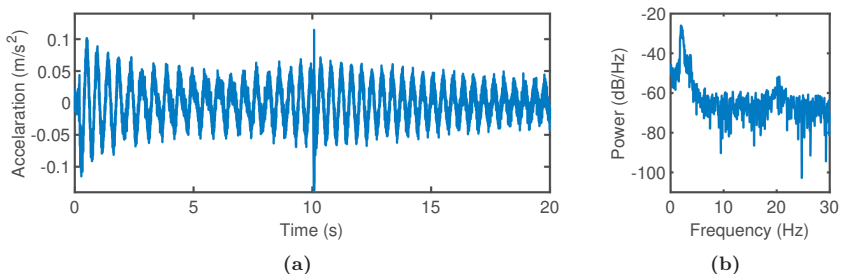
Figure 3.5: Test case 3: a) Full response of the bridge including the Traverse Phase (0-10s) and the Leaving Phase (10-20s) response. b) The power spectral density of the Traverse Phase.

3.4.2   Hilbert-Huang transform

Test case 1- unsprung mass

EMD decomposes the Traverse Phase response into six IMFs. The first two contain the relevant frequencies of the system, the bridge and the driving frequency, and the remaining four contain spurious modes with a frequency between 0-2 Hz. The first two IMFs and their frequency content are plotted in Figure 3.6a and Figure 3.6b.

(a)   (b)
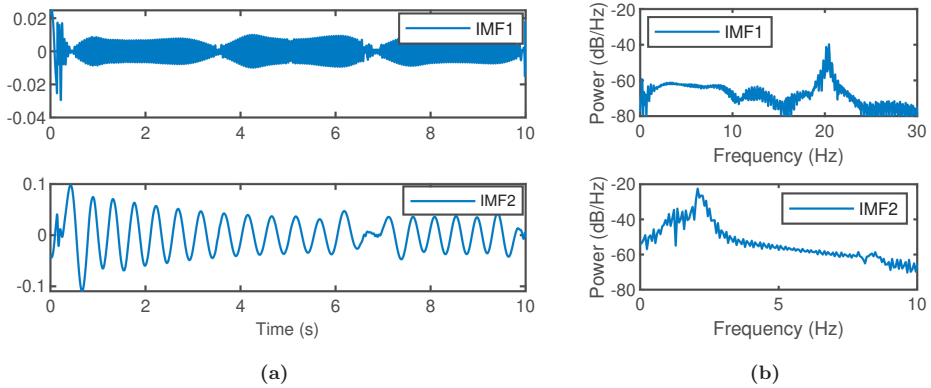
Figure 3.6: For test case 1: a) IMF1 and IMF2 obtained by applying EMD to the Traverse Phase response and, b) the frequency content of IMF1 and IMF2.

As expected, it can be seen that the first IMF carries the high frequency component (20 Hz) and the second IMF carries the low frequency component (2 Hz). Moreover, Figure 3.6b shows that IMF2 is a mono-component signal since the frequency plot contains a single dominant frequency peak. Therefore, the bridge instantaneous frequency (IF) can be extracted by applying the Hilbert Transform to IMF2. Figure 3.7 shows the instantaneous frequency (IF) plot resulting from the Hilbert transform. It reveals how the resonance frequency of the bridge changes during the passage of the mass. There are two important observations: firstly, it can be seen that the beginning and the end part of the IF are disrupted due to the signal edge effect. Secondly, the IF shows a waviness which is known as the intra-wave frequency modulation [38].

It can be concluded that for a system without closely spaced frequency components EMD adequately works when there is no noise and subsequently no mode-mixing. Furthermore, if the IMF is a mono-component signal, HHT can reveal the general
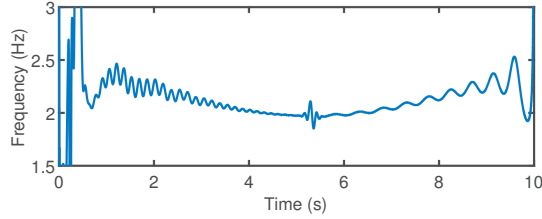
Figure 3.7: The IF of test case 1 obtained by applying the HT to IMF2

trend of the time-varying IF but due to the intra-wave modulations it cannot provide a precise time sequence of the IF.

Test case 2- sprung mass

EMD decomposes the Traverse Phase signal of the second test case into 6 IMFs. The first two IMFs and the associated frequency contents are shown in Figure 3.8a and Figure 3.8b respectively.

(a)　　　　(b)
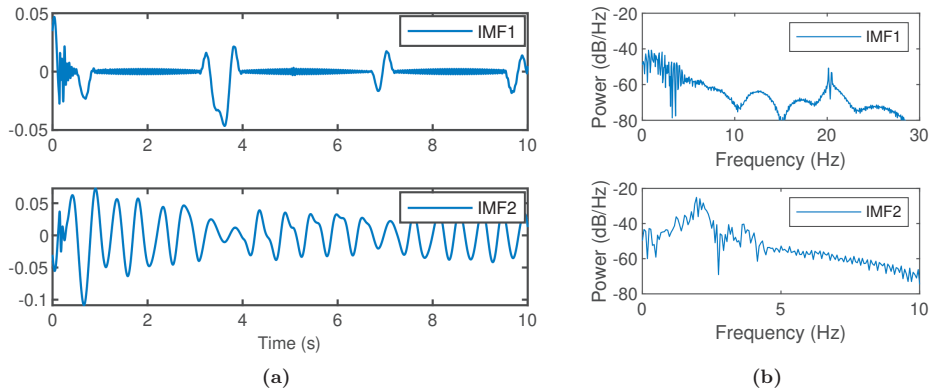
Figure 3.8: For test case 2: a) IMF1 and IMF2 obtained by applying EMD to the Traverse Phase response and, b) the frequency content of IMF1 and IMF2

It can be seen in Figure 3.8b that IMF1 carries two frequency components, the first component is around $2\,\text{Hz}$ and the second component is around $20\,\text{Hz}$. Moreover, Figure 3.8b for IMF2 shows two frequency peaks. The first peak is around the bridge frequency ($2\,\text{Hz}$) and the second one is around the vehicle frequency ($3\,\text{Hz}$). The two

main observations are: 1) the bridge resonance appears in two IMFs (IMF1 and IMF2), and 2) the bridge and the vehicle resonances, are mixed and both appear in IMF2. Both phenomena are known in literature as mode-mixing [48]. When mode-mixing occurs for a system resonance, the IMFs are not mono-component signals and as a result, the IF of the system resonances cannot be extracted by the Hilbert transform. The presence of either closely spaced frequency components or noise has been reported as the main cause of mode-mixing [49].

Rilling and Flandrini [50] extensively investigated the performance of EMD to decompose a signal which is composed of two closely spaced frequencies by means of experimental studies. They used the most general form for a discrete time two tone signal as:

$$x[n] = a_1 \cos(2\pi f_1 n + \psi_1) + a_2 \cos(2\pi f_2 n + \psi_2) \tag{3.7}$$

Their results revealed that the performance of EMD to separate a two-tone signal depends on the frequency and the amplitude ratio of its components. However, decomposing the bridge Traverse Phase response is even more complex. The amplitude of the vehicle response measured i.e. at the bridge mid-span while it is moving on the bridge is time-dependent. The contribution of the vehicle dynamics increases as the vehicle approaches the mid-span location and decreases again as it moves away. The largest contribution of the vehicle, as can be observed in Figure 3.4a, appears around 5 seconds as a noisy part. The time-dependent amplitude ratio can disrupt the extrema identification during the sifting process, which makes that the two resonances are mixed and cannot be extracted as two separate IMFs by the EMD method. As EMD is not capable of detecting the individual frequencies in the second test case, it will not be applied anymore to the even more complex test case 3.

3.4.3 Robust-Local Mean Decomposition

Test case 1- unsprung mass

Robust-LMD decomposes the Traverse Phase response of the first test case into five Product Functions (PFs) and the associated frequency modulated (FM) and amplitude modulated (AM) signals. Similar to EMD, the first two PFs contain the relevant frequencies of the system (the bridge and the driving frequency) and the remaining 4 contain spurious modes with a frequency between 0-2 Hz. Figure 3.9a shows PF1

and PF2 which should be examined for being a mono-component signal. Figure 3.9b presents the frequency content of PF1 and PF2. It can be seen that unlike PF2 which has one peak frequency, PF1 contains two frequency components. The bridge resonance (around 2 Hz) appeared in both PFs which means that mode-mixing has occurred.

(a)   (b)
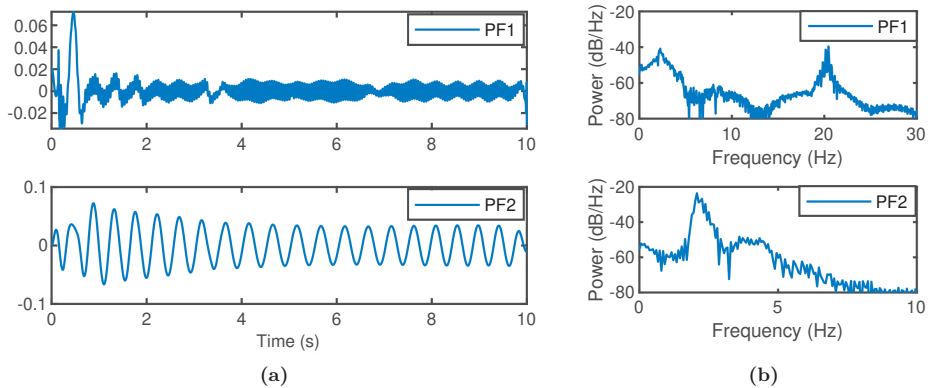
Figure 3.9: For test case 1: a) PF1 and PF2 obtained by applying Robust-LMD to the Traverse Phase response and b) the frequency content of PF1 and PF2.

Test Case 2- sprung mass

Robust-LMD is applied to the Traverse Phase response of the second test case. The first two PFs and their associated frequency spectral components are presented in Figures 3.10a and 3.10b. It can be seen in Figure 3.10b that the three frequency components of the system appeared in the first PF. Therefore, the first PF is not a mono-component signal. Moreover, it can be seen that the bridge frequency, a peak around 2Hz, appeared in both PFs. This observation proves that Robust-LMD is not able to decompose the Traverse Phase response of the second test case.

Wang et al. [35] performed a comparative study on the application of LMD and EMD to rotating machinery health diagnosis and concluded that LMD outperforms EMD. However, for the current study EMD outperforms LMD, since LMD encountered the mode-mixing even for test case 1. The Matlab code for the Robust-LMD function used for the current study is published in [33]. Possibly satisfactory results could be obtained if the parameters of the Robust-LMD algorithm are tuned differently.
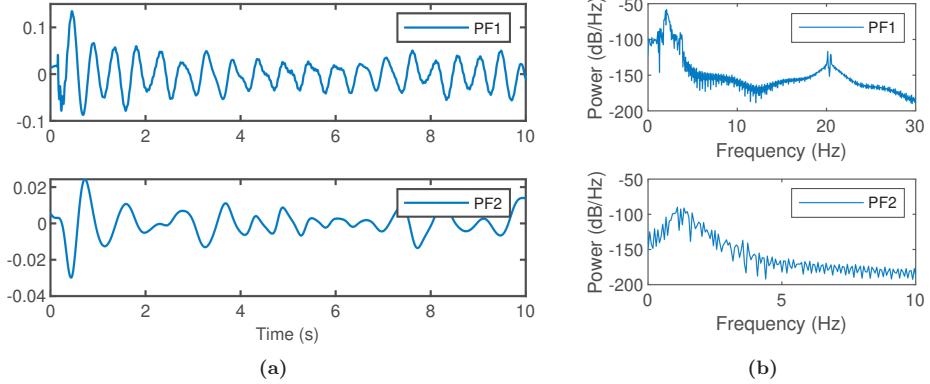
Figure 3.10: For test case 2: a) PF1 and PF2 obtained by applying Robust-LMD to the Traverse Phase response and b) the frequency content of PF1 and PF2.

Due to the lack of a sufficient body of research for application of LMD to structures, the cause(s) of failure cannot be further investigated and it is beyond the scope of the current work. However, it can be concluded that Robust-LMD is not a desirable technique since its performance depends on finding the proper parameters for a specific applied signal and the system dynamics.

3.4.4   Continuous Wavelet Transform

Test Case 1-unsprung mass

The previous subsections demonstrated that extracting the IF by applying HHT and Robust-LMD includes two steps: 1) decompose a composite signal into a series of the mono-component signals, and 2) extract the IF of mono-components. Unlike HHT and Robust-LMD, CWT is a process of decomposing a composite signal into a weighted sum of a series of base functions localized in both time and frequency [51]. The CWT of a composite non-stationary signal therefore shows how the energy is spread in frequency and time.

Figure 3.11b shows the CWT of the first test case. It can be observed that the frequency is plotted on a logarithmic scale. Moreover,the gray region outside the dashed white line shows where signal edge effects become significant. It is worth to remind that the edge effect has already been observed in Figure 3.7 for EMD. Furthermore,

Figure 3.11b shows the first resonance of the system around 2 Hz and It can be seen that the bridge resonance is presented as a blurred frequency ridge as indicated by the colored horizontal bands in the spectrum. In general, the high frequency wavelets are very narrow while the low ones are much broader [42]. Therefore, the frequency of a broad wavelet is spread out over a band of frequencies due to the low time resolution [44]. To illustrate this behaviour, the distribution of the energy (magnitude of the wavelet coefficients) over the frequency at the time instant 5 s is plotted in Figure 3.11a. The magnitudes of the different frequencies are shown with markers so this can slightly be seen as the frequency spectrum at 5 s, which is also represented by the color (intensities) in Figure 3.11b. The bridge frequency ridge is extracted by picking the peak frequency at each time instant. However, the blurred time-frequency representation can disrupt the peak picking process and may cause misinterpretation of the signal. Figure 3.11c shows a decent result, but it is not satisfactory for the purpose of IF determination because of the low time resolution.

Figure 3.11: For test case 1: a) The frequency content of the Traverse Phase at time instant 5 s obtained by CWT, b) the time-frequency representation obtained by CWT and c) the IF as a time-frequency ridge.

Test Case 2- sprung mass

Figure 3.12b displays the CWT of the second test case. The bridge and the vehicle resonances are successfully detected even though they are rather closely spaced. Again, it can be seen in Figure 3.12b that CWT provides a blurred time-frequency representation. Figure 3.12a displays the spread of the energy over the frequencies at 5 s where the two frequency peaks are associated to the bridge and the vehicle resonance respectively. The frequency ridges are extracted as explained for the previous test case and are presented in Figure 3.12c. Firstly, the scattered data are from the gray zone due to the signal edge effects. Secondly, the overall trends of the two ridges match the virtual IF constructed by the modal analysis (see Figure 3.2). Once the vehicle reaches the bridge mid-span, the first and the second resonance of the system reach 1.8 Hz and 3.8 Hz which exactly match with the first two resonances of the system obtained by the modal analysis as reported in Table 3.2. CWT works for this test case as well. However, the low time resolution and blurred peaks (see the distribution of the frequency components as the adjacent circles around peak values in Figure 3.12a) remain as a valid intrinsic issue while using CWT to extract the low time-dependent resonances of a system. Therefore, CWT will not be applied to the noisy Traverse Phase. As it mentioned earlier, the ultimate goal of extracting the bridge IF is to capture local events such as damage. Therefore, finding a time-frequency technique which provides a higher time resolution is still demanded.

3.4.5 Synchrosqueezed Wavelet Transform

Test Case 1- unsprung mass

The Synchrosqueezed transform aims to reduce the energy smearing that is observed with CWT and at the same time preserves the time resolution [44]. The time-frequency representation of the Traverse Phase response of the first test case is shown in Figure 3.13b. Firstly, the vertical axis shows a linear frequency scale as defined by the linear scale discretization of ω in Equation (4.3). The linear frequency scale provides a higher frequency resolution for low frequency components in comparison with CWT. Secondly, Figure 3.13b shows a sharp frequency ridge. The sharp frequency ridge illustrates that WSST reduces the energy smearing as is aimed for. Figure 3.13a presents the distribution of the energy over the frequency at the time instant 5 s, similar to

Figure 3.12: For test case 2: a) The frequency content of the Traverse Phase at time instant 5 s obtained by CWT, b) the time-frequency representation obtained by CWT and c) the IFs as the time-frequency ridges.

Figure 3.11a for CWT. It can be seen that unlike CWT, WSST shows a single and sharp peak frequency around the bridge resonance. Moreover, it can be seen that the markers in Figure 3.13a are dense unlike Figure 3.11a. This provides higher frequency resolution of WSST. Finally, the moving mass introduces a time-varying inertia and stiffness [52] and subsequently causes a time-varying resonance of the system which is clearly visible in Figure 3.13b and Figure 3.13c.

Figure 3.13: For test case 1: a) The frequency content of the Traverse Phase at time instant 5 s obtained by WSST, b) the time-frequency representation obtained by WSST and c) the IF as time-frequency ridge.

Test Case 2- sprung mass

WSST has been applied to the second case and Figure 3.15a is the time-frequency representation of the bridge Traverse Phase response of the second test case. It can be seen that there are two time-varying frequency components. The first frequency component starts at 2.3 Hz (the natural frequency of the bridge). The IF reaches the minimum value (1.8 Hz) when the vehicle is at mid-span. And then, the IF returns to a value of 2.3 Hz (bridge natural frequency) when the vehicle is at the end of the bridge.

(a)

(b)

(c)

Figure 3.14: For test case 2: a) The frequency content of the Traverse Phase at time instant 5 s obtained by WSST, b) the time-frequency representation obtained by WSST and c) the IF as time-frequency ridge.
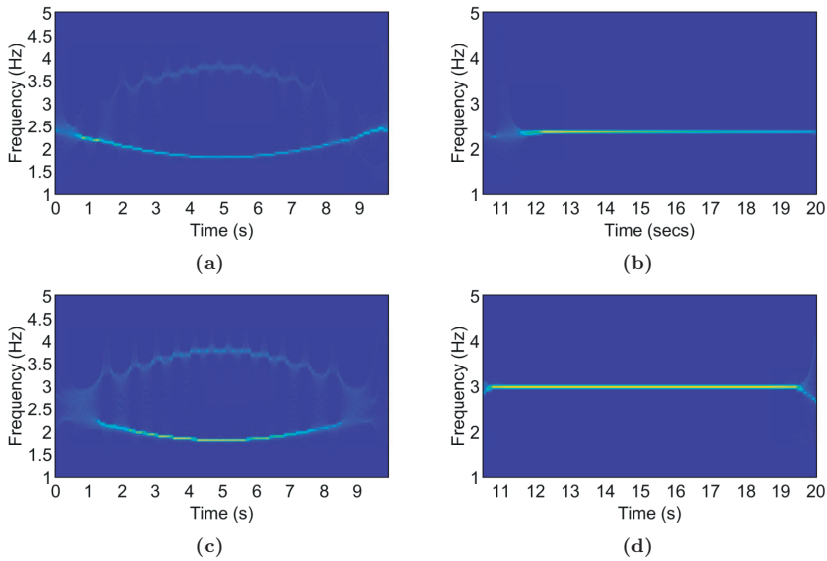
Figure 3.15: For test case 2 the time-frequency representations are obtained by applying WSST on: a) the Traverse Phase response calculated at the bridge mid-span, b) the Leaving phase response calculated at the bridge mid-span, c) the Traverse Phase response calculated at the moving vehicle, d) the Leaving phase response calculated at the moving vehicle

The second frequency component coming from the vehicle dynamics is not clear enough in the time-frequency representation of Figure 3.15a around the edge of the signal. Therefore the WSST has also been applied to the VBI response of the coupled system calculated at the moving vehicle. Figure 3.15c shows that the second frequency ridge starts from 3 Hz (the vehicle frequency) when the vehicle is at the beginning of the bridge, it increases to 3.8 Hz when the vehicle arrives at mid-span and again decreases to 3 Hz when it reaches the end of the bridge. Furthermore, Figure 3.15b and Figure 3.15d show the dynamic properties of the two individual systems, i.e. the bridge and the vehicle because they refer to the Leaving Phase response, in which the two do not interact anymore. When the individual systems are coupled and interact dynamically, the dynamic properties of the coupled system are changing, as shown in Figure 3.15a and Figure 3.15c.

The objective of the study was to find a technique which provides the IF of the system precisely. The result of the modal analysis reported in Table 3.2 and Figure 3.2 is used as th benchmark to verify and compare the results obtained by WSST. Figure 3.16 shows the IFs of the second test case extracted by WSST as the thick lines and the first two eigenfrequencies of the coupled system obtained by the modal analysis as the circles. It can be seen that apart from the edge of the signal, the IFs match well with the benchmark results.
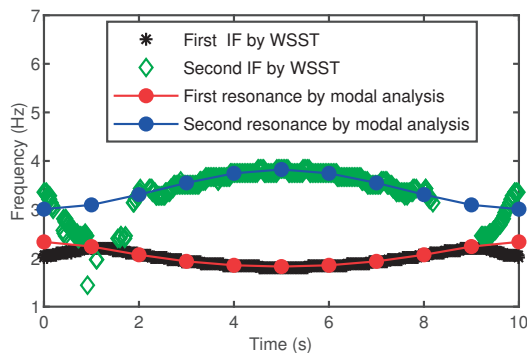
Figure 3.16: The IF of the coupled system obtained by WSST compared to the frequencies obtained with modal analysis

Test Case 3- sprung mass with noise

The performance of the WSST for the noisy signal is investigated in this test case. The SNR is 10 (see Figure 3.17b) and the result of applying the WSST is presented in Figure 3.17c. Figure 3.17a in comparison with Figure 3.14a shows that the added noise has mainly affected the driving frequency peak which is reflected by its lower amplitude for test case 3, whereas the bridge resonance frequency is not affected by the noise. Figure 3.17c shows that the IFs are not affected by added noise.
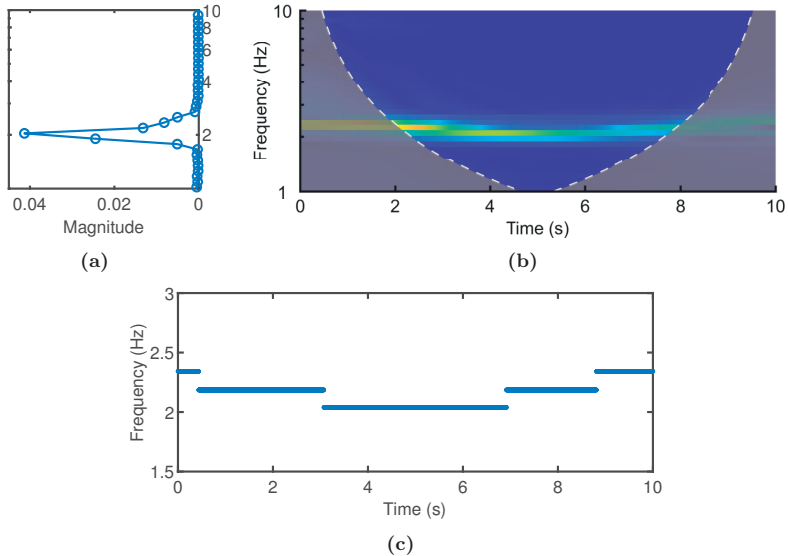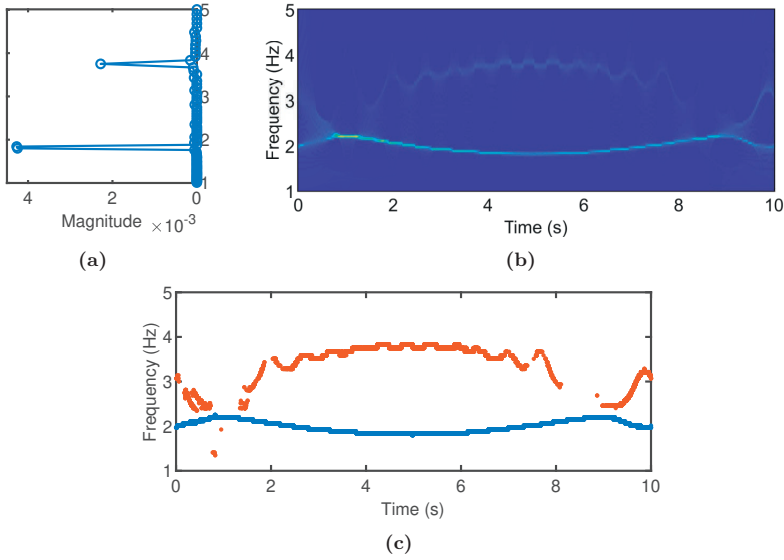

Figure 3.17: For test case 3: a) The frequency content of the Traverse Phase at time instant 5 s obtained by WSST, b) the time-frequency representation obtained by WSST and c) the IF as time-frequency ridge.

3.4.6   Concluding remarks of the numerical investigation

The IF of the first test case extracted by CWT and WSST are shown in Section 3.4.6 as the blue and the red dots respectively. As presented in Equation (4.2), to calculate the instantaneous frequency, $\omega_x(a, b)$, the wavelet transform, $W_x(a, b)$ appears in the denominator. Therefore, CWT and WSST represent the frequency in logarithmic and exponential scales respectively. To provide consistency and reproducibility of the
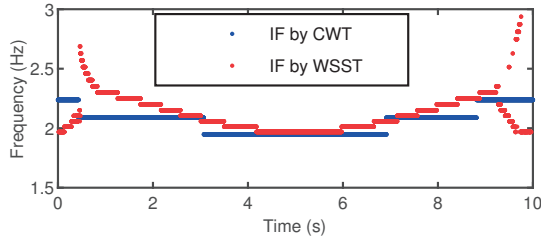
Figure 3.18: The IF of the first test case extracted by CWT and WSST

results, for both techniques Matlab functions with default settings are utilized. For a given signal, the frequency resolution depends on the number of samples, sampling frequency, time increment and the product of the number of voices per octave and the number of octaves. This product for the Travers Phase signal is equal to 100 for CWT and 384 for WSST. Therefore the frequency resolution of WSST is about 3.5 times higher than that obtained by CWT. It is worth mentioning that even if the frequency discretization for CWT increases, the blurry issue that arises from the spread of frequencies remains valid. To investigate this issue, the settings of the CWT function are modified to have a comparable frequency resolution for CWT and WSST for the test case 1. Figure 3.19 shows the results of applying the modified CWT. By comparing Figure 3.12a with Figure 3.19a it can be seen that by increasing the frequency discretization for CWT the energy distributes over more frequency components. Whereas, Figure 3.13a shows that for the same signal WSST squeezed the energy at the time instant 5 s in one frequency component. Thus, the blurry issue of CWT is due to the spread of energy over several frequencies instead of a single frequency component. This issue is intrinsic and will not be solved by increasing the frequency discretization.

An evaluation of the four investigated techniques is presented in Table 3.3. Firstly, EMD did not work for test case 2 due to the mode-mixing. Secondly, Robust-LMD did not work even for test case 1 due to the same issue. Finally, CWT and WSST are the two techniques which were able to capture the time-dependent resonances of the system. However, the accuracy of the obtained IFs are different. Therefore, it can be concluded that WSST is the only method which successfully analyses all the test cases. It can accurately capture the time-varying resonances of a noisy multi-component signal with closely spaced frequencies. The next section investigates whether WSST also properly
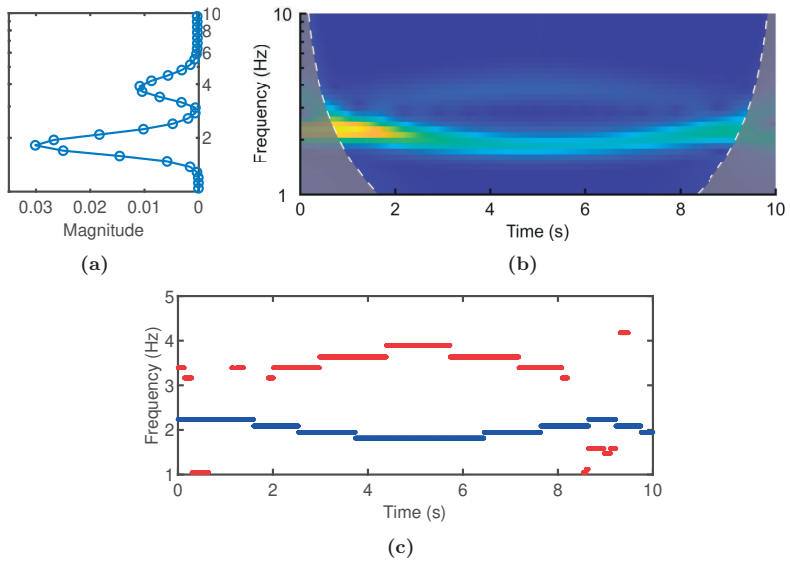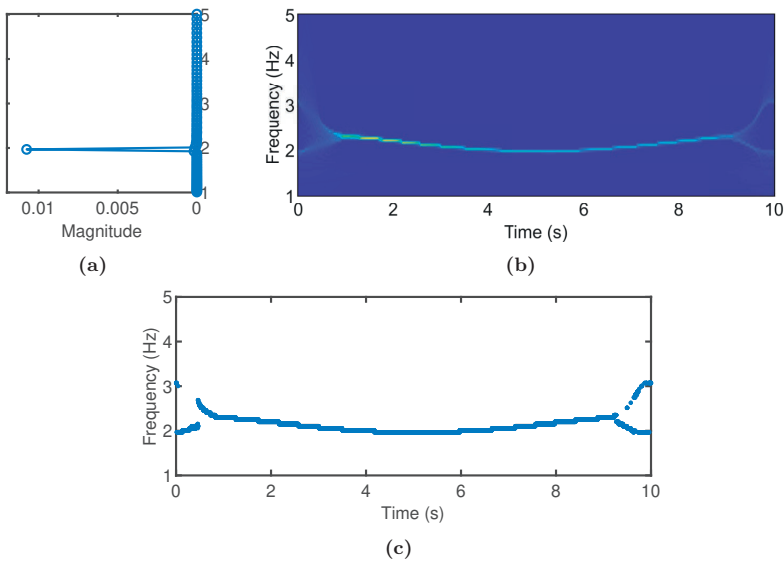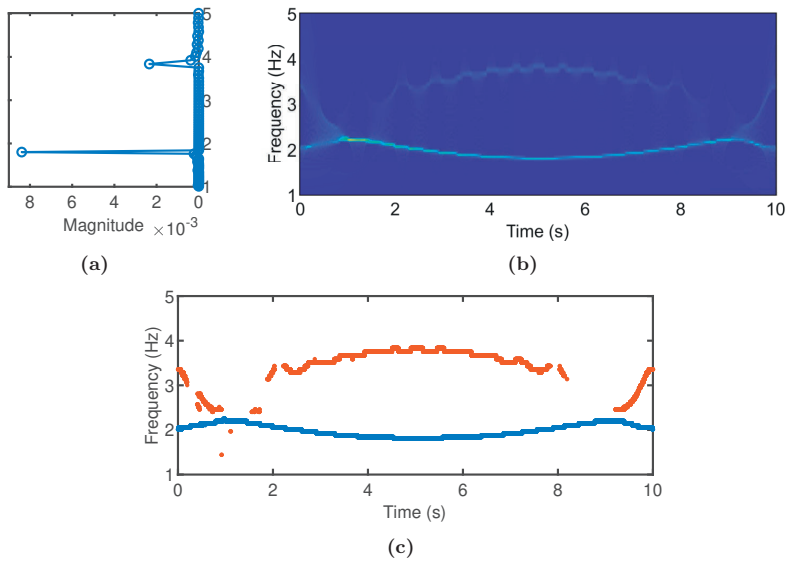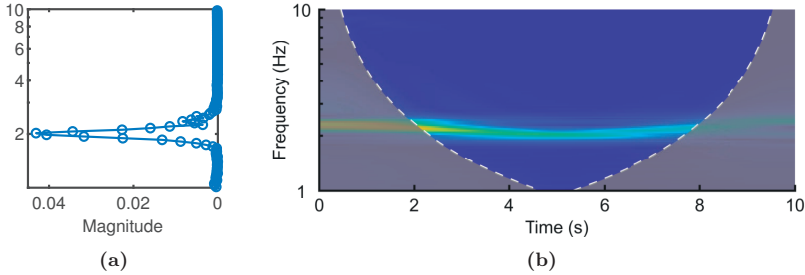
Figure 3.19: For test case 1: a) The frequency content of the Traverse Phase at time instant 5 s obtained by modified CWT, b) the time-frequency representation obtained by modified CWT.

performs for the field measurement of an existing bridge, the Boyne viaduct.

Table 3.3: Evaluation of the time-frequency analysis techniques for separating and localizing the components of a multi-component non-stationary signal

Method	Test Case 1	Test Case 2	Test Case 3
Robust-LMD	No	No	-
HHT	Yes	No	-
CWT	Yes	Yes	-
WSST	Yes	Yes	Yes

3.5   Verifying WSST by field measurements

The Boyne viaduct, a single track railway bridge as it exists today, was constructed in the early 1930s and consists of 15 semi-circular masonry arch spans and three simply supported steel-girder spans (Figure 3.20). The central steel-girder span is approximately 81 m long and has been instrumented with accelerometers and strain gauges. The strain gauges data have been used for the response phase separation and identifying the first and the last sample of the Traverse Phase. The data from the accelerometer installed at the mid-span of the bridge has mainly been used for the bridge health monitoring. The sampling frequency of the measurements is 2 kHz. The bridge fundamental frequency, 2.9 Hz, is obtained by a frequency analysis of the bridge free vibration.

The objective of this section is to prove that WSST is able to capture the IF of the coupled system from the train-bridge acceleration response. A detailed analysis of the

Figure 3.20: The Boyne Viaduct railway bridge in Drogheda, Ireland

IF thus obtained, i.e. investigating how the dynamic coupling affects the obtained IF, is beyond the scope of the present paper and will be subject of future work.

Different types of trains pass the Boyne bridge. Among a large data set of field measurements, two types of signals are identified for two different types of single vehicles crossing the bridge, 1) a locomotive and 2) an engineering/maintenance train as shown in Figure 3.21a and Figure 3.21b schematically. These cases most closely resemble the numerical cases investigated.
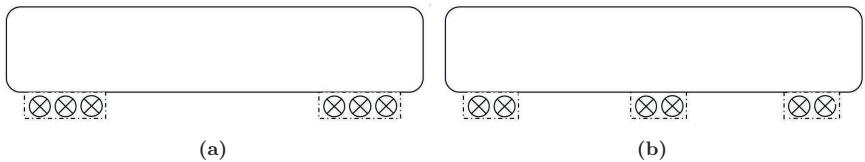
Figure 3.21: Schematic view of: a) 201 Class locomotive and, b) the engineering train.

A 201 Class locomotive has a total weight of 112.5 ton. The mass ratio between the locomotive and the Boyne bridge is around 20%, which is similar to the mass ratio used in the numerical model. WSST has been applied to the bridge response and the IF is extracted. Figure 3.22a displays the IF in a color density plot and the corresponding frequency ridge is shown in Figure 3.22b where the red dashed line separates the Traverse Phase and the Leaving Phase responses. It can be seen in Figure 3.22b that the IF ridge starts at 2.9 Hz and it is decreasing as the locomotive is approaching the bridge mid-span. When the vehicle is at mid-span the IF reaches its minimum value, 2.5 Hz. As the locomotive moves away, the IF returns again to 2.9 Hz.

The last second (9-10 s) of the signal corresponds to the Leaving Phase which contains the time-invariant bridge natural frequency, 2.9 Hz.
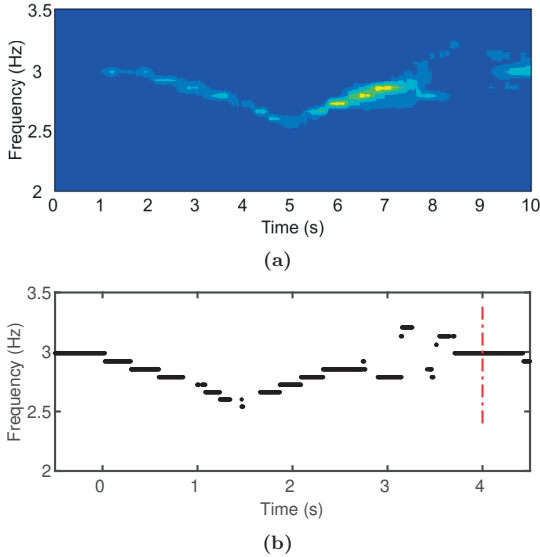
Figure 3.22: Time-frequency representation of the Boyne bridge obtained by WSST while a single 201 Class locomotive is passing over the bridge and, b) the corresponding frequency ridge.

The second example is a kind of maintenance train/truck (Figure 3.21b). The weight of this vehicle in unknown. WSST has been applied to the bridge response. Figure 3.23a displays the time-frequency representation in a color plot and the corresponding frequency ridges are shown in Figure 3.23b where again the red dashed line separates the Traverse Phase and the Leaving Phase responses. The observations are explained in the following.

Firstly, it can be seen in Figure 3.23b, there are two IFs during the Traverse Phase. The first IF starts at 2.9 Hz, decreases to 2.5 Hz and comes back to 2.9 Hz, which corresponds to the bridge resonance. The second one starts at 2.9 Hz, increases to 3.4 Hz and comes back to 2.9 Hz. Information of the vehicle is required to prove that this resonance corresponds to the vehicle but it is not available to the authors. However, considering the observations and the results obtained from the modelled bridge in

(a)

(b)
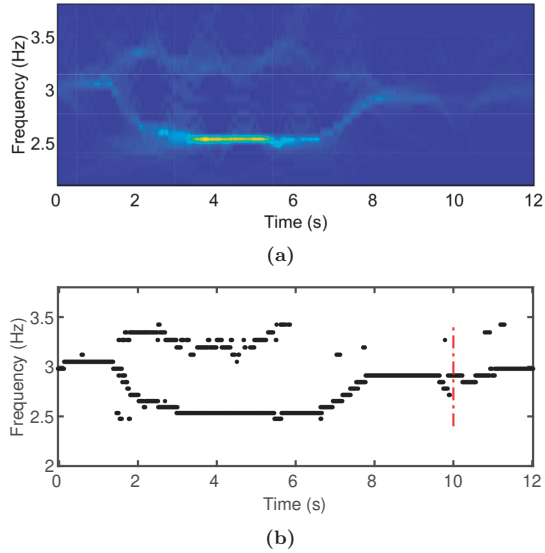
Figure 3.23: Time-frequency representation of the Boyne bridge obtained by WSST while a maintenace train is passing over the bridge and, b) the corresponding frequency ridges.

(a)

(b)
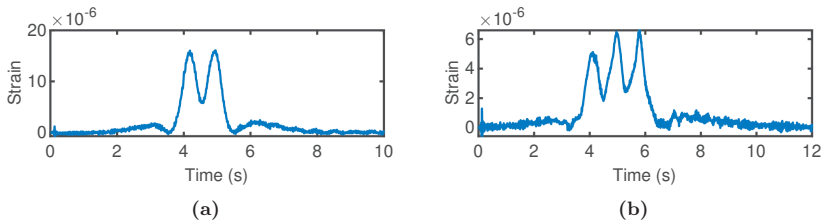
Figure 3.24: (a) the Boyne bridge strain response for the passage of: a) a 201 Class locomotive and, b) a single maintenance train

Section 3.4.5 (see Figure 3.15a), the second IF probably corresponds to the vehicle resonance.

Secondly, it can be seen in Figure 3.24a and Figure 3.24b that the maximum strain for the maintenance truck is less than half of the maximum strain for the locomotive, indicating that this vehicle has a much lower weight. However, the minimum value that the IF reaches, for both cases, is 2.5 Hz. It can be concluded that the mass is not the only parameter which affects the IF. Moreover, through the strain signal, Figure 3.24b, and the schematic view of the vehicle, Figure 3.21b it can be seen that the axles configuration and the axles distance of this vehicle is different from the locomotive (see Figure 3.24a and Figure 3.21a). this could therefore well be one of the other parameters which affects the time-dependent resonance of the coupled system.

Finally, the overall trend of the IF obtained from the bridge response to the passing maintenance train is different from the one obtained for the crossing of the locomotive. This is likely to be attributed to the different axles configuration and subsequently, load distribution. Axle distances are identified in [31] as an important parameter in the dynamic response of the bridge, a statement that seems to be confirmed by the results shown here.

3.6   Conclusion

A vehicle-bridge interaction has been simulated in ABAQUS to generate a coupled system with closely spaced frequency components and time varying resonances. This study aimed at performing a time-frequency analysis and extracting the Instantaneous Frequency (IF) of the system. To capture the time-varying resonances of the system, EMD, Robust-LMD, CWT and WSST have been applied on the Traverse Phase response. It has been observed that EMD is not able to decompose the Traverse-Phase signal into a set of mono-component signals due to mode-mixing. Although CWT is able to separate the frequency components, it cannot accurately localize them in time and it can be concluded that:

- Robust-LMD is not able to decompose the Traverse-Phase response into a set of purely frequency modulated signals (PFs) even for the test case 1 when the spectral components are not close.

- WSST has significantly enhanced CWT and has provided a sharper time-frequency representation by synchrosqueezing the wavelet scale variable into the instantaneous frequency.

- WSST is able to extract the IF of the modelled bridge from the simulated Traverse Phase response, also when it contains noise and closely spaced frequencies. The obtained IFs by applying WSST are well matched with the resonances obtained for the coupled system which has been loaded statically.

- WSST is able to extract the IF of the Boyne viaduct from the VBI acceleration response of a single passing vehicle. The time-dependent resonance of the Boyne bridge extracted from the Traverse Phase is in agreement with the bridge fundamental frequency obtained from the Leaving Phase. It also has been shown that the bridge interacts differently with a different vehicle, resulting in a different time-frequency representation.

The step-wise modal analysis created a benchmark to discriminate the bridge and the vehicle dynamics (see Figure 3.2). The extracted frequency ridges are very well matched with the step-wise modal analysis results. The IFs of the coupled system yield information about the bridge and the train dynamics, which can ultimately be used for vibration-based health monitoring of bridges. A bridge is traversed during its service life by different trains with different configurations. Although the current study proves that the IF can be extracted, which is an important first step in the process of VBI based monitoring of bridges, it is not yet clear which train parameters affect the IF and how each of these parameters influences the dynamic coupling between the train and the bridge. These topics are currently being addressed in ongoing research, by modeling and analyzing the response of full length trains passing a bridge.

3.7 Acknowledgments

Bibliography

[1] Casciati F, Casciati S, Faravelli L, Vece M. Validation of a Data-fusion Based Solution in view of the Real-Time Monitoring of Cable-Stayed Bridges. *Procedia Engineering* 2017; 199: 2288-2293. doi: 10.1016/j.proeng.2017.09.279

[2] Faravelli L, Ubertini F, Fuggini C. System identification of a super high-rise building via a stochastic subspace approach. *Smart Structures and Systems* 2011; 7(2): 133-152. doi: 10.12989/sss.2011.7.2.133

[3] Casas JR, Moughty JJ. Bridge Damage Detection Based on Vibration Data: Past and New Developments. *Frontiers in Built Environment* 2017; 3(4). doi: 10.3389/fbuil.2017.00004

[4] Staszewski WJ, Wallace DM. Wavelet-based Frequency Response Function for time-variant systems—An exploratory study. *Mechanical Systems and Signal Processing* 2014; 47(1-2): 35-49. doi: 10.1016/j.ymssp.2013.03.011

[5] Spiridonakos MD, Fassois SD. Non-stationary random vibration modelling and analysis via functional series time-dependent ARMA (FS-TARMA) models – A critical survey. *Mechanical Systems and Signal Processing* 2014; 47(1-2): 175-224. doi: 10.1016/j.ymssp.2013.06.024

[6] Dziedziech K, Staszewski WJ, Uhl T. Wavelet-based modal analysis for time-variant systems. *Mechanical Systems and Signal Processing* 2015; 50-51: 323-337. doi: 10.1016/j.ymssp.2014.05.003

[7] He WY, Ren WX, Zuo XH. Mass-normalized mode shape identification method for bridge structures using parking vehicle-induced frequency change. *Structural Control and Health Monitoring* 2018; 25(6). doi: 10.1002/stc.2174

[8] Lin STK, Lu Y, Alamdari MM, Khoa NLD. Field test investigations for condition monitoring of a concrete culvert bridge using vibration responses. *Structural Control and Health Monitoring* 2020; 27(10). doi: 10.1002/stc.2614

[9] Spiridonakos MD, Fassois SD. Parametric identification of a time-varying structure based on vector vibration response measurements. *Mechanical Systems and Signal Processing* 2009; 23(6): 2029-2048. doi: 10.1016/j.ymssp.2008.11.004

[10] Cohen L. Time-frequency distributions-a review. *Proceedings of the IEEE* 1989; 77(7): 941-981. doi: 10.1109/5.30749

[11] Wong KY. Instrumentation and health monitoring of cable-supported bridges. *Structural Control and Health Monitoring* 2004; 11(2): 91-124. doi: 10.1002/stc.33

[12] Yan BF, Miyamoto A. A comparative study of modal parameter identification based on wavelet and Hilbert-Huang transforms. *Computer-Aided Civil and Infrastructure Engineering* 2006; 21(1): 9-23. doi: DOI 10.1111/j.1467-8667.2005.00413.x

[13] He XH, Hua XG, Chen ZQ, Huang FL. EMD-based random decrement technique for modal parameter identification of an existing railway bridge. *Engineering Structures* 2011; 33(4): 1348-1356. doi: 10.1016/j.engstruct.2011.01.012

[14] Sayed MA, Kaloop MR, Kim E, Kim D. Assessment of acceleration responses of a railway bridge using wavelet analysis. *KSCE Journal of Civil Engineering* 2016; 21(5): 1844-1853. doi: 10.1007/s12205-016-1762-0

[15] Yu DH, Ren WX. EMD-based stochastic subspace identification of structures from operational vibration measurements. *Engineering Structures* 2005; 27(12): 1741-1751. doi: 10.1016/j.engstruct.2005.04.016

[16] Moughty JJ, Casas JR. A State of the Art Review of Modal-Based Damage Detection in Bridges: Development, Challenges, and Solutions. *Applied Sciences-Basel* 2017; 7(5). doi: ARTN 510 10.3390/app7050510

[17] Chen JUN. Application of Empirical Mode Decomposition in Structural Health Monitoring: Some Experience. *Advances in Adaptive Data Analysis* 2009; 01(04): 601-621. doi: 10.1142/s1793536909000321

[18] Connolly DP, Kouroussis G, Laghrouche O, Ho CL, Forde MC. Benchmarking railway vibrations – Track, vehicle, ground and building effects. *Construction and Building Materials* 2015; 92: 64-81. doi: 10.1016/j.conbuildmat.2014.07.042

[19] Zhang W, Li J, Hao H, Ma H. Damage detection in bridge structures under moving loads with phase trajectory change of multi-type vibration measurements. *Mechanical Systems and Signal Processing* 2017; 87: 410-425. doi: 10.1016/j.ymssp.2016.10.035

[20] Pakrashi V, O'Connor A, Basu B. A Bridge-Vehicle Interaction Based Experimental Investigation of Damage Evolution. *Structural Health Monitoring: An International Journal* 2009; 9(4): 285-296. doi: 10.1177/1475921709352147

[21] Hester D, Gonzalez A. A wavelet-based damage detection algorithm based on bridge acceleration response to a vehicle. *Mechanical Systems and Signal Processing* 2012; 28: 145-166. doi: 10.1016/j.ymssp.2011.06.007

[22] Reddy DM, Krishna P, Sathesa . Innovative method of empirical mode decomposition as spatial tool for structural damage identification. *Structural Control and Health Monitoring* 2015; 22(2): 365-373. doi: 10.1002/stc.1676

[23] Kunwar A, Jha R, Whelan M, Janoyan K. Damage detection in an experimental bridge model using Hilbert-Huang transform of transient vibrations. *Structural Control and Health Monitoring* 2013; 20(1): 1-15. doi: 10.1002/stc.466

[24] Aied H, Gonzalez A, Cantero D. Identification of sudden stiffness changes in the acceleration response of a bridge to moving loads using ensemble empirical mode decomposition. *Mechanical Systems and Signal Processing* 2016; 66-67: 314-338. doi: 10.1016/j.ymssp.2015.05.027

[25] Beskhyroun S, Oshima T, Mikami S. Wavelet-based technique for structural damage detection. *Structural Control and Health Monitoring* 2009: n/a-n/a. doi: 10.1002/stc.316

[26] Nguyen KV. Comparison studies of open and breathing crack detections of a beam-like bridge subjected to a moving vehicle. *Engineering Structures* 2013; 51: 306-314. doi: 10.1016/j.engstruct.2013.01.018

[27] Li JZ, Su MB, Fan LC. Natural Frequency of Railway Girder Bridges under Vehicle Loads. *Journal of Bridge Engineering* 2003; 8(4): 199-203. doi: 10.1061/(Asce)1084-0702(2003)8:4(199)

[28] Law SS, Zhu XQ. Dynamic behavior of damaged concrete bridge structures under moving vehicular loads. *Engineering Structures* 2004; 26(9): 1279-1293. doi: 10.1016/j.engstruct.2004.04.007

[29] Roveri N, Carcaterra A. Damage detection in structures under traveling loads by Hilbert-Huang transform. *Mechanical Systems and Signal Processing* 2012; 28: 128-144. doi: 10.1016/j.ymssp.2011.06.018

[30] Marchesiello S, Bedaoui S, Garibaldi L, Argoul P. Time-dependent identification of a bridge-like structure with crossing loads. *Mechanical Systems and Signal Processing* 2009; 23(6): 2019-2028. doi: 10.1016/j.ymssp.2009.01.010

[31] Cantero D, Kaustell lM, Karoumi R. Time–frequency analysis of railway bridge response in forced vibration. *Mechanical Systems and Signal Processing* 2016; 76-77: 518-530. doi: 10.1016/j.ymssp.2016.01.016

[32] Smith JS. The local mean decomposition and its application to EEG perception data. *J R Soc Interface* 2005; 2(5): 443-54. doi: 10.1098/rsif.2005.0058

[33] Liu ZL, Jin YQ, Zuo MJ, Feng ZP. Time-frequency representation based on robust local mean decomposition for multicomponent AM-FM signal analysis. *Mechanical Systems and Signal Processing* 2017; 95: 468-487. doi: 10.1016/j.ymssp.2017.03.035

[34] Daubechies I, Lu JF, Wu HT. Synchrosqueezed wavelet transforms: An empirical mode decomposition-like tool. *Applied and Computational Harmonic Analysis* 2011; 30(2): 243-261. doi: 10.1016/j.acha.2010.08.002

[35] Wang YX, He ZJ, Zi YY. A Comparative Study on the Local Mean Decomposition and Empirical Mode Decomposition and Their Applications to Rotating Machinery Health Diagnosis. *Journal of Vibration and Acoustics-Transactions of the Asme* 2010; 132(2). doi: Artn 021010 10.1115/1.4000770

[36] Jiang QT, Suter BW. Instantaneous frequency estimation based on synchrosqueezing wavelet transform. *Signal Processing* 2017; 138: 167-181. doi: 10.1016/j.sigpro.2017.03.007

[37] Wu HT, Flandrin P, Daubechies I. One or Two Frequencies? The Synchrosqueezing Answers. *Advances in Adaptive Data Analysis* 2011; 03(01n02): 29-39. doi: 10.1142/s179353691100074x

[38] Huang NE, Shen Z, Long SR, et al. The empirical mode decomposition and the Hilbert spectrum for nonlinear and non-stationary time series analysis. *Proceedings of the Royal Society a-Mathematical Physical and Engineering Sciences* 1998; 454(1971): 903-995. doi: 10.1098/rspa.1998.0193

[39] Huang NE, Shen SSP. *Hilbert-Huang Transform and Its Applications*. Interdisciplinary Mathematical SciencesWorld Scientific . 2005

[40] Huang NE, Wu Z, Long SR, Arnold KC, Chen X, Blank K. On Instantaneous Frequency. *Advances in Adaptive Data Analysis* 2011; 01(02): 177-229. doi: 10.1142/s1793536909000096

[41] Sadowsky J. The Continuous Wavelet Transform - a Tool for Signal Investigation and Understanding. *Johns Hopkins Apl Technical Digest* 1994; 15(4): 306-318.

[42] Daubechies I. *Ten Lectures on Wavelets*. CBMS-NSF Regional Conference Series in Applied Mathematics . 1992

[43] Fugal DL. Conceptual wavelets in digital signal processing : An In-depth, Practical Approach for the Non-mathematician. In: Space & Signals Technical Pub.

[44] Daubechies I, Maes S. *A nonlinear squeezing of the continuous wavelet transform based on auditory nerve models*book section 20: 527-546; New York: CRC Press. 1st edition ed. 1996

[45] Saleeb A, Kumar A. Automated Finite Element Analysis of Complex Dynamics of Primary System Traversed by Oscillatory Subsystem. *Computational Methods in Engineering Science and Mechanics* 2011; 12(4): 184-202. doi: 10.1080/15502287.2011.580830

[46] Amezquita-Sanchez JP, Adeli H. Signal Processing Techniques for Vibration-Based Health Monitoring of Smart Structures. *Archives of Computational Methods in Engineering* 2014; 23(1): 1-15. doi: 10.1007/s11831-014-9135-7

[47] Lu Y, Mao L, Woodward P. Frequency characteristics of railway bridge response to moving trains with consideration of train mass. *Engineering Structures* 2012; 42: 9-22. doi: 10.1016/j.engstruct.2012.04.007

[48] Wu Z, Huang NE. Ensemble Empirical Mode Decomposition: A Noise-Assisted Data Analysis Method. *Advances in Adaptive Data Analysis* 2009; 01(01): 1-41. doi: 10.1142/s1793536909000047

[49] Fosso OB, Molinas M. Method for Mode Mixing Separation in Empirical Mode Decomposition. *IEEE Transactions on Signal Processing* 2017. doi: arXiv:1709.05547v1

[50] Rilling G, Flandrin P. One or Two Frequencies? The Empirical Mode Decomposition Answers. *IEEE Transactions on Signal Processing* 2008; 56(1): 85-95. doi: 10.1109/tsp.2007.906771

[51] Feng Z, Liang M, Chu F. Recent advances in time–frequency analysis methods for machinery fault diagnosis: A review with application examples. *Mechanical Systems and Signal Processing* 2013; 38(1): 165-205. doi: 10.1016/j.ymssp.2013.01.017

[52] Ouyang HJ. Moving-load dynamic problems: A tutorial (with a brief overview). *Mechanical Systems and Signal Processing* 2011; 25(6): 2039-2060. doi: 10.1016/j.ymssp.2010.12.010

4

A damage detection approach based on extracting Instantaneous Frequency of vehicle-bridge acceleration response by Wavelet Synchrosqueezed Transform [1]

abstract

In bridge structural health monitoring, typically the dynamic response of the system is used to assess the health condition of the bridge. However, the dynamic interaction between a bridge and a passing vehicle imposes non-stationarity on the system response, whereby the bridge modal parameters become time-dependent and detecting damage, for example, based on the bridge modal parameters, becomes challenging. Dynamic vehicle-bridge interaction (VBI) responses have mainly been investigated for damage detection through identifying signal singularities and abrupt changes. The singularities are usually associated with high-frequency components (relative to the bridge

---

natural frequencies), and it is demanding to isolate the damage-induced singularities from those caused by either an operational condition, i.e., track irregularities, or noise. Unlike the high-frequency range, the influence of damage on the resonance frequency of the coupled system has not been fully explored. The present study proposes the shape of the bridge instantaneous frequency as a damage sensitive feature in which the influence of the vehicle dynamics can be excluded. This study demonstrates the feasibility of a damage detection approach based on the bridge instantaneous frequency by applying Wavelet Synchrosqueezed Transform (WSST). In this approach the bridge instantaneous frequency variation induced by damage is distinguished from the bridge instantaneous frequency variation induced by the vehicle. Several damage scenarios that are implemented numerically are analyzed to verify the method's performance. The results demonstrate that a high resolution instantaneous frequency extracted from the VBI dynamic response outperforms the resonance frequency in determining the local disruption, leading to detecting the damage. A Damage Index (DI) is also proposed as an attempt to quantify the damage severity.

4.1   Introduction

Structural Health Monitoring (SHM) systems aim at identifying damage to assess the structural integrity and safety of a structure. Moreover, the obtained damage information can serve as an input for Bridge Management Systems (BMSs) to guide and manage the maintenance activities during the service life of bridges. An SHM system can provide information at different levels regarding the condition of a bridge where the primary level is detecting damage. Several techniques have been developed for damage detection in bridges. The majority can be grouped into four categories. The first group involves model-based techniques, which are based on updating the parameters of an analytical or numerical model such that the model matches the real measurements [1–3]. However, these techniques are not always efficient because the bridges are massive structures with a complex geometry. Moreover, the accuracy of the results is dependent on the accuracy of the developed model. The second group contains the data-driven methods (DDMs) that are not supported by physical models such as neural network [4, 5], machine learning [6], feature extraction and pattern recognition [7–10]

techniques. The third group which is the traditional approach, contains the modal-based damage detection techniques [11, 12] based on extracting and monitoring the modal properties, which can vary due to the presence of damage. The fourth group contains structural health monitoring techniques based on time-frequency analysis of the Vehicle-Bridge interaction (VBI) response. The current study proposes a damage detection approach based on the instantaneous and natural frequency of the bridge extracted from the bridge forced and free vibration response, respectively. Therefore, the following literature review is on the last two groups where the bridge vibration, free or forced, has been utilized for damage detection.

The standard technique for modal identification is Modal Analysis (MA). Input-output methods or Experimental Modal Analysis (EMA) techniques involve applying a known input, such as a Dirac impulse load, to the structure and measuring the vibration response. To create a desired forcing function, devices such as impact hammers, shakers, or drop weights are required [13]. However, they are not efficient and applicable for a bridge in regular operation. Then the Output-only Modal Analysis (OMA) is adopted for a system stationary output while the unmeasured input can be considered as white noise [14]. Hence, the response of the structure to an ambient excitation such as wind load or its free vibration due to a passing vehicle is suitable for OMA [15–17]. Ambient vibration is generally of small magnitude, which cannot be helpful for all bridges [18]. Since EMA and OMA are not efficiently applicable for all bridges, railway bridges are generally monitored by extracting the bridge dynamic properties through the free vibration response, which occurs once a passing train has just left the bridge [18]. However, the extracted modal parameters, using the bridge free vibrations, before and after the damage occurrence are global and averaged features that may not be sensitive to damage as a local event [19]. Most damage detection researches have shown that a discontinuity appears in the forced vibration signal when the moving load crosses over damage [20–24], so the forced vibration response may be more sensitive to damage than the free vibration. The VBI response that refers to the coupled dynamic response of a bridge and a moving vehicle has been widely studied in the literature for damage detection in bridges by analyzing the bridge response (*direct methods*) or the vehicle response (*indirect methods*). VBI has also been applied for Moving Force Identification (MFI) from a vehicle response or a bridge response [25, 26]. A general overview of MFI techniques can be found in [27].

To narrow down, the scope of the current study is damage detection techniques for bridges that analyze the VBI response measured on the bridge (*direct methods*). In order to position the current study among existing techniques in scope, Table 4.1 summarizes these studies. Each approach is presented via five attributes: 1) the considered signal, 2) the damage sensitive feature (DSF), 3) the applied signal processing method, 4) the way the vehicle dynamics are simulated and, 5) the validation approach. In the following, some of the attributes ar discussed to distinguish the proposed method.

Regarding the considered signal, Table 4.1 shows that the bridge time-deflection response (typically taken at the mid-span location) has been mostly used. However, there are motivations to study the bridge acceleration rather than the deflection signal. Firstly, it might not be possible to measure the bridge deflection signal at mid-span directly. Secondly, in comparison with the deflection signal, the bridge acceleration signal is more sensitive to damage [22]. The acceleration signal contains more information about damage as well as noise, making it challenging but also valuable to analyze. Therefore, measuring the bridge acceleration is considered more practical than measuring the bridge deflection.

Regarding the applied technique Table 4.1 shows that Empirical Mode Decomposition (EMD) [21] and Ensemble Empirical Mode Decomposition (EEMD) [24] were applied to the acceleration response of the damaged bridge models induced by a constant moving force. They aimed to capture the singularities that appeared in a series of Intrinsic Mode Functions (IMFs) corresponding to high-frequency components. Table 4.1 further shows that Continuous Wavelet Transform (CWT) is one of the most applied methods, since the basic principle of the wavelet-based damage detection techniques is detecting singularities, and abrupt changes [37]. Hester et al. [22] applied CWT to a modeled bridge acceleration response and concluded that in the coefficient matrix, the damaged strips have a higher energy content than the healthy strips if the frequencies are distant from the natural frequencies. Later, they [20] assumed that the damage was already detected, and they investigated how a singularity changes with damage location and severity. Regardless of the applied method, a commonality among the above methods is the DSF is based on singularities that appear in the response of a damaged structure, but do not exist in its healthy response [20]. The singularities are usually associated with high-frequency components (in comparison with the bridge natural frequencies), and it is demanding to isolate the damage-induced singularities

Table 4.1: An overview of recent damage detection approaches

Research study	Considered response [1]	Damage Sensitive Feature [2]	Applied technique [3]	Moving object	Validation
Huseynov et al [28]	$\ddot{x}$	rotation	rotation influence line	series of constant forces	Numerically experimentally
Weiwei et al [29]	$x, \dot{x}, \ddot{x}$	phase trajectory	low-pass filter & moving average	constant force & mass	Numerically experimentally
He et al. [30]	x	moving frequency	DWT	constant force & vehicle	Numerically
Aied et al [24]	$\ddot{x}$	discontinuity in IMF	EEMD	a constant force	Numerically
Yu et al. [31]	x	Wavelet coefficient	CWT	a constant force	Numerically experimentally
Nguyen [32]	x	instantaneous frequency	CWT	a half-vehicle	Numerically
Gonzales et al. [20]	$\ddot{x}$	mid-span 'static' deflection and acceleration	MAF	a constant force & a vehicle	Numerically
Khorram et al. [33]	x	Wavelet coefficients	CWT & Factorial Design	a constant force	Numerically
Weiwei et al. [34]	$\dot{x}$	wavelet coefficient	CWT	a constant force	Numerically
Hester et al. [22]	$\ddot{x}$	wavelet coefficient	CWT	a constant force	Numerically
Meredith et al. [21]	$\ddot{x}$	high peaks in IMFs	MAF followed by EMD	a constant force	Numerically
Roveri et al. [23]	x	instantaneous frequency	HHT	constant force	Numerically
Pakrashi et al. [35]	ε	Wavelet coefficient & Wavelet phase	CWT	vehicle	Numerically experimentally
Zhu et al. [36]	x	Wavelet coefficient	CWT	constant force	Numerically

[1] $x, \dot{x}, \ddot{x}$ and ε represent the bridge displacement, velocity, acceleration and strain response.
[2] IMF: Intrinsic Mode Function.
[3] DWT: Descrete Wavelet Transform, CWT: Continouse Wavelet Transform, EMD: Empirical Mode Decomposition, EEMD: Ensemble Empirical Mode Decomposition, MAF: Moving Average Filter, HHT: Hilbert Huang Transform.

from those caused by either an operational condition (track irregularities) [38] or noise [29]. This might be a reason why they are efficient for simulated signals or laboratory experiments but not for field applications.

Moreover, in most of the above studies, the vehicle is mainly modeled as a constant

force, whereas the vehicle-bridge dynamic interactions are completely excluded. Those studies that utilized vehicle models did not explicitly investigate the influence of the vehicle on the system response and the damage detection approach. In general, a moving force model is suitable for the cases where either the weight of the vehicle is much smaller than the bridge or the effect of the dynamic behavior of the vehicle is not of interest [39]. For trains, it is known that the train weight is not negligible and the trains thus affects the dynamic properties of the VBI system [40]. Therefore, for the current study, the vehicle is modeled as a point mass to include the influence of the vehicle mass on the system dynamics response.

To overcome the limitations as mentioned above, the feasibility of a damage detection concept based on the following axioms will be studied;

- The bridge free vibration mainly reflects the global dynamics properties, which may overshadow a small and local variation triggered by the passing vehicle and captured by the vehicle-bridge coupled dynamic response.

- A damage-induced singularity originates from a sudden stiffness change between two bridge elements once the vehicle passes over a damaged element. This sudden stiffness change causes a deviation in the time-dependent resonance of the system.

- A passing vehicle, depending on its (dynamic) properties, can affect the bridge resonance frequencies. Thus, upfront the damage investigation, the bridge forced and free vibrations are required to identify their frequency difference in a healthy state.

- The vehicle is modeled as a point mass to impose the bridge resonance frequency change due to the operational condition (i.e. added mass) as occurs in practice.

- a high-resolution time-frequency analysis technique is required to extract the VBI system's time-dependent resonances as accurately as possible. Wavelet SynchroSqueezed Transform (WSST) is used for the current study as its performance has been investigated and validated [41].

The following section will explain the methodology in three steps: 1) phase separation, 2) frequency extraction and, 3) frequency analysis. A numerical model has been used to validated the complete damage detection approach, which is presented in

Methodology section. The results are discussed in Results and discussion section, and the final section provides the conclusions. It is worth mentioning that a large amount of vibration data of a real bridge, the Boyne viaduct is available. The bridge condition is considered healthy due to recent refurbishment activities. Therefore, the first two steps, the phase separation and the frequency extraction, have been verified with the field measurement data of the Boyne viaduct.

4.2   Methodology

Generally, a bridge vibration response due to a passing train contains three phases: 1) the entrance phase, 2) the traverse phase, and 3) the leaving phase. The entrance phase covers the period right before the train enters the bridge, and the part of the vibration signal associated with this phase is not investigated in this paper. The traverse phase is the period that the train is either partly or entirely on the bridge, and the leaving phase is the period right after the train has left the bridge. The traverse and the leaving phase correspond to the bridge forced and free vibrations, respectively. The traverse phase is known as the vehicle-bridge interaction response (VBI), representing the response of the coupled system of both bridge and vehicle.

The flowchart of the conventional damage detection technique based on monitoring the variation of the bridge natural frequency is presented in Figure 4.1 where f_b and f_m are the baseline and the measured bridge natural frequency extracted from the leaving phase response.

It is known that a discontinuity emerges in the response when the moving mass crosses a damaged element. Both the traverse and the leaving phase signals contain local and global information. However, the global properties dominate in the leaving phase, whereby slight variations induced by damage may be overshadowed. Therefore, the traverse phase is believed to be more sensitive to damage than the free vibration response. The flowchart of the proposed concept presented in Figure 4.2 shows that the proposed method extends the traditional method by including both the traverse phase and the leaving phase response and accordingly utilizing the bridge instantaneous and natural frequency respectively.

The challenge of utilizing the traverse phase response is that the traverse phase, in addition to damage, is also sensitive to the operational conditions. Therefore, the pro-

posed algorithm for a VBI system starts by setting a baseline instantaneous frequency extracted from the bridge traverse phase, $\mathcal{F}_b$ for a passing vehicle type. If different types of trains pass the bridge, a train type should be defined as the target vehicle to set $\mathcal{F}_b$. A parallel study is investigating the definition of the target vehicle type, which is out of the scope of the current study. The traverse phase provides a baseline for a healthy bridge. An instantaneous frequency extracted from a measured traverse phase response, $\mathcal{F}_m$, can then differ from $\mathcal{F}_b$ due to; 1) a variation of the operational conditions or 2) the presence of damage. Therefore, the source of the instantaneous frequency difference must be identified first. The shape correlation ρ and the magnitude variation δ are proposed to identify the source of $\mathcal{F}_b$ variation. If the difference is caused by damage, then δ can be used as damage index. The proposed damage index is an attempt to quantify damage severity. Moreover, the local baseline deviation around the damage location shows the potential of the proposed method for damage localization. However, the focus of the current study is on detecting damage. Damage
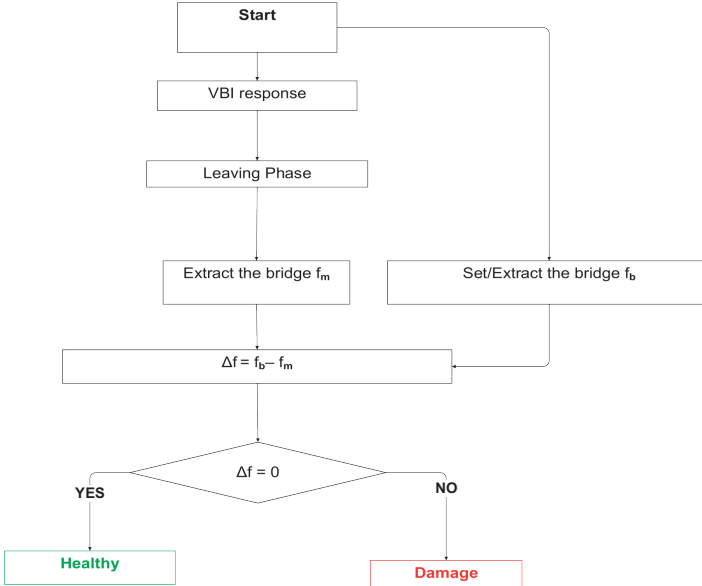
Figure 4.1: The flowcharts of the damage detection techniques based on the bridge natural frequency extracted from the leaving phase.

localization and damage quantification are out of the scope of the current study. The proposed concept is presented in three analysis steps; 1) phase separation, 2) frequency extraction, 3) frequency analysis.

4.2.1 Phase separation

Phase separation refers to splitting the entire response into the entrance, traverse, and leaving Phase responses. As these phases represent different systems with different
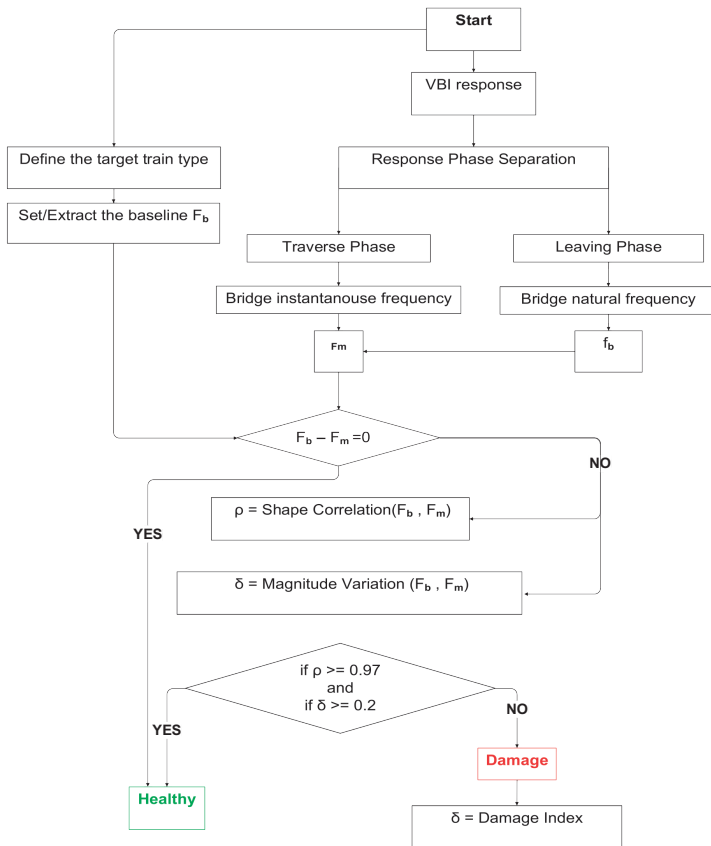
Figure 4.2: The flowcharts of the damage detection techniques based on the VBI system instantaneous frequency extracted from the traverse phase.

dynamics properties, the phase separation step is of paramount importance. Even though phase separation is relatively straightforward, it is a foundational block of the proposed concept. The phase separation step is performed based on the position of a train on the bridge, see Figure 4.3. The traverse phase starts when the first wheel set of the train enters and ends when the last wheel set leaves the bridge. This phase describes the forced response of the bridge due to the moving train, including the train-bridge dynamic interaction. The leaving phase is the free vibration of the bridge. Figure 4.3 shows a schematic view of the phase separation for a sample signal. This signal was measured by an accelerometer installed at mid-span of the Boyne viaduct in Ireland [42]. It can be seen that there is no visible sign in the time signal on when the train enters or leaves the bridge meaning that the phase separation is not straightforward for field data. The exact moments of the entrance and exit of the train can be identified by knowing the train velocity and the location of the accelerometer. The train velocity calculation can be carried out in several ways. In this study, it is obtained from the driving frequency, $f_{dr} = V_{vehicle}/L_{bridge}$ which is present in the frequency content of the bridge dynamic response [43]. The driving frequency is the inverse of the time that a train with a velocity V needs to pass a bridge with a length of L. By extracting the driving frequency for a bridge with a known length, the average vehicle velocity can be calculated.
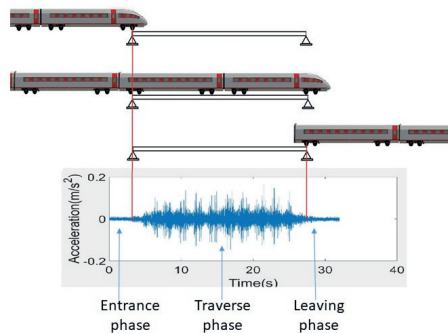
Figure 4.3: Schematic view of the phase separation

4.2.2 Frequency Extraction

The most challenging step of this methodology is the frequency extraction. Although the traverse and the leaving phase both contain the bridge response, they represent different systems. The traverse phase contains the response of the vehicle-bridge coupled system where the time-dependent mass distribution on the bridge leads to a time-variant system, whereas the leaving phase, as the bridge free vibration, represents a time-invariant system. In other words, the dominant frequency components of the leaving phase are the bridge natural frequencies, whereas the traverse phase contains the time-dependent frequency components that originate from the bridge, the vehicle, and the track vibration. The first challenge of the time-frequency analysis of the traverse phase, knowing that a VBI response contains closely-spaced spectral components due to the vehicle-bridge dynamic coupling [44], is to distinguish the bridge resonance from other resonances. A reliable and efficient approach is first to extract the bridge natural frequency from the leaving phase and then trace it back in the traverse phase. The bridge natural frequency extracted from the leaving phase is used as the reference to trace the VBI system time-dependent resonance corresponding to the bridge natural frequency. Including both the traverse and the leaving phase response and analyzing them individually as two separate systems is an essential base of the proposed concept to distinguish the bridge resonances from the system resonances.

The second challenge of the time-frequency analysis of the traverse phase is to extract the time-dependent resonance of the bridge as accurate as possible. A high-resolution and sharp time-frequency representation may reflect more information about a local signal disruption than a low-resolution or blurry time-frequency representation. Therefore, a high resolution time-frequency method is required to extract the instantaneous frequencies of the vehicle-bridge interaction response. The performance of Empirical Mode Decomposition (EMD), Local Mean Decomposition (LMD), The Continuous Wavelet Transform (CWT) and the Wavelet SynchroSqueezed Transform (WSST) has been investigated and it has been concluded that among the aforementioned methods WSST can separate the time-dependent resonances of the VBI system and capture the time-dependent variation of the resonances of the system without the prerequisite for the signal to be mono-component [41]. Moreover, the performance of WSST has been

validated for the field data of Boyne bridge in previous work of the authors [41]. In the following WSST is presented briefly.

The continuous wavelet transforms the one-dimensional time signal $x(t)$ into a two-dimensional quantity, $W(a,b)$, where a and b are the translation and the scale variables respectively and the function ψ is called the 'mother' wavelet.

$$W_x(a,b) = \int x(t) a^{-1/2} \psi\left(\frac{t-a}{b}\right) \tag{4.1}$$

However, the time frequency representation is somewhat blurred since $W(a,b)$ is spread out over a region around a on the time-scale [45]. Daubechies et al. [45] observed during the time-frequency analysis of audio signals for speaker identification that, the oscillatory behavior of the signal at time b indicates the original frequency ω, despite the fact that $W(a,b)$ is smeared out in a (scale), regardless of the amplitude of a. The process of synchrosqueezing tries to make the resulting time-scale image of CWT more precise.

In summary, WSST [46] has three steps. Step one is calculating the continuous wavelet transform of a time signal, $x(t)$ by Equation (4.1). Step two is calculating the instantaneous frequency by:

$$\omega_x(a,b) = \frac{\frac{\partial W_x(a,b)}{\partial b}}{2\pi i W_x(a,b)} \tag{4.2}$$

where the frequency variable ω_x and the scale variable a are binned and computed only at discrete values a_k, with $a_k - a_{k-1} = (\Delta a)_k$. The third step is to re-assign the scale variable a to the frequency variable ω by calculating the Synchrosqueezed transform, T_x as:

$$T_x(\omega_l,b) = (\Delta\omega)^{-1} \sum_{a_k} W(a_k,b) a_k^{-3/2} (\Delta a)_k \tag{4.3}$$

The transform function $T_x(\omega_l,b)$ is determined over time, only at the centers ω_l of the subsequent bins $[\omega_l - \frac{1}{2}\Delta\omega, \omega_l + \frac{1}{2}\Delta\omega]$, with $\Delta\omega = \omega_l - \omega_{l-1}$.

4.2.3 Frequency analysis

The extracted instantaneous frequency from the traverse phase provides a baseline for a healthy bridge. The bridge instantaneous frequency extracted from a measured response can deviate from the baseline due to variation of the operational conditions or

due to the presence of damage. It is worth noting that the frequency variation due to
the seasonal effect is not investigated in this study. The operational conditions are com-
monly considered to be the length, mass, and velocity of the vehicles. For the current
study, however, only the vehicle's mass is investigated as a variable operational condi-
tion since its influence on the bridge frequency is well known. Although the vehicle's
mass and the damage can both affect the traverse phase response, their impacts are on
different scales. The operational condition affects the bridge instantaneous frequency
globally, whereas the damage imposes a local variation in the bridge instantaneous
frequency. Once the moving mass crosses a damaged section with a lower stiffness, a
discontinuity appears in the response. This local discontinuity causes the instantaneous
frequency deviation. The proposed damage detection method is based on the deviation
of the baseline instantaneous frequency ($\mathcal{F}_b$) by calculating two features; 1) the baseline
shape correlation, ρ and, 2) the magnitude variation, δ. In statistics, the Pearson cor-
relation coefficient calculates a linear correlation measure between two data sets. The
baseline shape correlation calculates the global shape correlation between a measured
instantaneous frequency ($\mathcal{F}_m$) and the baseline instantaneous frequency ($\mathcal{F}_b$).

$$\rho(\mathcal{F}_b, \mathcal{F}_m) = \frac{1}{n-1} \sum_{i=1}^{n} \left(\frac{\mathcal{F}_{b,i} - \mu_{\mathcal{F}_b}}{\sigma_{\mathcal{F}_b}} \right) \left(\frac{\mathcal{F}_{m,i} - \mu_{\mathcal{F}_m}}{\sigma_{\mathcal{F}_m}} \right) \tag{4.4}$$

where μ and σ are the mean and standard deviation of the instantaneous frequency as
a time series with n samples [47]. A low correlation coefficient suggests a considerable
difference in shape and therefore, a local variation of the bridge instantaneous frequency,
which can indicate damage. On the contrary, a change in operational or environmental
conditions can also lead to a change in the response, but this will be a more global
change which leads to a high correlation coefficient. However, a small amount of damage
may not lead to a low correlation coefficients. Therefore, the magnitude variation, as the
second feature, is introduced to quantify the deviation of the measured instantaneous
frequency, $\mathcal{F}_m$ from the baseline instantaneous frequency, $\mathcal{F}_b$.

$$\delta(\mathcal{F}_b, \mathcal{F}_m) = \frac{\sum_{i=1}^{n-1}[(\mathcal{F}_{b,i} + \mathcal{F}_{b,i+1}) - (\mathcal{F}_{m,i} + \mathcal{F}_{m,i+1})]}{\sum_{i=1}^{n-1}[(\mathcal{F}_{b,i} + \mathcal{F}_{b,i+1}) - 2f_b]} \tag{4.5}$$

where f_b refers to the bridge fundamental frequency, which is constant in time and
a scalar value (see Figure 4.6). Whereas the instantaneous frequency of the traverse

phase yields a curve indicating that the bridge resonance continuously changes in time depending on the location of the moving mass (see Figure 4.6). The denominator of Equation (5.1) calculates the area bounded by $\mathcal{F}_b$ and f_b for the intact bridge. It, therefore, corresponds to the variation of the baseline instantaneous frequency of the intact bridge induced by the operational condition. Once the instantaneous frequency of a measured response differs from the baseline, which would be the case when damage is present, then the bounded area between $\mathcal{F}_b$ and $\mathcal{F}_m$ is a nonzero value that quantifies the magnitude variation and it can be a negative or positive value.

4.3   Numerical Model

Although a large amount of vibration data is available for the Boyne bridge, the measurements are not applicable for the validation of the proposed damage detection approach, as recent refurbishments have removed all damage that was potentially present. Hence, to verify the proposed approach, a bridge is modeled numerically.

   All finite element simulations are conducted in two-dimensional space in ABAQUS where the analysis scheme is chosen to be the Newmark implicit time integration, assuming an average acceleration during each time step. Linear Timoshenko beam elements were used. The bridge model (the center part of 50 m) has 200 beam elements of 1 m thickness and 0.5 m width with Young's modulus of $E = 210$ GPa, density of $\rho = 7860$ kg/m^3. The fundamental frequency of the bridge model is 2.1 Hz. According to Eurocode EN 1991-2 (2003) the bridge fundamental frequencies for a span length between 20-100 m are in the range 1.7-4 Hz. The bridge model parameters are adopted from [36, 48] where the bridge length and its fundamental frequency are in the acceptable range. Damping is modeled by implementing Rayleigh damping with the coefficients of $\alpha = 0.001$ and $\beta = 0.001$. The benchmark simulation corresponds to a point mass equal to 10% of the bridge mass which slides with a speed of 5 m/s over the bridge. The mass slides through a node to surface interaction, while a hard contact model is used [49].

   The bridge model is modified to obtain the bridge free vibration, while the mass is not present on the bridge. To this end, an approaching and leaving length are added before and after the bridge to properly locate the mass during the forced and free vibration phases. The length of the approaching and the leaving parts are 25m
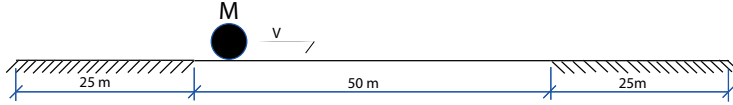
Figure 4.4: Schematic of the numerical model, showing the 50 m span and 25 m approaching and leaving sections.

and both are modelled with beam elements that are clamped in all their nodes. The approaching part is not strictly necessary, but it is used to provide symmetry to the structure.

To calculate the bridge acceleration, three dynamic analysis steps are implemented, corresponding to the mass approaching, crossing and leaving the bridge, representing the entrance, traverse and the leaving phase displayed in Figure 4.3.

The stiffness (or equivalently the elastic modulus E) of the elements at the damage location is reduced [29] to implement damage on the bridge. The locations $L/2$ and

Table 4.2: The healthy and damage scenarios that have been investigated numerically

Test case	vehicle-bridge mass ratio (%)	Stiffness reduction (%)	damaged element (No.)
Baseline simulation			
1	10	-	-
Variable operational condition			
2	5	-	-
3	15	-	-
4	20	-	-
5	25	-	-
Damage type 1 at L/2			
6	10	30	1
7	10	50	1
8	10	70	1
Damage type 1 at 3L/4			
9	10	30	1
10	10	50	1
11	10	70	1
Damage type 2 around mid-span			
12	10	30	2
13	10	30	3

$3L/4$ are selected to introduce the damage. Two types of damage with different severity are investigated based on the assessment of Boyne viaduct as a case study [42]. For the first type, damage grows locally, similar to pitting corrosion or a loose connection. This phenomenon is implemented by reducing the stiffness of a single element. For the second type, the damage propagates along the elements, similar to general corrosion. This damage is implemented by reducing the stiffness of multiple elements around the damage location.

In addition to the baseline simulation, four groups of simulations are executed to verify the proposed approach for various operational conditions and health states. In the first group, moving masses equal to 5%, 15%, 20%, and 25% of the bridge mass are used, and the bridge is considered healthy. In the second group, local damage is implemented with different severities at location $L/2$ (mid-span). In the third group, the location of the damage is moved to $3L/4$. Group four is implemented to investigate propagated damage around the bridge mid-span. Table 4.2 provides an overview of the four groups of simulations that aim at investigating the sensitivity and performance of the proposed damage detection approach for various VBI system states.

4.4   Results and discussion

4.4.1   Baseline simulation

The bridge forced, and free vibration responses are calculated using the proposed VBI model according to the baseline simulation in Table 4.2. The first Eigen frequency of the bridge model obtained in Abaqus is 2.1 Hz. This frequency matches well with the analytical value of 2.08. Moreover, to verify WSST, as the accuracy of the applied technique, the bridge frequency extracted from the leaving phase by applying WSST is equal to 2.1 Hz, which is well matched with the analytical value.

Figure 4.5 shows the simulated VBI system response evaluated at the bridge mid-span for the baseline simulation.

The moving mass induces non-stationarity into the signal, meaning that the bridge fundamental frequency changes in time. The bridge frequency variation is not visible in the time signal, since the variation is small. The figure looks very similar to a typical field measurement on a bridge where the level of the bridge acceleration and also the noise during the traverse phase are higher than in the leaving phase. The

high frequency component appearing in the traverse phase is an artificial effect of the numerical simulation that corresponds to the inverse of the time taken by the mass for passing a numerical grid. This effect does not exist in the field data. However, usually bridge vibration field data looks noisy due to the vibration traces of the train and the track components. The first step of the proposed approach, as presented in the section Phase separation, is required since the bridge forced and free vibration responses are in practice not recognizable from the time domain signal as presented in Figure 4.3. However, this is not the case for the numerical simulation where the entrance, traverse and the leaving phase response are implemented in three different analysis steps. The signal for the entrance phase is a zero acceleration vector which is not plotted and not used for this study. The traverse phase and the leaving phase will be analyzed based on the proposed approach in the section Methodology.

The second step is to extract the bridge fundamental frequency by applying WSST to the signal of the leaving phase. Figure 4.6 is the time-frequency representation of the leaving phase response. This representation shows the distribution of the energy over the frequency range at each time instance.

It shows the bridge frequency is constant at 2.1 Hz as expected for a stationary signal. WSST is then applied to the traverse phase response to trace back the frequency component of 2.1 Hz during the traverse phase. The time frequency representation of the traverse phase is shown in Figure 4.6. The bridge instantaneous frequency as a
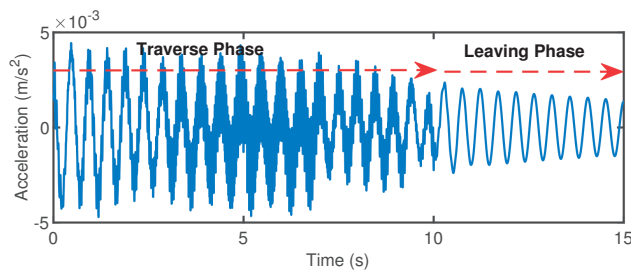
Figure 4.5: The forced (traverse phase) and the free (leaving phase) vibration of the baseline simulation response calculated at the bridge mid-span.
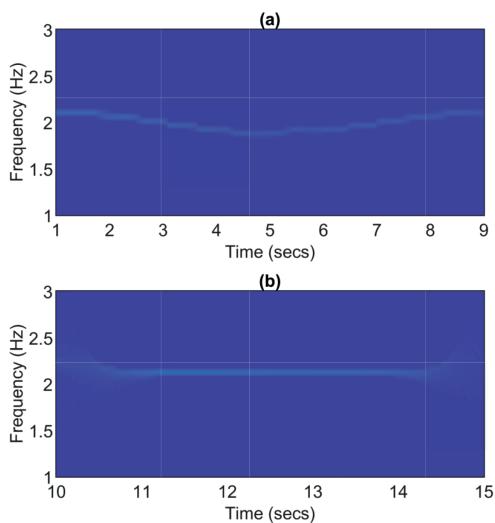
Figure 4.6: The instantaneous frequency of the healthy bridge extracted by WSST from (a) the traverse phase, (b) the leaving phase

time-frequency array can be obtained by extracting the frequency ridge. The bridge baseline instantaneous frequency, $\mathcal{F}_b$ is presented in Figure 4.7 in blue.

$\mathcal{F}_b$ is presented for the time period 1-9 s instead of 0-10 s. The reason is to avoid signal end effects which might cause disruption of the frequency ridge. It can also
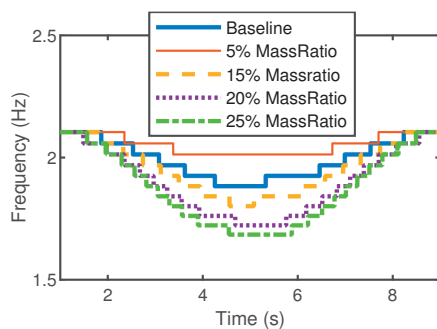
Figure 4.7: The instantaneous frequency of the bridge forced response induced by different vehicle mass.

be observed that the time frequency array is step-wise rather than continuous due to the limited frequency resolution of the WSST results. $\mathcal{F}_b$ as presented in Figure 4.7 displays that the bridge resonance when the vehicle passes the bridge mid-span ($t = 5$ s) is 1.9 Hz. It shows that the operational condition (added mass) has indeed reduced the bridge natural frequency by 9.5%.

4.4.2 Variable operational condition

Up to this stage, the first test case is performed, and the system baseline frequency variation corresponding to the healthy state of the bridge is provided. It has already been mentioned that the resonances of a VBI system can deviate from the baseline either due to the dynamic interaction between the sub-systems or due to damage. In this section, test cases 2-5 are defined such that the mass, as the operational condition, is changed to 0.5, 1.5, 2, and 2.5 times the value used in the baseline simulation (test case 1). Figure 4.7 shows the extracted instantaneous frequency for the baseline and variable operational condition test cases.

It can be clearly seen that the mass change leads to a different system and, subsequently, a different time-frequency content compared to the baseline. Moreover, it can be seen that the curvature of the instantaneous frequency of the systems corresponds to the vehicle mass ratios. In Figure 4.7, the top instantaneous frequency (plotted in red) is for the system with the lowest vehicle-bridge mass ratio (5%) and the bottom one (plotted in green) is for the system with the highest vehicle-bridge mass ratio (25%).

For a test case, once the obtained instantaneous frequency, $\mathcal{F}_m$ is different from the baseline instantaneous frequency, $\mathcal{F}_b$ the shape correlation, ρ and the magnitude variation, δ should be investigated. ρ and δ are calculated for $\mathcal{F}_b$ and $\mathcal{F}_m$ for a test case by utilizing Equation (4.4) and Equation (5.1) respectively. For the variable operational condition test cases (2-5) with the mass ratios of 5%, 15%, 20%, and 25% the shape correlation coefficients are equal to 0.94, 0.98, 0.97, 0.97 respectively and the magnitude variation yielding the values -0.56, 0.35, 0.91 and 1.14 respectively. Apart from test case 2, for test cases 3-5, the shape correlation coefficients are larger than 0.97 and the magnitude variation values are larger than 0.2. For the intact bridge, when the vehicle mass changes $\mathcal{F}_b$ is affected globally as displayed in Figure 4.7. Therefore, The magnitude variation which calculates the bounded area between $\mathcal{F}_b$ and $\mathcal{F}_m$ (Equation (5.1)) becomes a larger value in comparison with a local $\mathcal{F}_b$ deviation like damage.

It can be concluded that the high correlation coefficients, $\rho \geq 0.97$ and a relatively large magnitude variation, $\delta \geq 0.2$ imply that the source of the frequency change is the operational condition.

The shape correlation of test case 2 is 0.94 which is lower than the shape correlation coefficients of test cases 3-5 and the magnitude variation is negative. The denominator of Equation (5.1) is always a positive value, however, the numerator can be negative or positive depending on $\mathcal{F}_b$ and $\mathcal{F}_m$. For the second test case the mass ratio (5%) is smaller than the mass ratio of the baseline test case (10%). As displayed in (Figure 4.7), $\mathcal{F}_m$ for test case 2 appears above the baseline, $\mathcal{F}_b$ and accordingly, the magnitude variation becomes negative. A negative magnitude variation implies a change in operational condition or an increase of the system stiffness which is not expected in the case of damage. Therefore, regarding the 13 test cases of the current study, the source of the baseline deviation for test case with negative magnitude variation is the operational condition.

4.4.3   Variable damage severity at the bridge mid-span

This section investigates test cases 6-8 corresponding to three damage scenarios. The scenarios are defined such that the bridge mid-span element is damaged with different severity levels. All the steps of the proposed approach are performed, and $\mathcal{F}_m$ for each damage case is presented in Figure 4.8.

It can be seen that for the 30% , 50% and 70% damage, $\mathcal{F}_m$ deviates from $\mathcal{F}_b$ around the time when the moving mass crosses the damaged element. The correlation

Figure 4.8: The bridge baseline $\mathcal{F}_b$ and $\mathcal{F}_m$s for the bridge having damage at $L/2$ caused by various damage severity levels

coefficients, ρ for the test cases corresponding to the 30%, 50%, and 70% damage cases are 0.98, 0.92, and 0.90, respectively. $\mathcal{F}_m$ of the first damage case still highly correlates with the baseline due to the small amount of damage. Therefore, the shape correlation is not sufficient to reveal the source of the baseline deviation. The baseline magnitude variation is required. δ for test cases 6-8 are equal to 0.08, 0.30, and 0.48, respectively.

Figure 4.9 displays the shape correlation and the magnitude variation for all test cases. Test case 6-8 are displayed with red marker in Figure 4.9. In Figure 4.9 different test scenarios are displayed in different colors, and the marker size corresponds to the damage size. It can be seen that by increasing damage, the shape correlation decreases, and the magnitude variation increases. However, the scale of the increase in magnitude variation for the damaged cases (test cases 6-8) is different from those for variable operational conditions (test cases 1-5). A small magnitude variation implies a local variation like damage. In contrast, a relatively large magnitude variation, $\delta \geq 0.2$ is caused by the operational condition where the baseline instantaneous frequency changes along the entire bridge span. For example, consider test case 3, where the vehicle mass is changed, and test case 6, when the bridge mid-span element is damaged. For both test cases, the shape correlation value is the same and equal to 0.98. However, the
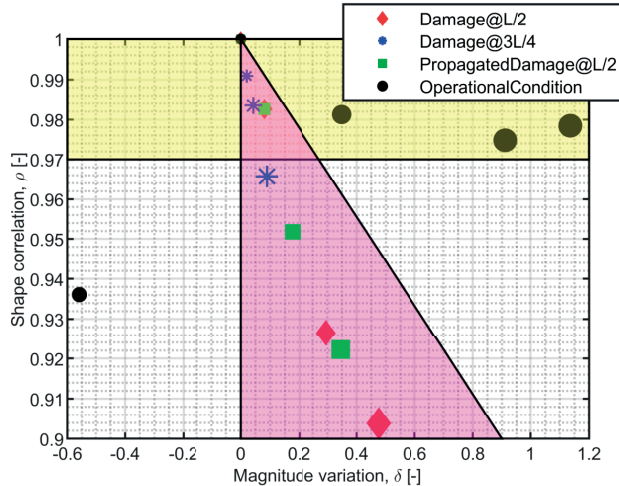
Figure 4.9: The magnitude variation and the shape correlation for the damaged test cases and the variable operational conditions test cases.

magnitude variation for test case 2, where the vehicle mass is changed, is 0.35, and it is much larger than 0.08, the magnitude variation of test case 6, where the bridge is damaged at mid-span. Therefore, for the cases where the shape correlation, ρ is greater or equal to 0.97 the magnitude variation, δ is the determining factor. For the damage cases, by increasing the damage, ρ decreases and δ does not strongly increase as displayed by the steep trend line with pink background in Figure 4.9. However, for the healthy bridge by increasing the operational condition, ρ remains high ($\rho \geq 0.97$) and δ continues to increase ($\delta \geq 0.2$) displayed by the near horizontal trend line with yellow background in Figure 4.9. For a case with high shape correlation ($\rho >= 0.97$) and small magnitude variation ($\delta < 0.2$), where the two background colors overlap in Figure 4.9, the method cannot distinguish if the baseline deviation is caused by change in operational condition or damaged. That is the limit of the sensitivity of the proposed method.

4.4.4 Variable damage severity at the bridge three-quarter

The objective of this part is to investigate the performance of the proposed damage detection technique for the cases where the damage location is far from the sensor node, which in this case is assumed to be located at mid-span. Test cases 9-11 are investigated in this section, where the damage size and severity are similar to the previous section. The only difference is that the damage is relocated to $3L/4$ of the bridge span while the measurement point of the vibration is at the bridge mid-span. The damage location is 12.5 m (25% of the bridge span) away from the measurement point. The instantaneous frequency corresponding to each damage severity is extracted and displayed in Figure 4.10. The correlation coefficients corresponding to the 30%, 50% and 70% damage at $3L/4$ are equal to 0.99, 0.98 and 0.96. The correlation coefficients for the damage cases at the three-quarter span length of the bridge are higher than the shape correlation for the damage cases at the bridge mid-span. It is explained by the distance between damage and observation point and by the fact that the change of the baseline frequency is already smaller at that location. Since the first vibration mode of the bridge has its maximum deflection at the mid-span, the mid-span will also be the most sensitive place to capture the dynamic variation properties. The performance of the method can be improved in the future by adding more sensors.

The magnitude variation values for test cases 9-11 are 0.02, 0.04, and 0.09, where the small magnitude variation values imply the local variation like damage. For example, consider test case 3 and 10, where the shape correlation for both is 0.98. However, the magnitude variation of test case 3 corresponding to the change of operational condition is 0.35, which is much larger than 0.04, the magnitude variation of the damaged bridge. Therefore, the baseline frequency deviation is caused by damage when a combination of a decrease in correlation coefficient and a limited magnitude variation occurs. It can be concluded that even for the cases where the damage is relatively small and far from the bridge mid-span, the proposed method can still properly detect the different damage severity levels.

4.4.5 Variable damage length at the bridge mid-span

This final subsection aims at investigating an extended damage scenario around mid-span. To do so, the 30% stiffness reduction at the mid-element is extended to two and three adjacent elements. For each case, the instantaneous frequency is plotted in Figure 4.11.

The results of test cases for the propagated damage at the bridge mid-span are plotted in green in Figure 4.9. The shape correlation coefficient values for test cases 6,12, and 13 corresponding to the bridge having one, two, and three damaged elements at the bridge mid-span are 0.98, 0.95, and 0.92. The magnitude variation values for test cases 6, 12, and 13 are equal to 0.08, 0.18, and 0.35. For test cases 12 and 13, the shape correlation is smaller than 0.97, implying that the baseline instantaneous
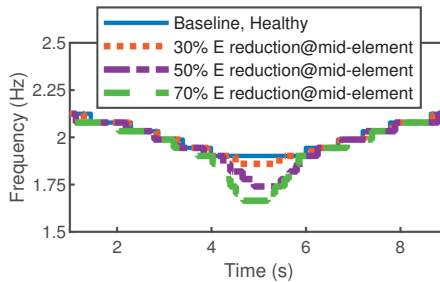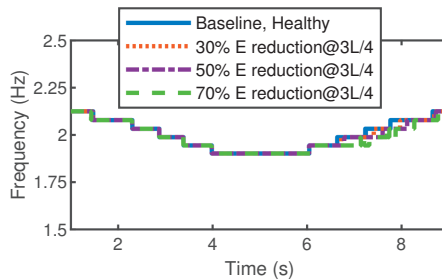

Figure 4.10: The bridge baseline $\mathcal{F}_b$ and $\mathcal{F}_m$s for the bridge having damage at $3L/4$ caused by various damage severity levels

frequency deviates due to damage. For test case 6, where the shape correlation is high, 0.98, the magnitude variation is 0.08, and it is smaller than 0.2. Therefore it represents a damaged bridge.

4.5   Summary

The results of the two proposed features; the shape correlation (ρ) and the magnitude variation (δ) between the baseline ($\mathcal{F}_b$) and a measured instantaneous frequency ($\mathcal{F}_m$ for test cases 2-13 are summarized in Table 4.3. Figure 4.9 shows the magnitude variation versus the shape correlation for all test cases. It can be seen that the pattern of the results of the damaged cases is different from the cases with varying operational condition. The vehicles with different masses are displayed with the black circles where the increasing size of the marker implements the increase of the mass ratio from 10% to 15%, 20% and 25%. By increasing the mass ratio, the magnitude variation increases where the shape correlations are about 0.98. Regarding the damage cases, it can be seen that by increasing damage severity or length, the shape correlation coefficient decreases, whereas, the magnitude variation remains relatively low. Moreover, the shape correlation coefficients for the damage cases at the three-quarters length of the bridge are higher than the shape correlations coefficients for the same amount of damage but at the bridge mid-span.
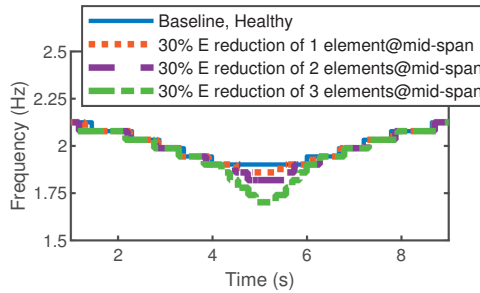
Figure 4.11: The bridge baseline $\mathcal{F}_b$ and $\mathcal{F}_m$s for the bridge having various sizes of damage around $L/2$

Table 4.3: The healthy and damage scenarios that have been investigated numerically

Test case	vehicle-bridge mass ratio (%)	Stiffness reduction (%)	damaged element (No.)	ρ	δ
Baseline simulation					
1	10	-	-	1	0
Variable operational condition					
2	5	-	-	0.94	-0.56
3	15	-	-	0.98	0.35
4	20	-	-	0.97	0.91
5	25	-	-	0.97	1.14
Damage type 1 at L/2					
6	10	30	1	0.98	0.08
7	10	50	1	0.92	0.30
8	10	70	1	0.90	0.48
Damage type 1 at 3L/4					
9	10	30	1	0.99	0.02
10	10	50	1	0.98	0.04
11	10	70	1	0.96	0.09
Damage type 2 around mid-span					
12	10	30	2	0.95	0.18
13	10	30	3	0.92	0.35

4.6 Performance of the WSST versus FFT and CWT

A comparison between the proposed approach and the conventional technique, using the FFT of the leaving phase response, is performed to demonstrate the first three axioms of the proposed method addressed in the Introduction. Conventionally, the change in the natural frequencies of the bridge obtained from the free vibration response is used as an indication of damage. Figure 4.12b shows that the bridge natural frequency does not change for different vehicle masses, whereas a slight frequency reduction for the most severe damage case can be seen in Figure 4.12d. This observation verifies the first axiom of the proposed method, stating that the bridge free vibration mainly reflects the global dynamic properties. Moreover, Figure 4.12b and Figure 4.12d show that the different cases yield a clear difference in the magnitude of the Power Spectral Density (PSD). However, this does not distinguish the effects of the damage and operational conditions. Figure 4.12a and Figure 4.12c show the frequency content of the traverse
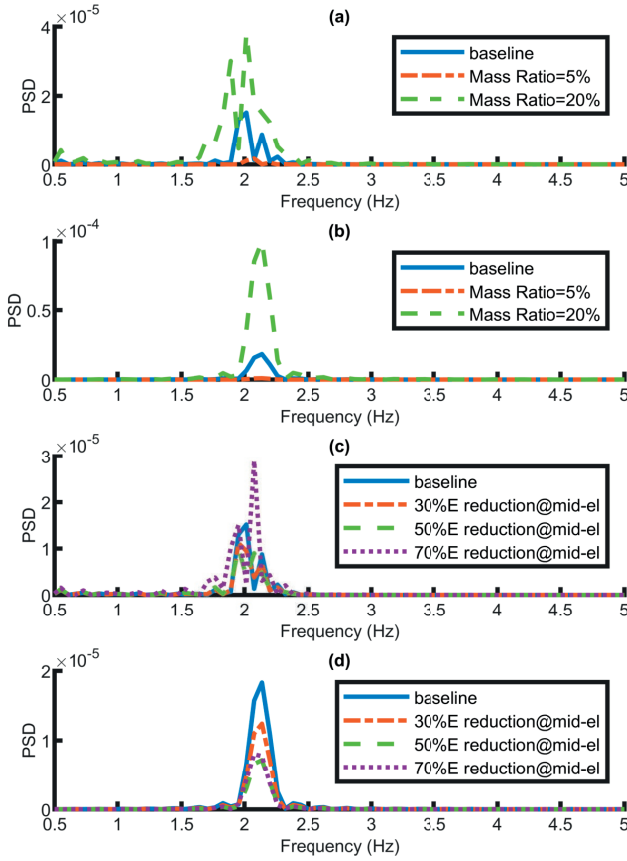
Figure 4.12: The PSD of a) the traverse phase for the variable operational conditions, b) the leaving phase response for variable operational conditions, c) the traverse phase in case of damage and, d) the leaving phase in case of damage.

phase for variable operational conditions and the damaged cases, respectively.

The figures show that the traverse phase response is much more sensitive than the free vibration response to both sources since the change of the baseline peak frequencies is more visible in the traverse phase, and this observation verifies the third axiom of the

proposed method. However, using only the frequency content of the VBI response is not adequate and reliable since the traverse phase response represents a non-stationary response which means that the frequency content of the signal changes over time. Therefore, looking at the frequency content and interpreting the changes of the peak frequencies is not informative to learn about the changes caused by time-dependent and local events such as damage. This observation verifies the second axiom, which utilizes the Instantaneous Frequency of the VBI system instead of the resonance frequency.

As addressed in the last axiom of the proposed method, a high-resolution time-frequency analysis technique is required to extract the system instantaneous frequency, as the enabler, as accurately as possible. Therefore, the performance of the WSST is compared with CWT as the widely used time-frequency technique. To provide consistency and re-producibility of the results, Matlab functions with default settings are utilized for both techniques. Figure 4.13 shows the instantaneous frequency extracted by the WSST and CWT for the different conditions of the bridge. Figure 4.13a shows the instantaneous frequency of the healthy bridge extracted by WSST and CWT in red and black, respectively.

It can be seen that the resolution of the extracted frequency ridge by the CWT is much lower than the IF extracted by WSST. The fundamental difference between the CWT and WSST is about the frequency resolution and the interested readers are referred to [41]. Regarding the damaged bridge Figure 4.8 has already shown that the shape of the bridge instantaneous frequency changes due to 30% and 50% damage at the bridge mid-span element. However, it can be seen in Figure 4.13b and Figure 4.13c that the frequency ridge extracted by CWT for these two damage cases are nearly similar. Therefore, it can be concluded that WSST outperforms CWT to detect local events like damage.

4.7 Performance of the WSST with noise

Noise is the main difference between a measured bridge response and the corresponding simulated response. Noise is a determining factor that challenges the damage detection techniques based on finding response singularities and wavelet coefficients. However, those techniques are verified numerically or experimentally in a controlled laboratory
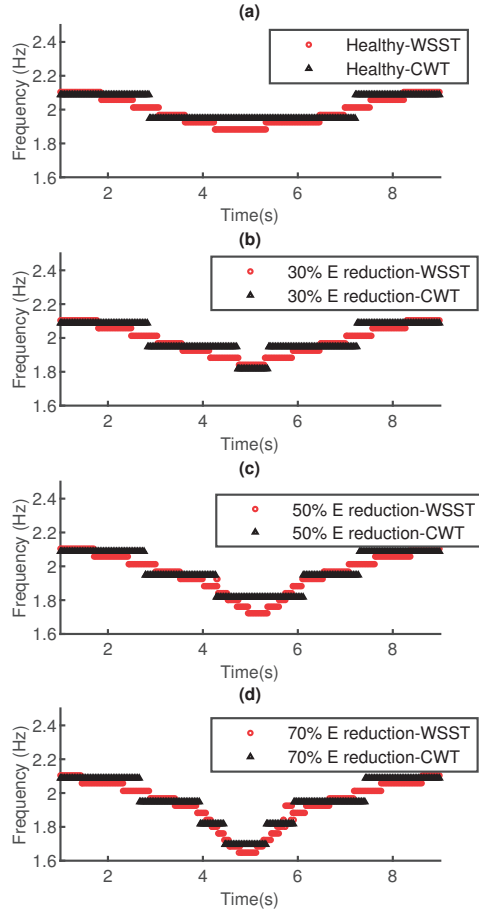
Figure 4.13: The bridge instantaneous frequency extracted by WSST and CWT for a) the healthy bridge, an the damaged bridge with b) 30% c) 50% d) 70% E reduction at the mid-span element.

environment. When the damage-sensitive feature is defined based on the signal disruption once damage occurs, the performance of the techniques in distinguishing the

damage from the noise is questionable. However, it is not the case for the current study's proposed approach, where the VBI system's instantaneous frequency, which is in a low frequency range, is utilized as the damage-sensitive feature. White noise corresponding to the signal-to-noise ratio (SNR) of Boyne viaduct (as the case study) equal to 10 is added to the simulated bridge response to verify the performance of the proposed approach. Figure 4.14 presents the bridge instantaneous frequency extracted from the simulated signal without noise in color and with noise in black. It can be seen that the noise has not affected the bridge instantaneous frequency. For further investigation, higher noise levels with lower SNR are added to the response. Three SNR levels, 10, 5, and 0.1 are added to the bridge simulated response in healthy and damaged conditions. To evaluate the influence of the added noise, the shape correlation coefficient between the bridge instantaneous frequency extracted from the traverse phase response with the different noise levels is calculated and presented in Figure 4.15. It can be seen that the correlation coefficients corresponding to the three noise levels and the four bridge conditions are similar and not dispersed, which verifies the robustness of the WSST concerning noise. Therefore, it can be concluded that the proposed damage detection technique is not sensitive to noise.

It should be noted that the proposed method has been applied to a series of simulated signals for which the results are promising. The combination of the variable operational condition and damage will be considered in future work. However, based on the current study results, it is believed that for the case of the combined variables, the proposed method can distinguish the variable operational condition and the damage, although the proposed damage index needs to be adapted to the new situation in future work.

4.8   Conclusion

A method has been proposed that extends the traditional damage detection techniques based on the bridge natural frequencies extracted from the bridge free vibration. This study presented a concept for damage detection in (railway) bridges based on the instantaneous frequency analysis of the bridge forced and free vibration responses. Within this concept, based on the bridge natural frequency extracted from the bridge free vibration f_b , a healthy baseline ($\mathcal{F}_b$) was obtained by applying the Wavelet Synchrosqueezed
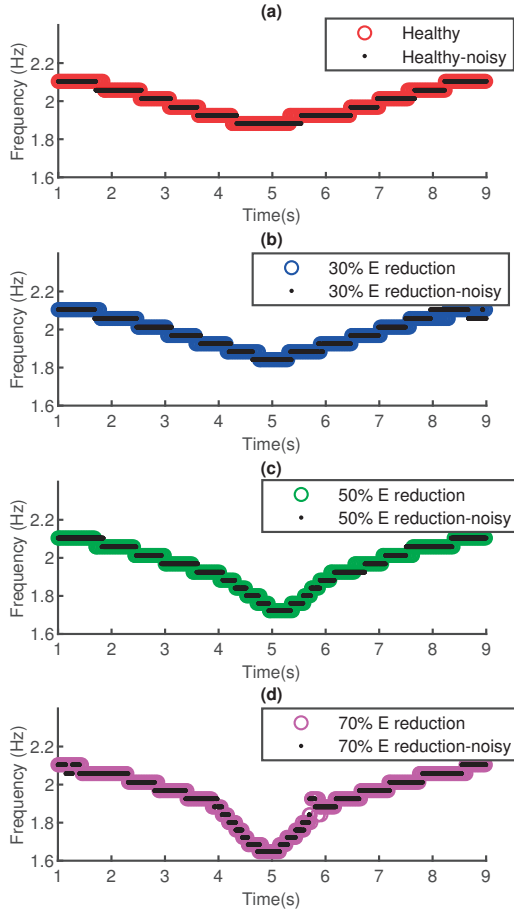
Figure 4.14: The bridge instantaneous frequency extracted from the simulated signal with and without noise for a) the healthy bridge, an the damaged bridge with b) 30% c) 50% d) 70% E reduction at the mid-span element.

transform (WSST) to the bridge forced vibration response. The objective was to understand how well WSST is capable of filtering information related to damage and
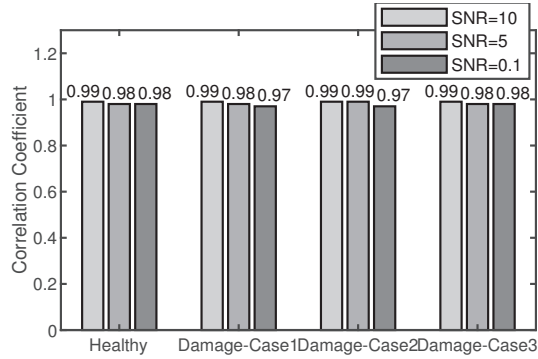
Figure 4.15: The correlation coefficient between the bridge baseline instantaneous frequency extracted from the bridge simulated signals without noise and with noise.

separate it from other sources of variation in the signal. The shape correlation ρ and the magnitude variation δ proposed to distinguish the global and the local deviation of the bridge baseline instantaneous frequency induced by variable operational conditions and damage, respectively. Finally, if the source of the baseline deviation is damage, then the magnitude variation, δ can be used as a damage index. The proposed damage index is a preliminary step towards damage quantification. Furthermore, for the damaged test cases, the local deviation of the baseline instantaneous frequency around the damage location shows the potential of the proposed method for damage localization. However, damage localization is out of the scope of the current study. Including the baseline simulation, 13 test cases have been analyzed to verify the performance of the proposed method. The results show that;

- Information on the time-variant resonance frequency is highly valuable and more informative than the natural frequency, extracted from the bridge free-decay, to detect local events like damage.

- The instantaneous frequency of the vehicle-bridge interaction response obtained with the WSST outperforms the CWT due to the higher resolution for the lower frequency range.

- The bridge baseline instantaneous frequency deviates due to damage or operational condition. The damage can be distinguished from the variation of the

operational condition using the combination of the shape correlation coefficients (ρ) and the magnitude variation (δ).

- For damaged bridge, the magnitude variation (δ) is a first step towards quantification of the damage.

The current study investigated a moving mass model. A next step is to perform an experimental study to verify the findings. Moreover, future work will extend the model to more realistic moving masses with a dual suspension system and more complex yet more realistic dynamic behavior.

4.9 Acknowledgments

Bibliography

[1] M. I. Friswell, Damage identification using inverse methods, Philos Trans A Math Phys Eng Sci 365 (1851) (2007) 393–410. `doi:10.1098/rsta.2006.1930`.
URL `https://www.ncbi.nlm.nih.gov/pubmed/17255045`

[2] R. V. Farahani, D. Penumadu, Damage identification of a full-scale five-girder bridge using time-series analysis of vibration data, Engineering Structures 115 (2016) 129–139. `doi:10.1016/j.engstruct.2016.02.008`.
URL `http://www.sciencedirect.com/science/article/pii/S0141029616000900`

[3] J. Li, S. S. Law, H. Hao, Improved damage identification in bridge structures subject to moving loads: Numerical and experimental studies, International Journal of Mechanical Sciences 74 (2013) 99–111. `doi:10.1016/j.ijmecsci.2013.05.002`.

[4] D. Li, Y. Wang, W.-J. Yan, W.-X. Ren, Acoustic emission wave classification for rail crack monitoring based on synchrosqueezed wavelet transform and multi-branch convolutional neural network, Structural Health Monitoring 20 (4) (2020) 1563–1582. `doi:10.1177/1475921720922797`.

[5] L. Sun, Z. Shang, Y. Xia, S. Bhowmick, S. Nagarajaiah, Review of bridge structural health monitoring aided by big data and artificial intelligence: From condition assessment to damage detection, Journal of Structural Engineering 146 (5) (2020). `doi:10.1061/(asce)st.1943-541x.0002535`.

[6] A. Malekjafarian, F. Golpayegani, C. Moloney, S. Clarke, A machine learning approach to bridge-damage detection using responses measured on a passing vehicle, Sensors (Basel) 19 (18) (2019). `doi:10.3390/s19184035`.
URL `https://www.ncbi.nlm.nih.gov/pubmed/31546759`

[7] M. Silva, A. Santos, E. Figueiredo, R. Santos, C. Sales, J. C. W. A. Costa, A novel unsupervised approach based on a genetic algorithm for structural damage detection in bridges, Engineering Applications of Artificial Intelligence 52 (2016) 168–180. `doi:10.1016/j.engappai.2016.03.002`.
URL `<GotoISI>://WOS:000379631100016`

[8] G. Comanducci, F. Magalhaes, F. Ubertini, A. Cunha, On vibration-based damage detection by multivariate statistical techniques: Application to a long-span arch bridge, Structural Health Monitoring-an International Journal 15 (5) (2016) 505–524. doi:10.1177/1475921716650630.
URL <GotoISI>://WOS:000383039500002

[9] A. Santos, E. Figueiredo, M. Silva, R. Santos, C. Sales, J. C. W. A. Costa, Genetic-based em algorithm to improve the robustness of gaussian mixture models for damage detection in bridges, Structural Control & Health Monitoring 24 (3) (2017). doi:ARTNe188610.1002/stc.1886.
URL <GotoISI>://WOS:000394426500012

[10] H. Babajanian Bisheh, G. Ghodrati Amiri, M. Nekooei, E. Darvishan, Damage detection of a cable-stayed bridge based on combining effective intrinsic mode functions of empirical mode decomposition using the feature selection technique, Inverse Problems in Science and Engineering 29 (6) (2020) 861–881. doi:10.1080/17415977.2020.1814280.

[11] M. B. P. Scott W. Doebling, Charles R. Farrar, A summary review of vibration-based damage identification methods, The Shock and Vibration Digest (1998).

[12] J. J. Moughty, J. R. Casas, A state of the art review of modal-based damage detection in bridges: Development, challenges, and solutions, Applied Sciences-Basel 7 (5) (2017). doi:ARTN51010.3390/app7050510.
URL <GotoISI>://WOS:000404449000074

[13] M. Dilena, M. P. Limongelli, A. Morassi, Damage localization in bridges via the frf interpolation method, Mechanical Systems and Signal Processing 52-53 (2015) 162–180. doi:10.1016/j.ymssp.2014.08.014.

[14] C. Rainieri, G. Fabbrocino, Operational Modal Analysis of Civil Engineering Structures, 2014. doi:10.1007/978-1-4939-0767-0.

[15] L. Zhang, R. Brincker, An overview of operational modal analysis: Major development and issues, in: International Operational Modal Analysis Conference, pp. 179–190.

[16] A. P. Ojeda, Matlab implementation of an operational modal analysis technique for vibration-based structural health monitoring, Master of science (2012).
URL http://hdl.handle.net/1721.1/74412

[17] K.-C. Chang, C.-W. Kim, Modal-parameter identification and vibration-based damage detection of a damaged steel truss bridge, Elsevier (2016). doi:122(2016) 156173.

[18] D. Cantero, M. Ülker Kaustell, R. Karoumi, Time–frequency analysis of railway bridge response in forced vibration, Mechanical Systems and Signal Processing 76-77 (2016) 518–530. doi:10.1016/j.ymssp.2016.01.016.

[19] J. U. N. Chen, Application of empirical mode decomposition in structural health monitoring: Some experience, Advances in Adaptive Data Analysis 01 (04) (2009) 601–621. doi:10.1142/s1793536909000321.

[20] A. Gonza´lez, D. Hester, An investigation into the acceleration response of a damaged beam-type structure to a moving force, Journal of Sound and Vibration (2013). doi:10.1016/j.jsv.2013.01.024.

[21] J. Meredith, A. Gonzalez, D. Hester, Empirical mode decomposition of the acceleration response of a prismatic beam subject to a moving load to identify multiple damage locations, Shock and Vibration 19 (5) (2012) 845–856. doi: 10.3233/Sav-2012-0693.
URL <GotoISI>://WOS:000309518800009

[22] D. Hester, A. Gonzalez, A wavelet-based damage detection algorithm based on bridge acceleration response to a vehicle, Mechanical Systems and Signal Processing 28 (2012) 145–166. doi:10.1016/j.ymssp.2011.06.007.
URL <GotoISI>://WOS:000301549900011

[23] N. Roveri, A. Carcaterra, Damage detection in structures under traveling loads by hilbert-huang transform, Mechanical Systems and Signal Processing 28 (2012) 128–144. doi:10.1016/j.ymssp.2011.06.018.
URL <GotoISI>://WOS:000301549900010

[24] H. Aied, A. Gonzalez, D. Cantero, Identification of sudden stiffness changes in the acceleration response of a bridge to moving loads using ensemble empirical mode decomposition, Mechanical Systems and Signal Processing 66-67 (2016) 314–338. `doi:10.1016/j.ymssp.2015.05.027`.
URL `<GotoISI>://WOS:000362861700020`

[25] E. Obrien, C. Carey, J. Keenahan, Bridge damage detection using ambient traffic and moving force identification, Structural Control and Health Monitoring 22 (12) (2015) 1396–1407. `doi:10.1002/stc.1749`.

[26] E. J. Obrien, P. J. McGetrick, A. Gonzalez, A drive-by inspection system via vehicle moving force identification, Smart Structures and Systems 13 (5) (2014) 821–848. `doi:10.12989/sss.2014.13.5.821`.

[27] L. Yu, T. H. T. Chan, Recent research on identification of moving loads on bridges, Journal of Sound and Vibration 305 (1-2) (2007) 3–21. `doi:10.1016/j.jsv.2007.03.057`.
URL `<GotoISI>://WOS:000247904000002`

[28] F. Huseynov, C. Kim, E. J. Obrien, J. M. W. Brownjohn, D. Hester, K. C. Chang, Bridge damage detection using rotation measurements – experimental validation, Mechanical Systems and Signal Processing 135 (2020). `doi:10.1016/j.ymssp.2019.106380`.

[29] W. Zhang, J. Li, H. Hao, H. Ma, Damage detection in bridge structures under moving loads with phase trajectory change of multi-type vibration measurements, Mechanical Systems and Signal Processing 87 (2017) 410–425. `doi:10.1016/j.ymssp.2016.10.035`.

[30] W.-Y. He, S. Zhu, Moving load-induced response of damaged beam and its application in damage localization, Journal of Vibration and Control 22 (16) (2016) 3601–3617. `doi:10.1177/1077546314564587`.

[31] Z. Yu, H. Xia, J. M. Goicolea, C. Xia, Bridge damage identification from moving load induced deflection based on wavelet transform and lipschitz exponent, International Journal of Structural Stability and Dynamics 16 (05) (2016). `doi:10.1142/s0219455415500030`.

[32] K. V. Nguyen, Comparison studies of open and breathing crack detections of a beam-like bridge subjected to a moving vehicle, Engineering Structures 51 (2013) 306–314. `doi:10.1016/j.engstruct.2013.01.018`.

[33] A. Khorram, M. Rezaeian, F. Bakhtiari-Nejad, Multiple cracks detection in a beam subjected to a moving load using wavelet analysis combined with factorial design, European Journal of Mechanics - A/Solids 40 (2013) 97–113. `doi:10.1016/j.euromechsol.2012.12.012`.

[34] W. W. Zhang, J. Geng, Z. L. Zhao, Z. H. Wang, Numerical studies on wavelet-based crack detection based on velocity response of a beam subjected to moving load, Damage Assessment of Structures X, Pts 1 and 2 569-570 (2013) 854–+. `doi:10.4028/www.scientific.net/KEM.569-570.854`.
URL `<GotoISI>://WOS:000326409000106`

[35] V. Pakrashi, A. O'Connor, B. Basu, A bridge-vehicle interaction based experimental investigation of damage evolution, Structural Health Monitoring: An International Journal 9 (4) (2009) 285–296. `doi:10.1177/1475921709352147`.

[36] X. Q. Zhu, S. S. Law, Wavelet-based crack identification of bridge beam from operational deflection time history, International Journal of Solids and Structures 43 (7-8) (2006) 2299–2317. `doi:10.1016/j.ijsolstr.2005.07.024`.
URL `<GotoISI>://WOS:000236608200025`

[37] V. Pakrashi, B. Basu, A. O' Connor, Structural damage detection and calibration using a wavelet–kurtosis technique, Engineering Structures 29 (9) (2007) 2097–2108. `doi:10.1016/j.engstruct.2006.10.013`.

[38] W. Zhai, X. Sun, A detailed model for investigating vertical interaction between railway vehicle and track, Vehicle System Dynamics 23 (sup1) (2008) 603–615. `doi:10.1080/00423119308969544`.

[39] W. Zhai, Z. Han, Z. Chen, L. Ling, S. Zhu, Train–track–bridge dynamic interaction: a state-of-the-art review, Vehicle System Dynamics 57 (7) (2019) 984–1027. `doi:10.1080/00423114.2019.1605085`.

[40] X. H. He, X. G. Hua, Z. Q. Chen, F. L. Huang, Emd-based random decrement technique for modal parameter identification of an existing railway bridge, Engineering Structures 33 (4) (2011) 1348–1356. doi:10.1016/j.engstruct.2011.01.012. URL <GotoISI>://WOS:000289026900028

[41] N. Mostafa, D. Di Maio, R. Loendersloot, T. Tinga, Extracting the time-dependent resonances of a vehicle–bridge interacting system by wavelet synchrosqueezed transform, Structural Control and Health Monitoring (2021). doi:10.1002/stc.2833.

[42] L. Connolly, L. Prendergast, N. Mostafa, R. Loendersloot, Report on assessment of bridges, Report (2017).

[43] Y. Lu, L. Mao, P. Woodward, Frequency characteristics of railway bridge response to moving trains with consideration of train mass, Engineering Structures 42 (2012) 9–22. doi:10.1016/j.engstruct.2012.04.007.

[44] D. P. Connolly, G. Kouroussis, O. Laghrouche, C. L. Ho, M. C. Forde, Benchmarking railway vibrations – track, vehicle, ground and building effects, Construction and Building Materials 92 (2015) 64–81. doi:10.1016/j.conbuildmat.2014.07.042.

[45] I. Daubechies, S. Maes, A nonlinear squeezing of the continuous wavelet transform based on auditory nerve models, 1st Edition, CRC Press, New York, 1996, book section 20, pp. 527–546. doi:10.1201/9780203734032.

[46] I. Daubechies, J. F. Lu, H. T. Wu, Synchrosqueezed wavelet transforms: An empirical mode decomposition-like tool, Applied and Computational Harmonic Analysis 30 (2) (2011) 243–261. doi:10.1016/j.acha.2010.08.002. URL <GotoISI>://WOS:000286705400008

[47] W. Kirch, Encyclopedia of Public Health, Springer Netherlands, 2008. doi:10.1007/978-1-4020-5614-7_2569. URL https://doi.org/10.1007/978-1-4020-5614-7_2569

[48] M. A. Mahmoud, Effect of cracks on the dynamic response of a simple beam subject to a moving load, Proceedings of the Institution of Mechanical Engineers

Part F-Journal of Rail and Rapid Transit 215 (3) (2001) 207–215. `doi:Doi10.1243/0954409011531521`.
URL `<GotoISI>://WOS:000172080600006`

[49] A. Saleeb, A. Kumar, Automated finite element analysis of complex dynamics of primary system traversed by oscillatory subsystem, Computational Methods in Engineering Science and Mechanics 12 (4) (2011) 184–202. `doi:10.1080/15502287.2011.580830`.

5

The influence of vehicle dynamics on the time-dependent resonances of a bridge [1]

abstract

In bridge structural health monitoring, the response of the bridge while the vehicle is on the bridge, is called a vehicle-bridge interaction (VBI) response. If the vehicle and the bridge are dynamically coupled, the VBI response depends on the bridge's and the vehicle's dynamic properties. Therefore, the damage detection techniques based on the bridge resonances become questionable due to the dynamic coupling between the bridge and the vehicle. This study investigates the influence of vehicle dynamics on the bridge's time-dependent resonances. Vehicle-Induced Delta Frequency (VIDF) represents the changes in the bridge's time-varying resonances resulting from the vehicle-bridge interaction, while Damage-Induced Delta Frequency (DIDF) accounts for the additional alterations caused by bridge damage. The dynamic interaction between vehicles and bridges (VBIs) is characterized by the frequency ratio between the vehicle (super-system) and the bridge (sub-system). The vehicle frequency is influenced by its dynamics, particularly the suspension systems. Two vehicle models, single suspension and dual suspension vehicles representing passenger trains and freight trains,

---

[1]This chapter is reproduced from: Mostafa, N., Di Maio, D., Loendersloot, R. & Tinga, T. (2023). The influence of vehicle dynamics on the time-dependent resonances of a bridge. Advances in Bridge Engineering, 4, No. 22.

respectively, are analyzed to assess the significance of vehicle dynamics on VIDF and DIDF. The results demonstrate that both vehicle models experience resonance, which magnifies the dynamic response to damage. However, not all types of vehicles possess the desired dynamic characteristics for effective bridge health monitoring. Trains with single suspension systems exhibit more pronounced changes in the bridge's frequency response. This characteristic makes them more suitable for effective bridge health monitoring and damage detection.

5.1   Introduction

Degradation of bridge structures due to environmental and traffic factors is inevitable. The collapse of such structures might result in civil and economic casualties. Therefore, a maintenance strategy capable of detecting or even predicting potential failure is crucial to ensure the safety and reliability of bridges. Structural Health Monitoring (SHM) approaches are nowadays prevalent in evaluating structural reliability and damage detection during the service life of civil structures such as bridges. SHM approaches intend to directly or indirectly assess the condition of the bridge structures while they are in operation. Therefore, the input of the SHM systems is mainly the vehicle-bridge interaction (VBI) response.

A vehicle-bridge interaction (VBI) refers to the dynamic coupling between a bridge and a passing vehicle, resulting in a time-varying process. The dynamic response of the VBI system is influenced by the dynamic properties of both the vehicle and the bridge. Understanding the dynamic interaction between vehicles and bridges is important for both direct and indirect approaches to bridge damage detection. In indirect approaches [1, 2], either the passing vehicle [3] or both the vehicle and the bridge [4] are instrumented. The focus of the current study is on the direct approach, where the VBI response is collected through instrumented bridges.

The VBI models available in the literature have evolved from moving constant force models to complete train-track-bridge interaction models [5]. Moving constant force models have been widely used to model the cases where either the weight of the vehicle is much smaller than the weight of the bridge or the vehicle-bridge dynamic coupling is not of interest [5]. Therefore, such a model cannot capture the dynamic interaction between

the vehicle and the bridge. A more detailed and computationally more expensive multi-body vehicle model is normally implemented to verify safety, ride comfort, and the stability of bridges [6–9] or to investigate the wheel-rail vertical interactions in case of track irregularities [10, 11] mainly in the domain of high-speed trains and not focusing on the condition of the bridge. Despite the different interests, the common challenge is the extracting of the dynamic characteristics during the passage of the train, as they are important for condition assessment of the bridge as argued in [12, 13].

Track irregularities are an important source of complexity in the dynamics response. Short-wavelength track irregularities contribute to noise in trains and the environment [14], while long-wave irregularities induce low-frequency vertical oscillations in high-speed trains, where the oscillation frequency is directly proportional to the train's speed [15], and in cases where the train's speed is low, this frequency can be less than 1 Hz. Since this study is focused on low-speed trains, track irregularities are not further taken into account. It should be noted though that deformation of the bridge due to the presence of the train is not considered to be track irregularity and is taken into account.

There is a rich literature on the implementation of a moving single-stage suspension vehicle on a bridge employing various numerical methods for different purposes such as time-frequency analysis [16], extracting instantaneous frequency (IF) [17], damage detection [18], and so on. Li et al. [19] modeled a moving vehicle with a primary suspension system on a simply supported beam and obtained the fundamental frequency of the bridge utilizing a step-wise solution of the eigenvalue problem at each step of numerical integration. A similar approach was utilized in [20] where the bridge resonance is again calculated based on the solution of the eigenvalue problem. Yang et al. [21] developed a closed-form solution for the frequencies of a VBI system by including only the first mode shape of the system where the vehicle is modeled as a 1-DOF sprung mass. Cantero et al. [22] extracted the resonance of a modeled bridge subjected to a moving sprung mass by applying the singular value decomposition technique (SVD) to capture the variation of the bridge resonance [23]. Marchesiello et al. [24] applied continuous wavelet transform (CWT) on the measured acceleration response of a scaled bridge-like structure under a moving train without any suspension, and the time-dependent bridge resonance was successfully extracted. The main objective of the above studies was either applying or developing different approaches to extract the time-dependent resonances of bridges

meaning that the influence of the vehicle dynamics on the time-dependent resonances of bridges in healthy or damaged conditions is not fully explored.

The influence of the vehicle dynamics on the dynamic response is addressed in some field measurements. Cantero et al. [22] experimentally applied CWT to a truck-induced bridge vibration, but no clear pattern of energy distribution in the time-frequency domain was found [22]. Xin et al. [25] proposed an enhanced empirical wavelet transform (EWT) approach, based on the synchro-extracting transform (SET) [26], for the time-frequency analysis of a highway bridge under a controlled traffic event; i.e. the passing of two trucks. Li et al. [27] applied an enhanced short-time Fourier transform (STFT) based on synchro-extracting transform (SET) on the acceleration response of a cable-stayed single-lane highway bridge in Sydney under a passing truck and extracted the instantaneous frequency of the bridge. Regarding railway bridges, He et al. [28] applied the empirical mode decomposition (EMD) to the forced vibration response of a railway bridge in China, and by means of spectral analysis of the intrinsic mode functions (IMFs). They concluded that the modal frequencies of the bridge change due to the presence of the train. Cantero et al. [29] applied the Wavelet transform in combination with the modified Littlewood-Paley method on the response of the Skidtrask bridge in Sweden. The proposed method did not successfully identify the time-dependent bridge resonance from the bridge's forced vibration response.

Unlike a few successful time-frequency analyses for highway bridges under a moving truck, railway bridges have not been fully explored yet. It is suggested that the reason for the limited success compared to highway bridge analyses is the vehicle's secondary suspension system which aims to provide passenger ride comfort by isolating the vehicle body from the dynamic loads and vibrations between the wheel and rail [30]. This second-stage suspension system not only affects the train-bridge coupling but also introduces new vibrating modes that can affect the entire VBI system. It is concluded in [29] that for railway bridges, the dynamic interaction between the vehicle and the bridge is complex and highly dependent on the mechanical properties of the suspension systems and the distribution of the masses within the vehicle. Many advanced VBI models have been developed, but these have not been applied to analyze the dynamic coupling and the time-dependent resonances of the system for the purpose of condition monitoring or damage identification, which is the objective of the research of the authors. On the one hand, detailed models are sophisticated and computationally

expensive to investigate the vehicle-bridge interaction, on the other hand, modeling a multi-axle train as a single or dual suspension point mass may sound oversimplified. However, Fryba [31] stated that if the vehicle axle base is not comparable with the bridge span length, the vehicle can be modeled as a suspended lumped mass.

Given the earlier-mentioned importance of the number of suspension stages, the current study investigates 1) a single-suspension and, 2) a dual-suspension vehicle model, which are accurate yet simple models to deal with this complicated interaction to investigate the influence of the vehicle dynamics on the healthy and damaged bridge response. Note that freight trains have a single stage of suspension [32], locomotives can have one or two suspension stages, whereas passenger trains have two or more suspension stages to provide ride quality [33].

Previously, the authors recognized the importance of extracting the instantaneous frequency (IF) and showed in [12] that the Wavelet Synchro-Squeezed Transformation (WSST) outperforms methods like Short-Term Fourier Transformation (STFT) and Continuous Wavelet Transformation (CWT). In [13] it was then shown that the IF can be used to distinguish damage from operational conditions, such as the mass of the train, the temperature, etc. The train dynamics itself were only taken into account to a limited extent: a single sprung mass was used. In the current study, the performance of the damage detection, based on IF extraction via the WSST method and the proposed damage detection method technique will be evaluated for single and dual-suspension vehicle models. This paper therefore investigates the significance of the vehicle dynamics on the dynamic interaction between vehicles and bridges, by extracting the bridge's instantaneous frequency response under intact and damaged conditions. The vehicle-bridge dynamic interaction may mask or magnify the damage influence on the VBI system response. Utilizing those vehicles that magnify the damage leads to a more efficient SHM strategy since the data collection and, subsequently, the data analysis are optimized.

5.2 Model and Data Analysis Method

The single suspension vehicle model has been used before to investigate the influence of the vehicle dynamics on the bridge resonances [21]. The influence of the vehicle-bridge coupling on the damaged bridge response has not been explored. For a single

suspension vehicle model the determinant frequency ratio is defined as the vehicle (the super-system) frequency over the bridge (the sub-system) frequency. It has been concluded in [21] that the most substantial interaction occurs at resonance when the car-body bouncing (the vertical oscillation) frequency approaches the bridge frequency. However, the determinant frequency ratio for a dual suspension vehicle model cannot be defined by the car-body to the bridge frequency ratio due to the intermediate bogie suspension. For the dual-suspension vehicle model, the determinant frequency ratio is the bogie (the super-system) over the bridge (sub-system) frequency.

To set up a model with realistic parameters, characteristics of different trains with dual suspension systems are collected from literature sources and presented in Table 5.1. It can be seen that the car-body bouncing frequency varies in the range 0.52-1.32 Hz. In Eurocode EN 1991-2 (2003), the lower limit of the bridge fundamental frequency is given by $f_r = 23.58L^{-0.592}$ for a span length between 20-100 m, which results in a frequency range of 1.7-4 Hz. Therefore, it can be concluded that these two vibration modes, the car-body bouncing and the bridge bending for dual suspension vehicles, are well-separated and that resonance will not occur. The bogie bouncing frequency range as also presented in Table 5.1 is 2.3-8.6 Hz which overlaps with the bridge frequency range and can therefore cause resonance. Regarding freight trains, having only a single suspension, the car-body bouncing frequency range is 0.9-4 Hz [32], which also overlaps with the bridge frequency range.

Table 5.1: Vehicle dynamic properties for dual-suspension trains.

Train		Resonance frequency [Hz]		Component mass [kg]	
		Bogie	Car-body	Bogie	Car-body
ETR500-locomotive	[34]	4.83	0.65	3896	55976
ETR500-passenger	[34]	3.85	0.52	2760	34231
Thalys-237A	[35]	5.93	1.03	3261	53442
Thalys-237B	[35]	8.6	1.32	1400	28500
Thalys-237A	[35]	3.75	1.18	8156	40850
Eurostar-237A	[35]	6.5	1.1	3075	54200
Eurostar-237B	[35]	4.1	1.01	2363	22000
Eurostar-237B	[35]	2.86	0.96	9580	36000
ICE-passenger	[36]	5.84	0.67	2373	34000
ICE-locomotive	[36]	6.6	1.21	5600	61000
Hauling-locomotive	[37]	2.36	0.65	14860	87140
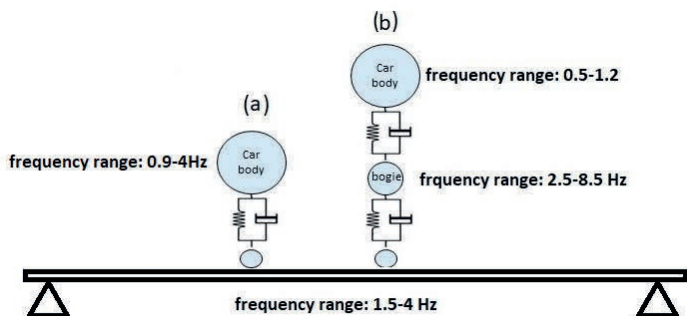
Figure 5.1: The vehicle models used in the current study.

Figure 5.1 presents a single suspension and a dual suspension vehicle model repre-
senting a freight train or a locomotive (a) and a passenger train (b) respectively. The
variation of the bouncing frequency is also displayed. The current study focuses on the
frequency ratio range of 0.55-1.7 for both vehicle models to shed light on the influence
of the vehicle dynamics on the coupled system frequency response in two conditions;
away-from-resonance, and near-resonance.

All finite element simulations are conducted in two-dimensional space in ABAQUS
where Euler-Bernoulli beam elements are used. An extended version of a simply sup-
ported beam is used to simulate the bridge numerically. The bridge model is extended
to obtain the bridge's free vibration, while the mass is not present on the bridge. To
this end, an approaching and leaving length are added before and after the bridge to
properly locate the mass during the forced and free vibration phases. The extension
sections are pinned to the ground, and they allow to generate the bridge response while
the vehicle is approaching and leaving the bridge. The bridge model (i.e. the center part
of 80 m) has 1600 rectangular beam elements of $A = 0.4\,\mathrm{m}^2$ cross section area and with
Young's modulus $E = 210\,\mathrm{GPa}$, density $\rho = 7860\,\mathrm{kg/m}^3$. The fundamental frequency
of the bridge model is 2.99 Hz. Rayleigh damping with the coefficients $\alpha = 0.001$ and
$\beta = 0.001$ is added to increase the stability of the solver and viscous damping with a
damping coefficient of $C = 10,000\,\mathrm{N\cdot s/m}$ (well below the critical damping: $\zeta \approx 4\cdot 10^{-3}$)
is added to limit the motion of the car body.

The damage detection concept proposed by the authors in [13] implies that the

bridge's forced vibration response is more sensitive to damage than the free vibration response. The proposed damage-sensitive feature is the bridge instantaneous frequency and the magnitude variation has been introduced. The magnitude variation δ quantifies the deviation of the measured instantaneous frequency for a VBI system, $\mathcal{F}_m$, from the baseline instantaneous frequency of the VBI system, $\mathcal{F}_b$.

$$\delta\left(\mathcal{F}_b, \mathcal{F}_m\right) = \frac{\sum\limits_{i=1}^{n-1}\left(\frac{1}{2}\left(\mathcal{F}_{b,i} + \mathcal{F}_{b,i+1}\right)\Delta t - \frac{1}{2}\left(\mathcal{F}_{m,i} + \mathcal{F}_{m,i+1}\right)\Delta t\right)}{\sum\limits_{i=1}^{n-1}\left(\frac{1}{2}\left(\mathcal{F}_{b,i} + \mathcal{F}_{b,i+1}\right)\Delta t - f_b\Delta t\right)} = \frac{\text{DIDF}}{\text{VIDF}} \qquad (5.1)$$

where f_b refers to the bridge fundamental frequency, which is constant in time and thus a scalar value. In the transient phase, the bridge frequency continuously changes in time (as defined by the time steps $i = 1 : n$) depending on the location of the vehicle. The denominator of Equation (5.1) calculates the area in the frequency versus time plot bounded by $\mathcal{F}_b$ and f_b for the intact bridge. It, therefore, corresponds to the change of the baseline instantaneous frequency of the intact bridge induced by the operational condition and is referred to as the Vehicle Induced Delta Frequency (VIDF). Once the instantaneous frequency of a measured response differs from the baseline, which would be the case when damage is present, then the bounded area between $\mathcal{F}_b$ and $\mathcal{F}_m$ is a nonzero value that quantifies the magnitude variation. The numerator of Equation (5.1) is therefore referred to as the Damage Induced Delta Frequency (DIDF). The magnitude variation δ thus is the ratio between the bridge instantaneous frequency variation induced by damage and the bridge instantaneous frequency variation induced by the vehicle.

5.3 Single suspension vehicle model

5.3.1 The influence of the vehicle dynamics on the intact bridge instantaneous frequency

The single suspension vehicle model represents a locomotive or freight train that in practice has a larger mass than the passenger trains. For the single suspension vehicle model the natural frequency of the vehicle (the super-system) is $\sqrt{(k_{car}/m_{car})}$ where the mass of the car is about 15%-35% of the bridge mass. In the current study, the vehicle mass ranges from 40 tons to 80 tons, denoted as m1 to m9. The mass values are

distributed within this range with a step size of 5 tons. The car mass is set such that it covers the common range of car masses presented in Table 5.1. Having the vehicle mass and the target frequency ratio range, the vehicle stiffness can be calculated. In the current study, the vehicle stiffness variation range is 9 MN/m to 40 MN/m, denoted as k1 to k9. These stiffness values are distributed within the specified range, with a step size of 3.875 MN/m. Therefore, by taking into account the 9 mass variations (m1 to m9) and the 9 stiffness variations (k1 to k9), this study involves the modeling of a total of 81 VBI systems.

Once the vehicle model properties are set, the influence of the vehicle dynamics on the instantaneous frequency of the intact bridge model is investigated. There are two approaches to obtain the instantaneous frequencies of VBI systems: 1) step-wise modal analysis and, 2) dynamic implicit analysis. The step-wise modal analysis aims to calculate the system resonances of the VBI system depending on the location of the vehicle on the bridge. The step-wise approach is computationally affordable, but it is a static approach that is not able to capture the local variation of the instantaneous frequency due to the presence of damage. A dynamic analysis is computationally expensive, yet it provides a high-resolution instantaneous frequency. Therefore, the step-wise modal analysis is used to quantify the intact bridge resonances, whereas the dynamic implicit integration scheme is used to calculate the damaged bridge acceleration response and investigate the influence of the vehicle dynamics on the instantaneous frequency of the damaged bridge.

The step-wise modal analysis starts by locating the vehicle on the left support of the bridge. For the next step, the vehicle is located at 10 m distant from its previous location. The steps are repeated until the vehicle reaches the bridge's right support. At each step, the eigenfrequencies of the system corresponding to the car-body bouncing and the bridge resonance are collected as a numerical array. Figure 5.2 presents a set of results of the step-wise modal analysis for the single suspension vehicle model with constant stiffness (k4) and variable mass (m1 to m9). The horizontal axis is labeled as the relative vehicle location which represents the ratio of the distance traveled by the vehicle on the bridge and the bridge length. The light blue area corresponds to the VIDF, as defined in Equation (5.1), since the VIDF is the area enclosed by the instantaneous frequency and the bridge frequency (dashed line in Figure 5.2).
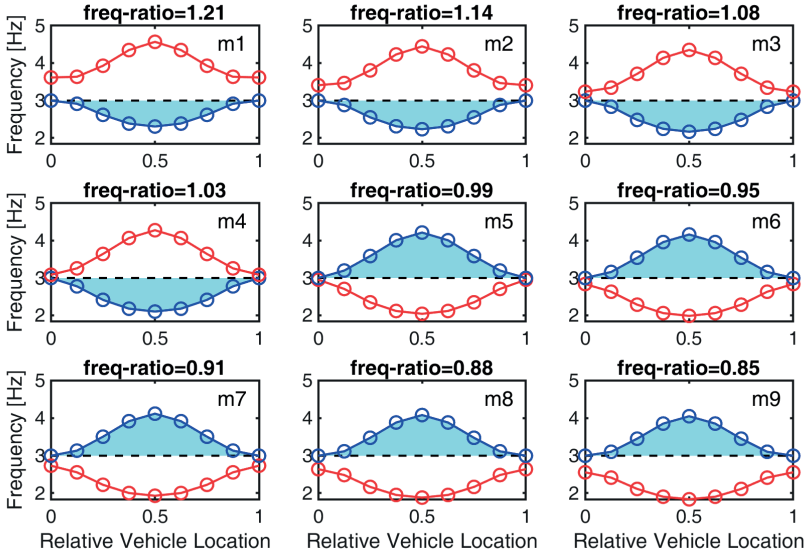
Figure 5.2: The bridge (blue marker) and the vehicle (red marker) frequency variation during a vehicle passage for a constant vehicle stiffness (k4, $k = 20.625\,\mathrm{MN/m}$) and nine different vehicle mass values (indicated by the resulting car-bridge frequency ratio). The bridge's fundamental frequency is displayed as a dashed black line. The light blue area corresponds to the VIDF.

The top-left corner subplot of Figure 5.2 represents a VBI system with the first two resonance frequencies of 2.9 Hz and 3.6 Hz corresponding to the bridge bending resonance frequencies and the car bouncing respectively. These values are visible when the vehicle is located at the left support. The bridge bending frequency (blue curve) appears as the first mode of the coupled system. While the vehicle moves towards the mid-span the bridge frequency decreases to 2.3 Hz when the vehicle is at the mid-span and again comes back to the initial value (2.9Hz) when the vehicle arrives at the right support. The vehicle frequency (red curve) increases to 4.5 Hz when the vehicle is located at the mid-span, and when the vehicle comes back to the right support the frequency also comes back to the initial value (3.6 Hz). This pattern is valid as long as the frequency ratio is larger than 1. Once the frequency ratio comes close to unity, this pattern is changed. It can be seen in the middle row, center plot of Figure 5.2 that the

vehicle frequency is now the first (lowest) mode of the coupled system and it decreases when the vehicle moves towards the bridge mid-span.

The way the resonance frequencies change can be explained by the relative motion of the bridge and the vehicle. The first resonance mode of the bridge-vehicle system is comparable to an in-phase motion of the vehicle mass and the bridge: the car body moves in the same direction as the bridge and follows its vertical displacement, as shown in Figure 5.3a. As a result, the instantaneous resonance frequency of the bridge decreases when the mass moves toward the mid-span position, similar to the effect of an added mass. The second resonance is comparable to an out-of-phase motion, where the vehicle mass and bridge move in opposite directions, as shown in Figure 5.3b. This is similar to the effect of an added stiffness and hence results in an increase of the instantaneous resonance frequency when the mass moves toward the mid-span position.
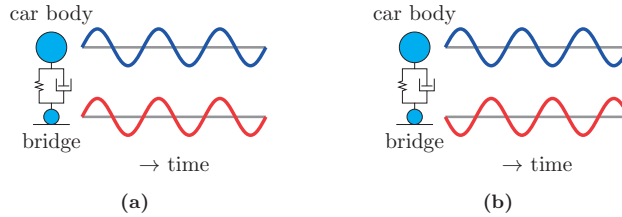
Figure 5.3: Mode shapes retrieved from the step-wise eigenfrequency analyses show that the car and the bridge move (a) in-phase or (b) out-of-phase.

The VIDF has been proposed to quantify the influence of vehicle dynamics on the vehicle-bridge coupled system. The VIDF as introduced in Equation (5.1) calculates the area bounded by $\mathcal{F}_b$: the bridge instantaneous frequency (blue curves in Figure 5.2) and f_b the bridge fundamental frequency (the dashed black line at 2.99 Hz in Figure 5.2) for the intact bridge. It can be observed in Figure 5.2 that the VIDF increases when the frequency ratio approaches unity and decreases when the frequency ratio gets smaller or larger than unity.

The VIDF is calculated for all 81 VBI systems and plotted against the frequency ratio in Figure 5.4. Each marker in Figure 5.4 corresponds to one of the VBI systems, where the color indicates the stiffness and the size of the marker the mass ratio (small: m1; large: m9). The solid markers correspond with the case shown in Figure 5.2 (k4,

m1-m9). As previously observed from Figure 5.2, the maximum value for the VIDF is reached at the resonance condition, where the frequency ratio equals unity.
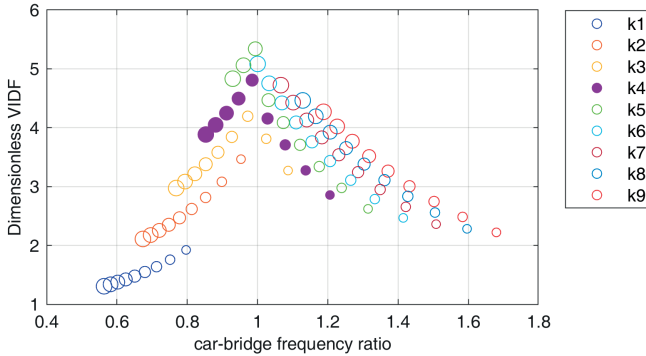
Figure 5.4: VIDF versus car-bridge frequency ratio. Each color corresponds to the stiffness k1 to k9, while the size of the marker represents m1 (small) to m9 (large). The set of solid markers is used as an example for the step-wise analysis.

Figure 5.4 shows in addition that the VIDF drops quicker when moving away from resonance for the VBI systems with a frequency ratio larger than unity compared to VBI systems with a frequency ratio smaller than unity. This is illustrated by the non-equal spacing between markers below and above resonance for the purple, solid markers (case k4, m1-m9). The VIDF for a given absolute distance from the resonance condition is lower for a frequency ratio higher than unity compared to that of a frequency ratio lower than unity. This behavior can be attributed to the different effects of added mass versus added stiffness on the change of the instantaneous frequency $\mathcal{F}_b$.

5.3.2 The influence of the vehicle dynamics on the damaged bridge instantaneous frequency

The numerator of Equation (5.1) introduces the Damage Induced Delta Frequency, DIDF. The main objective of this section is to quantify DIDF for the modeled VBI systems and investigate the influence of the vehicle dynamics on the DIDF. The question is in which situation the DIDF is magnified and thus when optimal conditions for bridge damage detection occur.
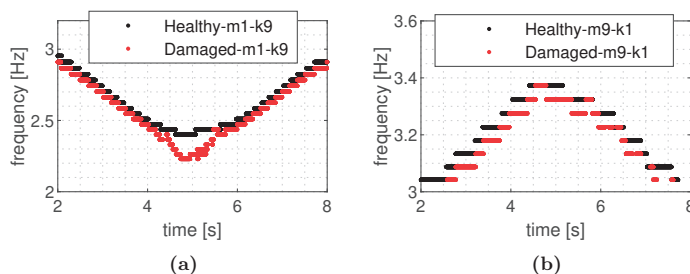
Figure 5.5: The intact and the damaged bridge instantaneous frequency ridges are displayed in black and red respectively, for two VBI systems; (a) the VBI system with a car-bridge mass ratio of 0.16 (m1) and a car-bridge frequency ratio of 1.68 and, (b) the VBI system with a car-bridge mass ratio of 0.32 (m9) and a car-bridge frequency ratio of 0.55.

The numerical model of the bridge in the current study consists of 1600 elements of 50 mm long. To implement damage, the stiffness of 16 elements along the bridge mid-span is reduced by 50%. The total length of the damaged area is thus about 1% of the bridge span length. The damage severity and length are kept constant for all step-wise modal analyses. The same mass and stiffness variations (9×9=81 VBI systems) are used as in the previous section. A more detailed study on the effect of various damage scenarios is presented in [13].

Among the 81 vehicle-bridge interaction (VBI) systems studied, two examples were selected to illustrate the instantaneous frequencies of the bridge in both intact and damaged conditions. Figure 5.5a shows the instantaneous frequency of the VBI system with the lowest car-bridge mass ratio of 0.16 (m1) and the highest car-bridge frequency ratio of 1.68 (corresponding with the highest stiffness case k9). This VBI system exhibits an in-phase regime, where the vehicle behaves as an added mass on the bridge, as depicted Figure 5.3a. In Figure 5.5a, the instantaneous frequency of the intact bridge is represented by the black curve, while the red curve represents the instantaneous frequency of the damaged bridge. The DIDF represents the bounded area between the frequency curves of the intact and damaged bridges. In Figure 5.5a, it is evident that the damaged bridge frequency curve (red curve) exhibits a local reduction around the area of damage. This reduction in the bridge's instantaneous frequency is attributed to the decreased stiffness of the damaged elements and the additional mass introduced by the vehicle.

A VBI system with the lowest vehicle-bridge frequency ratio is chosen as a second example. The instantaneous frequency of the VBI system with a car-bridge mass ratio of 0.32 (m9) and a car-bridge frequency ratio of 0.55 (the lowest frequency ratio, and lowest stiffness case k1) is shown in Figure 5.5b. This VBI system represents an out-of-phase regime, where the vehicle mass counteracts the bridge motion. Again, the black curve represents the intact bridge's instantaneous frequency, while the red curve represents the damaged bridge's instantaneous frequency. Unlike Figure 5.5a, where a larger frequency reduction was observed, Figure 5.5b shows only a marginal frequency reduction around the damage location. This is because the vehicle is effectively acting as an added stiffness in this case.

Only a subset of the 81 VBI systems is used to investigate the influence of the vehicle dynamics on the Damage Induced Delta Frequency (DIDF), considering the computational time of each individual dynamic simulation. The dynamic simulations are performed for 5 VBI systems with the highest vehicle stiffness value (k9, k =3.6MN/m) and for 5 VBI systems with the lowest vehicle stiffness value (k1, k =0.9Mn/m). Figure 5.6 displays the resulting DIDF for these two times 5 VBI systems, where the blue markers correspond with the lowest stiffness (k1) and the red markers with the highest stiffness (k9).
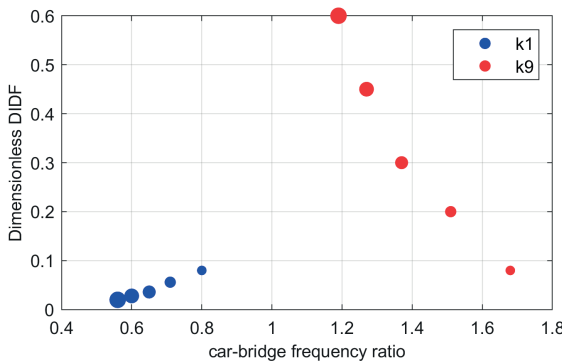
Figure 5.6: DIDF versus car-bridge frequency ratio. Blue markers correspond with k1, red with k9, while the size of the markers represents the mass ratio: m1 (smallest marker size), m3, m5, m7, and m9 (largest marker size).

The observed pattern of the DIDF is similar to that of the VIDF. A maximum is reached if the frequency ratio is unity. Moving away from resonance yields a decrease of the DIDF. The VBI systems having a frequency ratio lower than unity correspond to an out-of-phase motion of the bridge and vehicle, while the VBI systems with a frequency ratio higher than unity correspond to an in-phase motion of the bridge and vehicle. The size of the marker indicates the car-bridge mass ratio (m1, m3, m5, m7, and m9), which for both stiffnesses k1 and k9 is increasing with increasing frequency ratio. Similar to the VIDF, the DIDF drops quicker when moving away from the resonance condition for the in-phase case (frequency ratio > 1), compared to the out-of-phase case (frequency ratio < 1). The resonance condition is not reached for both sets of VBI systems. The mass ratio for the specific combination of bridge and train types under investigation would become very unrealistic. However, it can still be observed from the graph that the lower stiffness case (k1) shows significantly lower values for the DIDF than the higher stiffness case (k9).

It can be concluded that for a unique damaged bridge, different vehicles trigger the damage differently. Furthermore, the DIDF for VBI systems having a frequency ratio larger than unity seems to be larger than for the VBI systems having a frequency ratio less than unity. Finally, being close to resonance (i.e. frequency ratio equal to unity) magnifies the response to damage.

5.4   Dual suspension vehicle model

5.4.1   The influence of the vehicle dynamics on the intact bridge instantaneous frequency ridge

This section investigates the VIDF due to the primary suspension stage of the dual suspension vehicle model displayed in Figure 5.1. In this figure, also the common frequency range of the car body and the bogie system found in the literature are presented. As mentioned previously, the car-body bouncing frequency for dual suspension vehicles and the bridge bending frequency are well-separated, thus, resonance will not occur. However, the bogie bouncing frequency overlaps with the bridge frequency range and here resonance can occur.

For the dual suspension vehicle model, the car dynamics contribute to the vehicle-bridge dynamic interaction through the bogie. Through the current study, the fre-

quency ratio is the benchmark to compare the VBI systems with different vehicle models i.e. different super-systems. For the single suspension vehicle model the car and for the dual suspension vehicle model the combination of the bogie and the car dynamics serve as the super-system. Therefore, for the dual suspension vehicle model, the influence of the primary suspension is investigated by keeping the car mass and stiffness constant and changing the bogie properties. Also, the influence of the secondary suspension is explored by keeping the bogie properties constant and changing the car properties.

The influence of the primary suspension is presented here where the car mass (40 tons) and the car stiffness (0.91 Mn/m) are constant and the bogie mass and the bogie stiffness are tuned such that the frequency ratio ranges from 0.6-1.5. The bogie stiffness variation range is 1.268-3.96 MN/m and the bogie mass variation range is 6,117-13,677 kg. Each range is again divided into 9 steps, yielding a total of $9 \times 9 = 81$ VBI systems. Note that the car bouncing frequency is smaller than 1 Hz and it always appears as the first mode, which corresponds with the actual situation in passenger trains to ensure passenger comfort during the ride.

A step-wise analysis, similar to the one presented in Section 5.3 is done first. The results are shown in Figure 5.7, which displays the bridge and the bogie resonances in blue and red respectively for a fixed bogie mass and all bogie stiffnesses k1 to k9, covering the frequency ratio from 0.78 (top left subplot) to 1.18 (bottom right subplot).

The top left corner plot of Figure 5.2 and the bottom right corner plot of Figure 5.7, show two VBI systems having similar frequency ratios (around 1.18). It can be seen that the single suspension vehicle in comparison with the dual suspension vehicle model shows more dynamic interaction which yields a higher VIDF, which is visualized in both graphs by the light blue area enclosed by the blue curve and the black dashed line.

The VIDF as a function of the frequency ratio for all 81 VBI systems is presented in Figure 5.8. The different colors refer to the different bogie stiffness cases k1 to k9, while the size of the markers refers to the bogie-bridge mass ratio cases m1 (small) to m9 (large). The pattern for the dual suspension vehicle model is similar to the pattern observed for the single suspension vehicle model (see Figure 5.4). The maximum VIDF occurs when approaching a frequency ratio of one near resonance conditions, while the VIDF drops when moving away from a frequency ratio of unity. In out-of-phase motion regimes when the system is away from resonance, the VIDF tends to zero,
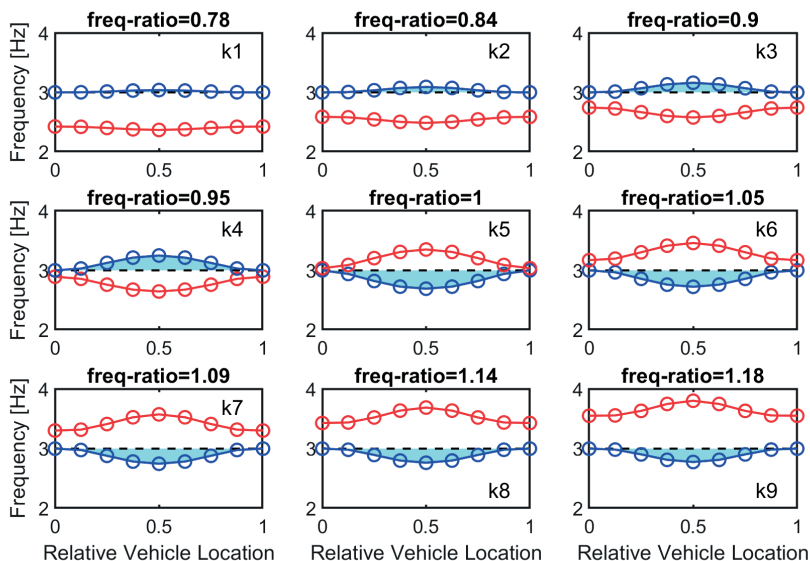
Figure 5.7: The bridge (blue marker) and the vehicle (red marker) frequency variation during a dual suspension vehicle passage for a constant bogie mass and nine different bogie stiffness values k1-k9. The bridge's fundamental frequency is displayed as a dashed black line. The light blue area corresponds to the VIDF.

whereas for in-phase regimes the VIDF tends to 0.4 far from resonance. This means that even for passenger trains with a double-stage suspension when the frequency ratio is larger than unity, the vehicle dynamics affect the bridge's instantaneous frequency. At resonance, VIDF reaches the maximum values which are lower than the maxima observed in Figure 5.4 of the VIDF at resonance of the single suspension vehicle model. Although the mass of the entire system is (nearly) the same for the single suspension and dual suspension systems, the car body has a more limited contribution to the change of the instantaneous frequencies, and hence the VIDF, compared to the bogie. Effectively, the motion of the car body is largely isolated from the bridge and bogie motion due to the low stiffness of the secondary suspension.

Another set of 81 (9×9) VBI systems is analyzed to further support the finding that the dual suspension system has a lower influence on the VIDF compared to the single
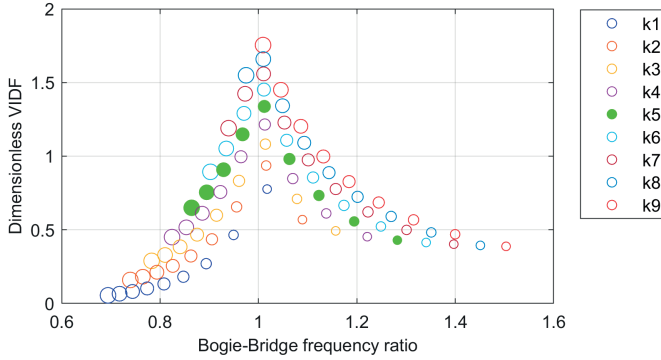
Figure 5.8: VIDF versus bogie-bridge frequency ratio. Each color corresponds to the primary stiffness (k1 to k9), while the size of the marker represents bogie mass (m1: small; m9: large). The solid markers show the case k5, m1-m9.

suspension system. The objective is now to investigate the impact of car mass and car stiffness on the bridge frequency rather than the bogie mass and bogie stiffness. The bogie mass (9580 kg) and the bogie stiffness (1.268 MN/m) are considered constant. The variation in car dynamics is examined for the bogie-bridge frequency ratio ranging from 0.8 to 1.4 by varying the car stiffness ranges in 9 steps from 0.9 to 3.6 MN/m, while the car mass varies in 9 steps between 40 and 80 tons. The VIDF values versus the frequency ratio, resulting from these analyses, are presented in Figure 5.9.

The blue markers in Figure 5.9, corresponding with the lowest secondary suspension stiffness and covering the full range of car body mass variation, all nearly coincided and result in the same VIDF value. This indicates that the car body mass has a very limited influence on the VIDF. The red markers, corresponding with the highest secondary suspension stiffness, show a larger variation in VIDF, but this is still a low amount of variation compared to the variation observed in Figure 5.8. In addition, the maximum value for the VIDF near resonance is also lower than in case the bogie mass and stiffness vary. Additionally, Figure 5.9 reveals that the variation in car body mass has a marginal effect on the VIDF for systems operating away from resonance conditions.
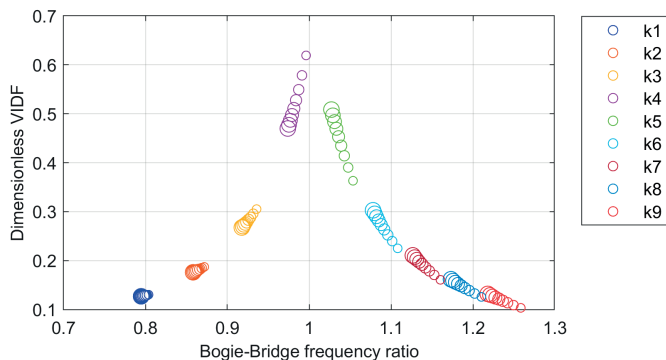
Figure 5.9: VIDF versus bogie-bridge frequency ratio. Each color corresponds to the secondary stiffness (k1 to k9), while the size of the marker represents car mass (m1: small; m9: large).

### 5.4.2 The influence of the vehicle dynamics on the damaged bridge instantaneous frequency

Based on the previous analysis, it can be concluded that the bogie dynamics play a crucial role in the vehicle-bridge dynamic interaction for passenger trains. Furthermore, it was observed that vehicles operating in the in-phase regime (frequency ratio > 1) amplify the VIDF more than in the out-of-phase regime (frequency ratio < 1). In this section, only the influence of the bogie dynamics on the DIDF for the dual suspension vehicle models in the in-phase regime is investigated. The vehicle model is configured with a constant bogie stiffness of $3.96\,\mathrm{MN/m}$ (k9) and a variation of the bogie mass between 6,117-13,677 kg. Only 5 steps (m1, m3, m5, m7, and m9) are used to limit the computational time. Figure 5.10 shows the corresponding DIDF. A similar pattern as in Figure 5.6 can be observed in Figure 5.10. The DIDF value drops when moving away from the resonance condition and seems to converge to approximately 0.1. The difference between the single-suspension and dual-suspension systems reduces with increasing frequency ratio, but close to resonance, the damage-induced variation in the instantaneous frequency is significantly larger for the single-suspension system. This observation is in line with the earlier observation that the change of the VIDF is also lower for the dual-suspension systems compared to that of the single-suspension

systems.
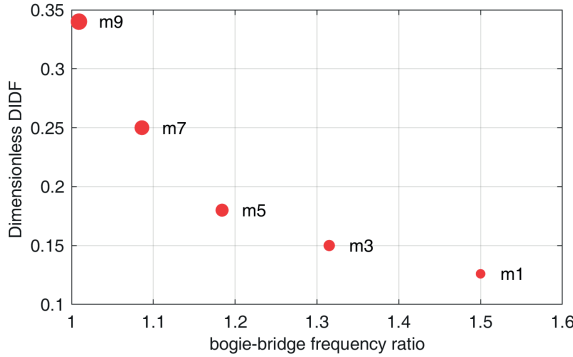
Figure 5.10: DIDF versus bogie-bridge frequency ratio. Results of the highest stiffness case (k9) are shown for mass ratios m1 (smallest marker size), m3, m5, m7, and m9 (largest marker size).

5.5   Discussion

The dynamic properties of the single-suspension vehicle model cannot be directly compared to those of the dual-suspension vehicle model. However, the frequency ratio between the super system (the vehicle) and the sub-system (the bridge) serves as a criterion for representing and comparing the vehicle-bridge dynamic interaction. Figure 5.11 provides a concise summary of the findings presented in Figure 5.6 and Figure 5.10 illustrating the DIDF for both the single suspension and dual suspension vehicle models. The figure specifically focuses on the in-phase regime for which the frequency ratio ranges from 1.2 to 1.5. In Figure 5.11 it is evident that as the vehicle approaches the resonance condition the DIDF increases for both vehicle models. The figure also clearly demonstrates a significant difference in DIDF between the single-suspension vehicle model representing freight trains or single locomotives and the dual-suspension vehicle model representing passenger trains. At a frequency ratio of 1.2, Figure 5.11 displays that the DIDF of the dual suspension vehicle is approximately 0.18 while, this value for the single suspension vehicle is approximately 0.6 which is roughly three times larger. Note that in both cases the total mass of the vehicle is the same.
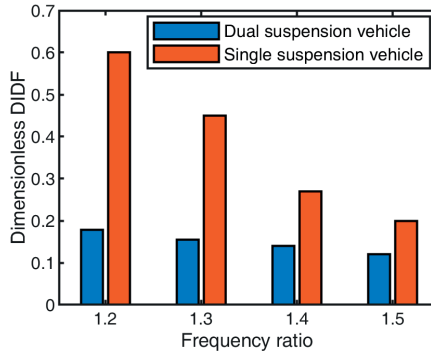
Figure 5.11: The DIDF of the single suspension and the dual suspension vehicle models for frequency ratios of 1.2 and 1.5.

This discrepancy in DIDF values can be attributed to the distinct characteristics of the suspension systems employed in each vehicle model. Compared to dual-suspension vehicles, the single-suspension vehicle exhibits a higher impact on the bridge dynamics which translates into a larger change of the bridge's instantaneous frequency when damage is present. This enhanced sensitivity enables the detection of smaller deviations in the bridge's frequency response, thereby facilitating the identification of potential damage in an earlier stage. These findings serve as guidelines for the design of bridge health monitoring systems, combined with a dedicated approach, which for example involves the deployment of dedicated vehicles designed specifically for the purpose of structural assessment.

5.6 Conclusion

The dynamic interaction between a vehicle and a bridge is numerically investigated for two vehicle models: a single-suspension and a dual-suspension vehicle. The instantaneous frequencies of the vehicle-bridge interaction (VBI) models for an intact and damaged bridge are extracted by performing a series of step-wise modal analyses and a series of transient response analyses. The Vehicle-Induced Delta Frequency (VIDF) was proposed earlier to quantify the influence of the vehicle dynamics on the response of the intact bridge. The Damage-Induced Delta Frequency (DIDF) was proposed as a damage-sensitive feature to quantify the influence of vehicle dynamics on damage

detection. The investigation of the Vehicle-Bridge Interaction (VBI) system response, conducted near resonance conditions, focused on a single-span simply supported bridge in the context of low-speed train operations. From this analysis, the following conclusions can be drawn:

- To ensure accurate and reliable bridge health monitoring and damage detection, it is crucial to select suitable train types. Not all types of trains possess the desired dynamic characteristics for effective bridge health monitoring.

- Trains with single suspension systems cause more pronounced changes in the bridge's frequency response than dual suspension trains, specifically the Vehicle-Induced Delta Frequency (VIDF) and Damage-Induced Delta Frequency (DIDF). This phenomenon can be attributed to the concept of interacting mass. In single suspension systems, the entire mass of the train, including the car body, interacts directly with the bridge. In contrast, dual suspension systems decouple the car body from the bridge, leading to a reduction in the mass interaction between the train and the bridge.

- In the case of dual-suspension vehicles, the outcomes demonstrate that the influence of the vehicle mass on the bridge frequency is negligible compared to the mass of the bogie. This observation aligns with the intended role of the secondary suspension system, which is primarily focused on enhancing ride comfort by effectively decoupling the car body from the undesired vibrations of the subsystems. Hence, when the objective is to analyze the impact of vehicle dynamics on the bridge's instantaneous frequency (VIDF) for dual-suspension vehicles, it is essential to focus on the characteristics and properties of the bogie rather than the car mass.

-

Bibliography

[1] Wang, Z.L., Yang, J.P., Shi, K., Xu, H., Qiu, F.Q., Yang, Y.B.: Recent advances in researches on vehicle scanning method for bridges. International Journal of Structural Stability and Dynamics **22**(15) (2022) https://doi.org/10.1142/s0219455422300051

[2] Yang, Y.B., Lin, C.W., Yau, J.D.: Extracting bridge frequencies from the dynamic response of a passing vehicle. Journal of Sound and Vibration **272**(3-5), 471–493 (2004) https://doi.org/10.1016/s0022-460x(03)00378-x

[3] Zhang, T.P., Zhu, J., Xiong, Z.L., Zheng, K.F., Wu, M.X.: A new drive-by method for bridge damage inspection based on characteristic wavelet coefficient. Buildings **13**(2) (2023) https://doi.org/10.3390/buildings13020397

[4] Sarwar, M.Z., Cantero, D.: Vehicle assisted bridge damage assessment using probabilistic deep learning. Measurement **206** (2023) https://doi.org/10.1016/j.measurement.2022.112216

[5] Zhai, W., Han, Z., Chen, Z., Ling, L., Zhu, S.: Train–track–bridge dynamic interaction: a state-of-the-art review. Vehicle System Dynamics **57**(7), 984–1027 (2019) https://doi.org/10.1080/00423114.2019.1605085

[6] Zhu, Z., Gong, W., Wang, L., Harik, I.E., Bai, Y.: A hybrid solution for studying vibrations of coupled train–track–bridge system. Advances in Structural Engineering **20**(11), 1699–1711 (2017) https://doi.org/10.1177/1369433217691775

[7] Zhang, N., Tian, Y., Xia, H.: A train-bridge dynamic interaction analysis method and its experimental validation. Engineering **2**(4), 528–536 (2016) https://doi.org/10.1016/j.Eng.2016.04.012

[8] Youcef, K., Sabiha, T., El Mostafa, D., Ali, D., Bachir, M.: Dynamic analysis of train-bridge system and riding comfort of trains with rail irregularities. Journal of Mechanical Science and Technology **27**(4), 951–962 (2013) https://doi.org/10.1007/s12206-013-0206-8

[9] Yang, Y.B., Yau, J.D.: Resonance of high-speed trains moving over a series of simple or continuous beams with non-ballasted tracks. Engineering Structures **143**, 295–305 (2017) https://doi.org/10.1016/j.engstruct.2017.04.022

[10] Zhai, W., Sun, X.: A detailed model for investigating vertical interaction between railway vehicle and track. Vehicle System Dynamics **23**(sup1), 603–615 (2008) https://doi.org/10.1080/00423119308969544

[11] Zhai, W.M., Cai, C.B.: Train/track/bridge dynamic interactions: Simulation and applications. Vehicle System Dynamics **37**(sup1), 653–665 (2016) https://doi.org/10.1080/00423114.2002.11666270

[12] Mostafa, N., Di Maio, D., Loendersloot, R., Tinga, T.: Extracting the time-dependent resonances of a vehicle–bridge interacting system by wavelet synchrosqueezed transform. Structural Control and Health Monitoring (2021) https://doi.org/10.1002/stc.2833

[13] Mostafa, N., Maio, D.D., Loendersloot, R., Tinga, T.: Railway bridge damage detection based on extraction of instantaneous frequency by wavelet synchrosqueezed transform. Advances in Bridge Engineering **3**(1), 12 (2022) https://doi.org/10.1186/s43251-022-00063-0

[14] Xin, T., Wang, P., Ding, Y.: Effect of long-wavelength track irregularities on vehicle dynamic responses. Shock and Vibration **2019**, 1–11 (2019) https://doi.org/10.1155/2019/4178065

[15] Hung, C.F., Hsu, W.L.: Influence of long-wavelength track irregularities on the motion of a high-speed train. Vehicle System Dynamics **56**(1), 95–112 (2017) https://doi.org/10.1080/00423114.2017.1346261

[16] Hester, D., Gonzalez, A.: A wavelet-based damage detection algorithm based on bridge acceleration response to a vehicle. Mechanical Systems and Signal Processing **28**, 145–166 (2012) https://doi.org/10.1016/j.ymssp.2011.06.007

[17] Roveri, N., Carcaterra, A.: Damage detection in structures under traveling loads by Hilbert-Huang transform. Mechanical Systems and Signal Processing **28**, 128–144 (2012) https://doi.org/10.1016/j.ymssp.2011.06.018

[18] Huseynov, F., Kim, C., Obrien, E.J., Brownjohn, J.M.W., Hester, D., Chang, K.C.: Bridge damage detection using rotation measurements – experimental validation. Mechanical Systems and Signal Processing **135** (2020) https://doi.org/10.1016/j.ymssp.2019.106380

[19] Li, J.Z., Su, M.B., Fan, L.C.: Natural frequency of railway girder bridges under vehicle loads. Journal of Bridge Engineering **8**(4), 199–203 (2003) https://doi.org/10.1061/(Asce)1084-0702(2003)8:4(199)

[20] Law, S.S., Zhu, X.Q.: Dynamic behavior of damaged concrete bridge structures under moving vehicular loads. Engineering Structures **26**(9), 1279–1293 (2004) https://doi.org/10.1016/j.engstruct.2004.04.007

[21] Yang, Y.B., Cheng, M.C., Chang, K.C.: Frequency variation in vehicle–bridge interaction systems. International Journal of Structural Stability and Dynamics **13**(02) (2013) https://doi.org/10.1142/s0219455413500193

[22] Cantero, D., Hester, D., Brownjohn, J.: Evolution of bridge frequencies and modes of vibration during truck passage. Engineering Structures **152**, 452–464 (2017) https://doi.org/10.1016/j.engstruct.2017.09.039

[23] Cantero, D., McGetrick, P., Kim, C.-W., Obrien, E.: Experimental monitoring of bridge frequency evolution during the passage of vehicles with different suspension properties. Engineering Structures **187**, 209–219 (2019) https://doi.org/10.1016/j.engstruct.2019.02.065

[24] Marchesiello, S., Bedaoui, S., Garibaldi, L., Argoul, P.: Time-dependent identification of a bridge-like structure with crossing loads. Mechanical Systems and Signal Processing **23**(6), 2019–2028 (2009) https://doi.org/10.1016/j.ymssp.2009.01.010

[25] Xin, Y., Hao, H., Li, J.: Time-varying system identification by enhanced empirical wavelet transform based on synchroextracting transform. Engineering Structures **196** (2019) https://doi.org/10.1016/j.engstruct.2019.109313

[26] Yu, G., Yu, M., Xu, C.: Synchroextracting transform. IEEE Transactions on Industrial Electronics **64**(10), 8042–8054 (2017) https://doi.org/10.1109/tie.2017.2696503

[27] Li, J., Zhu, X., Law, S.-s., Samali, B.: Time-varying characteristics of bridges under the passage of vehicles using synchroextracting transform. Mechanical Systems and Signal Processing **140** (2020) https://doi.org/10.1016/j.ymssp.2020.106727

[28] He, X.H., Hua, X.G., Chen, Z.Q., Huang, F.L.: EMD-based random decrement technique for modal parameter identification of an existing railway bridge.

Engineering Structures **33**(4), 1348–1356 (2011) https://doi.org/10.1016/j.
engstruct.2011.01.012

[29] Cantero, D., Ülker-Kaustell, M., Karoumi, R.: Time–frequency analysis of railway
bridge response in forced vibration. Mechanical Systems and Signal Processing
76-77, 518–530 (2016) https://doi.org/10.1016/j.ymssp.2016.01.016

[30] SKF Group: Railway Technical Handbook, Sweden (2011)

[31] Fryba, L.: Vibration of Solids and Structures Under Moving Loads. Noordhoff
International Publishing, Groningen (2013)

[32] Iwnicki, S., Spiryagin, M., Cole, C., McSweeney, T.: Handbook of Railway Vehicle
Dynamics. Handbook of Railway Vehicle Dynamics, CRC Press (2019). https:
//doi.org/10.1201/9780429469398 . https://www.routledgehandbooks.com/
doi/10.1201/9780429469398

[33] Spiryagin, M., Wolfs, P., Cole, C., Spiryagin, V., Sun, Y.Q., McSweeney, T.:
Design and Simulation of Heavy Haul Locomotives and Trains, CRC Press (2016).
https://doi.org/10.1201/9781315369792-4

[34] Liu, K., Roeck, G.D., Lombaert, G.: The effect of dynamic train–bridge interaction
on the bridge response during a train passage. Journal of Sound and Vibration
Volume 325(Issues 1–2), 240–251 (2009)

[35] Kouroussis, G., Verlinden, O., Conti, C.: Free field vibrations caused by high-speed
lines: Measurement and time domain simulation. Soil Dynamics and Earthquake
Engineering **31**(4), 692–707 (2011) https://doi.org/10.1016/j.soildyn.2010.
11.012

[36] Doménech, A., Museros, P., Martínez-Rodrigo, M.D.: Influence of the vehicle
model on the prediction of the maximum bending response of simply-supported
bridges under high-speed railway traffic. Engineering Structures **72**, 123–139
(2014) https://doi.org/10.1016/j.engstruct.2014.04.037

[37] Spiryagin, M., Sun, Y.Q., Cole, C., McSweeney, T., Simson, S., Persson, I.:
Development of a real-time bogie test rig model based on railway specialised

multibody software. Vehicle System Dynamics **51**(2), 236–250 (2013) https://doi.org/10.1080/00423114.2012.724176

6

Discussion

This chapter provides a broad reflection on the research performed. It first revisits the research questions that were formulated in Chapter 1 and provides the answers to these questions. Secondly, the limitations of the work are identified and the implications and potential solutions are discussed.

6.1 Answers to the research questions

This section will address the five research questions introduced in Chapter 1 one by one.

6.1.1 What are the failure mechanisms for bridges and how do they influence the bridge dynamics?

As shown in Chapter 2, the dominant failure mechanism in both steel and concrete bridges is corrosion. Given that the case study of this research project was a steel bridge, the primary focus of the research was the steel bridges.

Corrosion appears in various forms. However, irrespective of its specific form, the common thread of all forms is the gradual material loss. The consequence of the diminished section thickness is a localized stiffness reduction. This involves corrosion in the flanges where different steel beams are connected or corrosion of the steel beams themselves. In the first case, corrosion is highly localized but may lead to a loss of connection, resulting in a significant stiffness reduction. In the second case, stiffness reduction may be less severe but extends over a larger region. This rationale underlies

the two approaches to implementing damage in Chapter 4. One method involves local-
ized damage by severely reducing the stiffness of a few elements, while the other entails
propagated damage through a mild reduction in the stiffness of multiple elements.

The damage detection techniques that rely on the global response of the structure,
such as the free vibration response, are unable to detect these local stiffness changes.
Therefore, as argued in Chapter 3, the vehicle-bridge interaction (VBI) response was
used. Analyzing VBI responses to detect the localized stiffness reduction requires more
complex analysis methods than analyzing the global dynamic response, accurate ex-
traction of the system's instantaneous frequencies (see section 6.1.2), and a damage
metric (see section 6.1.3 and section 6.1.4).

In the numerical studies presented in Chapter 4 and Chapter 5, damage was modeled
by reducing the stiffness of one or more elements, and the modeling approach did not
involve detailed crack models or corrosion models. Crack or corrosion modeling is only
necessary for prognostics, whereas this research project is limited to diagnostics.

6.1.2   How to accurately extract the instantaneous frequency of the vehicle-bridge coupled system which carries time-dependent and local event information i.e. damage?

The VBI response of the Boyne Bridge (the case study of this project) exhibits closely
spaced low-frequency time-dependent resonances, all falling below 10Hz. This charac-
teristic holds for railway bridges with a span length of 20-100m, as discussed in Chap-
ter 5. This specific characteristic underscores the importance of employing a signal
processing method that can effectively perform two key tasks:

1. decompose along the frequency axis;

2. localize in the time axis the time-dependent resonances of the VBI system.

As presented in Chapter 3, the Wavelet Synchrosqueezed Transform (WSST) is a
time-frequency analysis tool, that utilizes wavelet transform to extract time-frequency
information. Subsequently, through reassignment, WSST synchrosqueezes the infor-
mation, yielding a more concise, sharper, and noise-resistant representation. Other
commonly used methods, such as Empirical Mode Decomposition (EMD), Robust Lo-
cal Mean Decomposition (LMD), and Continuous Wavelet Transform (CWT), were
found to face challenges such as mode-mixing or low resolution of the low-frequency

components which make them less effective for this specific case. WSST has been effectively employed to analyze the acceleration response of the Boyne Bridge during the passage of a locomotive and a maintenance truck, along with various simulated scenarios.

It is essential to recognize that the effectiveness of a signal processing method may vary, influenced by factors such as train speed, vehicle dynamics, and the nature of their interaction with the bridge. Consequently, there may be cases where an alternative signal processing method may prove more suitable.

6.1.3 How to identify damage based on the extracted instantaneous frequencies and distinguish between operational conditions and damage?

A key element in damage identification is separating operational and environmental variations from variations due to damage. In Chapter 4, the presented damage detection approach utilizes the bridge's fundamental frequency extracted from the free vibration as a reference to exclude the effect of operational and environmental variations. This concept is extended by incorporating the bridge's Instantaneous Frequency (IF) extracted from the forced vibration response.

The absence of a comprehensive understanding of the dynamic interactions in the system makes it challenging to interpret the extracted instantaneous frequencies (IF) and identify the source of IF variation, whether it be operational conditions or damage. Hence, a basic model is established to initially investigate the variations of the system IFs resulting from operational conditions and subsequently, those induced by damage.

The proposed damage detection approach introduces two metrics; the shape correlation ρ and the magnitude variation δ were proposed to distinguish the global and the local deviation of the bridge baseline instantaneous frequency induced by variable operational conditions and damage, respectively.

Developing a complete and detailed numerical model is complex and computationally expensive, which may lead to a complex and uninformative response. Therefore, the decision was made to initiate the modeling process with a basic model and gradually increase complexity, gaining insight into the system step by step. The implementation of damage involved reducing the stiffness of the bridge element(s), utilizing the knowledge obtained in section 6.1.

To simulate variable operational conditions of the train, different masses were employed. Other factors such as train length and velocity could also be considered as variable operational conditions however, varying the mass directly influences the instantaneous frequencies of the system which can be considered as a worst-case scenario.

The comparative studies in Chapter 4 have demonstrated that using the bridge's Instantaneous Frequency yields superior results compared to conventional techniques for detecting and assessing damage in bridges.

6.1.4 How do the dynamics of a passing vehicle affect the instantaneous frequency of the intact and damaged structure?

Chapter 5 addresses the influence of vehicle dynamics on both Vehicle-Induced Delta Frequency (VIDF) and Damage-Induced Delta Frequency (DIDF) for two vehicle models representing passenger trains and freight trains. For single-suspension vehicles, the car mass and car stiffness play a dominant role in influencing the dynamic response of the system. In contrast, for dual suspension vehicles, the bogie mass and bogie stiffness are the primary factors governing the system's behavior.

In all VBI models, a unique damage size was implemented. It has been observed that, for a VBI system with a frequency ratio larger than unity, approaching resonance conditions increases DIDF for both vehicle models.

6.1.5 What type of vehicle demonstrates superior performance in damage detection?

Chapter 5 showed that different vehicles exhibit varying interactions with the damage, leading to different effects on the Instantaneous Frequencies (IFs). The single-suspension vehicle model exhibits larger DIDF values compared to the dual-suspension system. More specifically, the type of vehicle that is particularly suitable for damage detection is freight trains or single locomotives.

6.2 Limitations and challenges

This subsection will identify a number of limitations of the present research, and discuss how these could be addressed in future research. Also, some practical guidelines are derived that can assist in implementing these techniques in real-world SHM on bridges.

6.2.1 Train speed

In the presented model in ABAQUS, the interaction between the vehicles and the bridge is simulated using an unsprung and sprung mass, both sliding with a constant speed of 5 m/s. The decision to set the vehicle speed to 5 m/s was inspired by the train speed observed on the Boyne viaduct, which was below 30 km/hr (8.3 m/s). This choice is relevant as it allows for insights into the bridge's response under conditions that resemble those of real train traffic. The primary focus of our study has been on low to normal-speed trains, such as those crossing the Boyne Bridge. It is crucial to acknowledge that the performance of the proposed method may vary when it is applied to high-speed trains. This variation stems from several key factors. One critical input of the proposed method is the accurate extraction of the instantaneous frequency of the bridge. However, as train speed increases, the length of the signal received by the sensors decreases, leading to a decrease in frequency resolution. This limitation can impact the method's ability to precisely capture the bridge's dynamic behavior. Moreover, high-speed trains often encounter track irregularities and variations in the rail network. These irregularities can introduce additional frequency components into the VBI response. These frequencies may overlap or interfere with the bridge's natural frequencies or vehicle dynamics, making it challenging to distinguish between them. Therefore, when simulating high-speed train scenarios, the potential influence of track irregularities on the vehicle-bridge dynamic interaction must be considered and investigated. Furthermore, the key distinction between normal trains and high-speed trains lies in their vehicle dynamics and the track. To assess their compatibility with a proposed method, one must first understand the dynamics of each subsystem, namely the vehicle, track, and bridge, to identify the interacting frequency components. If the high-speed train exhibits dynamic interaction with the bridge, further steps may be needed to fine-tune or optimize the method.

6.2.2 Train length and train type

The application of the Wavelet-Synchrosqueezed Transform (WSST) proved successful in extracting the Instantaneous Frequency (IF) response of the Boyne bridge during the passage of a single locomotive and a maintenance truck. The field measurements were briefly mentioned, and the responses of a maintenance train and a single locomotive

were utilized because they closely resembled the point mass case studied in the paper. It can be inferred from the results that dynamic interaction is more pronounced when the train length is shorter than the bridge span. When the train's length exceeds that of the bridge, the response unfolds in three sub-phases: the loading phase, where the train approaches and fully loads the bridge; the loaded phase, where the bridge remains fully loaded; and the unloading phase, where the train starts to leave the bridge. The dynamic interaction during these three phases differs from the case of a single vehicle. Consequently, the baseline instantaneous frequency should be reconstructed over the three sub-phases. Moreover, the findings underscore the importance of the vehicle mass interaction with the local damage. For long trains, the variations between the mass of consecutive carriages can be helpful in detecting damage because they may trigger different responses, which should not occur when no damage is present. This sensitivity to variations between carriages can be a valuable indicator of damage. However, it also implies that the damage must be in proximity to the sensor to be accurately captured and not masked by the mass distribution of the train.

Regarding the type of train, passenger trains designed for passenger comfort by decoupling the car mass from the bogie system may not be well-suited for structural monitoring because this design reduces the direct interaction between the train and the bridge. In the case of DMU (Diesel Multiple Unit) trains, limited dynamic interaction is expected. However, for long freight trains, more significant interaction between the bridge and the train is anticipated.

6.2.3 Model assumptions and their implications

In the presented model the mass slides through a node-to-surface interaction with a hard contact model where no friction is considered. While this modeling approach is useful for calculating the bridge response, it is important to acknowledge that it does not fully replicate the real-world scenario of a rolling wheel. The model can be extended to implement the rolling wheel model; however, it needs to be investigated whether it has an influence on the content of the bridge dynamic response, specifically in detecting damage, without adding excessive time, effort, and complexity to the model.

6.2.4 Noisy data

In the context of VBI analysis, field measurements are often subject to various sources of noise, such as environmental or sensor noise, or data transmission artifacts. The ability to accurately extract the bridge's IFs from VBI field measurements, even in the presence of noise, is of paramount importance for Structural Health Monitoring (SHM) applications. It ensures that the SHM strategy can be implemented effectively. Any method capable of accurately decomposing noisy VBI responses with closely spaced frequency components and extracting the Instantaneous Frequency with sufficient resolution can be utilized effectively. In the context of damage detection, noise was identified as a challenging factor that affects damage detection techniques relying on response singularities and wavelet coefficients, which are commonly used. However, the proposed damage detection approach, centered around the bridge instantaneous frequency (IF) in a low-frequency range, exhibits robustness against noise interference. This is confirmed in Chapter 4 where various noise levels were added to simulated bridge responses, and the robustness of WSST in noisy environments was confirmed.

6.2.5 Damage size

Regarding the damage size, it has been observed that in scenarios involving small damage, it becomes challenging to determine whether the source of the IF change is damage or the operational condition. However, continuous monitoring over time can provide valuable insights for distinguishing whether the changes are a result of damage or variations in operational conditions. As the damage worsens, the magnitude variation in the IFs will increase over time. This trend serves as an indicator of actual damage, as the damage-induced alterations intensify with the progression of deterioration. On the other hand, if the changes were primarily induced by variations in operational conditions, the magnitude variation would remain relatively stable over time, without significant changes. By carefully monitoring the magnitude variation in the bridge's IFs over extended periods, it becomes possible to discern between damage-induced changes and changes resulting from different operational conditions.

6.2.6   Damage localization

Regarding damage localization, the study proposed a damage index based on the magnitude variation of the baseline instantaneous frequency, which serves as a preliminary step toward damage quantification. The potential for damage localization was also demonstrated, although it was not a primary focus of the current study. Moreover, an observation was made that the method exhibited lower sensitivity to damage at three-quarters of the bridge length than to damage close to midspan. This was mainly attributed to the fact that the baseline frequency used for comparison was the bridge's Instantaneous Frequency corresponding to the first bending mode. The method can possibly be extended by using higher bending modes as well, given they are excited sufficiently strong.

6.2.7   Sensor positioning

The proposed damage detection method relies on the fundamental bridge bending frequency and has been successfully validated on the Boyne bridge, equipped with three accelerometers. Despite one sensor being broken, the data analysis was executed using information from the remaining two sensors. For a single-span bridge with symmetry and relatively simple geometry, like the Boyne bridge, it was determined that a minimum of three strategically placed sensors (at one-quarter, one-half, and three-quarter length of the span) for effective monitoring is sufficient to explore the bridge first three bending modes.

7

Conclusions & Recommendations

7.1 Conclusions

Based on the results of the previous chapters and in line with the discussion, the following conclusion can be drawn:

- Usually railway bridges, including the case study bridge in this research, exhibit closely spaced mode shapes. As trains pass, these mode shapes become time-dependent. This study explored four signal processing techniques; Robust Local Mean Decomposition (Robust-LMD), Empirical Mode Decomposition (EMD), Continuous Wavelet Transform (CWT), and Wavelet Synchrosqueezed Transform (WSST), to extract the time-dependent resonances of the vehicle-bridge dynamic response. Among these, WSST consistently emerged as the superior method for delivering accurate Instantaneous Frequencies and robust time-frequency representations across a range of scenarios. WSST successfully extracted Instantaneous Frequencies (IFs) for both modeled and real-world bridges, even in noisy and closely spaced frequency conditions. This versatility positions WSST as a superior tool for structural analysis and monitoring in various applications.

- When it comes to detecting local events such as damage, this study emphasizes the importance of employing the bridge forced vibration (VBI) and analyzing the instantaneous frequencies of the coupled system rather than relying solely on the bridge free vibration and its natural frequency. However, the VBI response carries the global dynamic interaction between the subsystems as well as local events such

as damage. Variations in a bridge's baseline instantaneous frequency, attributed to damage or operational changes, can be effectively differentiated through a combination of shape correlation coefficients (ρ) and magnitude variation (δ), thereby improving damage detection. The magnitude variation parameter (δ) plays a crucial role as an initial step in quantifying damage in a damaged bridge, contributing significantly to structural health assessment.

- This study reveals the critical importance of selecting suitable train types for accurate and reliable bridge health monitoring and damage detection. Not all train types possess the desired dynamic characteristics for effective bridge health assessment. Single suspension trains exhibit more pronounced changes in the bridge's frequency response, particularly in Vehicle-Induced Delta Frequency (VIDF) and Damage-Induced Delta Frequency (DIDF), due to increased interaction between train mass and the bridge. On the other hand, in dual-suspension vehicles, the influence of the vehicle mass on the bridge frequency is minimal compared to the mass of the bogie, emphasizing the need to focus on bogie characteristics when analyzing the impact of vehicle dynamics on the bridge's instantaneous frequency (VIDF). Additionally, both single-suspension and dual-suspension vehicle models experience resonance, amplifying the dynamic response to damage. This underscores the significance of considering resonance effects in bridge health monitoring strategies for various train types.

7.2   Recommendations

Based on the limitations of the present work, as discussed in Chapter 6, some scientific recommendations will be given. In addition, a number of recommendations for the practical application of this research are provided.

7.2.1   Scientific recommendations

From the discussed limitations of the current models and methods, the following suggestions for further research are given:

- It should be investigated to what extent the proposed method also works for high-speed trains. The initial step to assess the performance of the proposed method

for high-speed trains involves increasing the train speed without altering other parameters and attempting to extract the bridge's Instantaneous Frequency (IF) using WSST. If successful, the next two stages involve; 1) refining the vehicle dynamics and, 2) incorporating the track as a subsystem in the model. In case the initial attempt is unsuccessful, optimizing the WSST algorithm to improve its performance can be considered.

- To extend the model to the full train, including its length, the best approach, according to the author's knowledge, is to extend the model to a series of consecutive dual-suspension mass-spring systems evenly spaced at the axle base length. In other words, each carriage is replaced by a dual-suspension mass-spring system. The next step would involve conducting the step-wise modal analysis, placing these systems at different locations on the bridge, and attempting to reconstruct the baseline instantaneous frequency over the three phases of loading, fully loaded, and unloading. These results will reveal the dynamic interaction between the series of carriages and the bridge. These results will determine whether a dynamic interaction exists between the series of carriages and the bridge, and establish the baseline instantaneous frequency. The next step is to introduce damage and investigate how consecutive masses passing over the damaged area influence the baseline IF.

- In reality, wheels roll as they move across the bridge surface, leading to different load distributions compared to the sliding contact model used in the simulation. Therefore, to extend the model, it is recommended to include a rolling wheel model.

- The proposed method displayed less sensitivity to damage at three-quarters of the bridge length compared to damage near midspan. As mentioned, this was primarily attributed to using the first bending mode of the bridge as the baseline IF. To address this limitation, the method can be extended by using multiple baselines corresponding to different bridge modes. Incorporating multiple baselines may improve the method's sensitivity and provide enhanced capabilities for identifying damage locations.

7.2.2 Practical recommendations

For the implementation of the presented methods in SHM of real bridges, the following guidelines can be used:

- For a single-span bridge with symmetry and relatively simple geometry, the minimum number of sensors required could be limited to three strategically placed at one-quarter, one-half, and three-quarter length of the span. This recommendation aligns with the mentioned scientific recommendation to enhance the method by defining multiple baseline Instantaneous Frequencies (IFs) corresponding to the bridge's higher modes.

- Single suspension trains exhibit more pronounced changes in the bridge's frequency response and are therefore more suitable for SHM purposes. To be more precise, a single locomotive is preferable over a freight train for this method, as the mass of freight trains can vary. In contrast, locomotives typically have a constant mass, contributing to more consistent and reliable results.

- Conducting long-term monitoring, which can be expensive in terms of instrumentation and data acquisition, may raise concerns about sensor connections and data quality over time. Therefore, it is recommended to perform shorter measurements but repeat them periodically, such as every 6 months or once per year. Additionally, conducting measurements in the same season and at the same time of day helps minimize variations in environmental factors like noise or temperature, reducing uncertainties in the data. However, the feasibility of this approach depends on the accessibility of the bridge span for instrumentation. For bridges equipped with built-in monitoring systems, the data analysis scheme can be optimized by focusing on a specific vehicle type and setting up the baseline IF.

8

Publications

8.1 Journal papers

- Mostafa, N., Di Maio, D., Loendersloot, R. & Tinga, T. (2023). The influence of vehicle dynamics on the time-dependent resonances of a bridge. Advances in Bridge Engineering, 4, No. 22. https://doi.org/10.1186/s43251-023-00102-4

- Mostafa, N., Di Maio, D., Loendersloot, R. & Tinga, T. (2022). Railway bridge damage detection based on extraction of instantaneous frequency by Wavelet Synchrosqueezed Transform. Advances in Bridge Engineering, 3, No. 12. https://doi.org/10.1186/s43251-022-00063-0

- Mostafa, N., Di Maio, D., Loendersloot, R. & Tinga, T. (2021). Extracting the time-dependent resonances of a vehicle–bridge interacting system by wavelet synchrosqueezed transform. Structural Control & Health Monitoring, 28(12), 1-24. No. e2833. https://doi.org/10.1002/stc.2833

8.2 Conference papers

- Mostafa, N., Di Maio, D. & Loendersloot, R. (2022). Non-stationary Analysis of Vehicle-Bridge Interaction for Structural Health Monitoring of a Railway Bridge. Paper presented at the Fifth international conference on railway technology, Montpellier, France.

- Mostafa, N., Loendersloot, R., Di Maio, D. & Tinga, T. (2020). Application of wavelet synchro-squeezed transform (WSST) method to railway bridge health monitoring. In M. Papadrakakis, M. Fragiadakis & C. Papadimitriou (Eds.), Proceedings of EURODYN 2020 - XI International Conference on Structural Dynamics. pp. 1388-1396. National Technical University of Athens, Greece.

- Mostafa, N., Di Maio, D. & Loendersloot, R. (2020). Vehicle Bridge Interaction – Extracting the dynamic characteristics of the non-stationary train passing phase. In W. Desmet, B. Pluymers, D. Moens & S. Vandemaele (Eds.), Proceedings of ISMA 2020 - International Virtual Conference on Noise and Vibration Engineering and USD 2020 - International Conference on Uncertainty in Structural Dynamics. pp. 1511-1523.

- Mostafa, N., Loendersloot, R., Di Maio, D. & Tinga, T. (2018). Relative frequency, a damage sensitive feature for railroad bridges. Paper presented at the Fourth International Conference on Railway Technology 2018, Barcelona, Spain.

- Mostafa, N., Loendersloot, R., Tinga, T., Reitsema, A. D. & Hordijk, D. A. (2016). Monitoring dynamic stiffness that predicts concrete structure degradation. In J. Bakker, D. M. Frangopol & K. van Breugel (Eds.), Life-Cycle of Engineering Systems: Emphasis on Sustainable Civil Infrastructure IALCCE, the Netherlands.

Acknowledgements

I extend my sincere gratitude to my promoter, Professor Tiedo Tinga. Thank you for the invaluable technical discussions and feedback. Your extensive expertise, coupled with meticulous attention to detail, has been instrumental in shaping the quality of my work. Thanks to my co-supervisor, Dario Di Maio, for his guidance throughout my Ph.D. journey. I also want to express my gratitude to my daily supervisor, Richard Loendersloot. Richard, without your support, the completion of my Ph.D. would not have been possible. My Ph.D. journey extended beyond the anticipated duration, and throughout the challenges, your consistent support has been my guiding light. You are a remarkable mentor. To Debbie Zimmerman van Woesik, thank you for your warmth and kindness. Your support has been a source of comfort whenever I needed assistance. I Also express my gratitude to the two wonderful ladies, Annemieke and Nubia, with whom I shared the office. I found great enjoyment in being in the office.

My heartfelt appreciation goes to my husband, Mohammad. You have gone above and beyond to help me balance the roles of a full-time working woman, a mother of two, and a Ph.D. student. I express my deep gratitude and love to my children, Nikan and Nila. You inspire me to persevere and never give up.

I also want to express my appreciation to my parents, siblings, and friends. Your support has been invaluable.